

T
CDI
Ana
607.024
May 83

COMPUTER SIMULATION OF THE IONIC CRYSTAL-WATER INTERFACE

by

NICHOLAS ANASTASIOU

A thesis submitted in part fulfillment of the requirements for the degree of Doctor of Philosophy in the Faculty of Science of the University of London.

Department of Chemistry
Royal Holloway College
Egham Hill
Egham,
Surrey.

September 1982

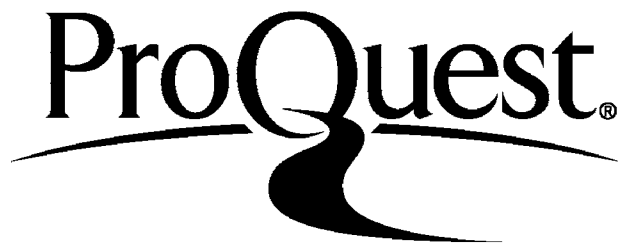
ProQuest Number: 10097504

All rights reserved

INFORMATION TO ALL USERS

The quality of this reproduction is dependent upon the quality of the copy submitted.

In the unlikely event that the author did not send a complete manuscript and there are missing pages, these will be noted. Also, if material had to be removed, a note will indicate the deletion.



ProQuest 10097504

Published by ProQuest LLC(2016). Copyright of the Dissertation is held by the Author.

All rights reserved.

This work is protected against unauthorized copying under Title 17, United States Code.
Microform Edition © ProQuest LLC.

ProQuest LLC
789 East Eisenhower Parkway
P.O. Box 1346
Ann Arbor, MI 48106-1346

ACKNOWLEDGEMENTS

I would like to express my thanks to
Professor K. Siggel for his excellent guidance
and assistance.

Dr. B. Fischer for valuable assistance during
the course of this work.

the S.E.R.C. and Unilever Research, in particular
for the award of a D.S.P. award.

My family for their constant
encouragement.

TO MY PARENTS

ABSTRACT

Computer simulation by the molecular dynamics technique has been used to investigate the liquid-crystal-water interface. The model consisted of a slab of water molecules in contact with a liquid-crystal phase. The simulation was carried out with the parameters found by Tosi and Ford were used for the liquid phase.

ACKNOWLEDGEMENTS

I would like to express my thanks to:

Professor K. Singer for his excellent guidance and enthusiasm.

Dr. D. Fincham for valuable assistance during the course of this work.

The S.E.R.C. and Unilever Research, in particular Dr. M. Lal, for a CASE award.

My family and friends for their constant encouragement.

ABSTRACT

Computer simulation by the molecular dynamic technique has been used to investigate the ionic crystal-water interface. The model consisted of a slab of sodium chloride in contact with water. The Born-Mayer-Huggins potential with the parameters found by Tosi and Fumi were used for the ion-ion interactions, water was modelled by the 'central-force potential' and the ion-water interaction by the potentials proposed by Heinzinger et al. The long range forces were evaluated by the Ewald method.

We investigated (a) a system in which only the water molecules were allowed to move while the ions were fixed (b) a system in which all particles could move. Attention was focused on (a) on the behaviour of the water molecules near the crystal surface, and in (b) on the mechanism of the solution process.

1.1	Non-Coulomb Forces, Potential Energy and Virial	26
1.2	Coulomb Force and Energy	27
1.3	The ∇^2 Method	34
1.4	Application to the Cryst-1	35
1.5	Application to Cryst-2	36

CHAPTER THREE- COMPUTER SIMULATION OF WATER AND AQUEOUS SOLUTIONS

2.1	Introduction	38
2.2	Water Model	40
2.3	Choice of Water Model	47
2.4	Comparison of ∇^2 and Ewald Method	48
2.5	Aqueous Solutions	49

CONTENTS

	Page No.
LIST OF DIAGRAMS	4
CHAPTER ONE: THE METHOD	
1.1 Introduction	9
1.2 Computational Details	12
1.3 The Monte Carlo Method	14
1.4 The Method of Molecular Dynamics	15
1.5 Equilibrium Properties	17
1.6 Time-dependent Phenomena	19
1.7 The Aim of the Work	23
CHAPTER TWO: IONIC SIMULATION	
2.1 Introduction	25
2.2 Interionic Pair Potential	27
2.3 Non-Coulomb Force, Potential Energy and Virial	28
2.4 Coulomb Force and Energy	29
2.5 The P ³ M Method	34
2.6 MDIONS on the Cray-1	35
2.7 Application of MDIONS	38
CHAPTER THREE: COMPUTER SIMULATION OF WATER AND AQUEOUS SOLUTIONS	
3.1 Introduction	39
3.2 Water Models	40
3.3 Choice of Water Model	47
3.4 Comparison of P ³ M and Ewald Methods	48
3.5 Aqueous Solutions	59

CHAPTER FOUR: COMPUTER SIMULATION OF IONIC CRYSTAL SLABS		
4.1	Introduction	62
4.2	Computational Details	65
4.3	Results and Discussion	68
4.4	Conclusion	83

CHAPTER FIVE: THE SODIUM CHLORIDE-WATER INTERFACE

5.1	Introduction	85
5.2	Computational Details	86
5.3	Simulation at 300K	96
5.4	Simulation at 480K	102
5.5	Conclusion	114

CHAPTER SIX: FIXED IONIC CRYSTAL-WATER INTERFACE

6.1	Introduction	115
6.2	Simulation at 300K	116
6.3	Simulation at 480K	135
6.4	Conclusion	157

REFERENCES

160

LIST OF FIGURES

- 1.1 Nearest image convention in evaluating pair interactions.
- 3.1 Point-charge representation of the water molecule for BNS and ST2 models.
- 3.2 Point-charge representation of the water molecule which corresponds to the CF model.
- 3.3 $g(r)$ obtained by P^3M method for CF water with 462 molecules, 300K.
- 3.4 $g(r)$ obtained by P^3M method for CF water with 216 molecules, 300K.
- 3.5 $g(r)$ obtained by Ewald method for CF water with 216 molecules, 200K.
- 3.6 VACF obtained by Ewald method for CF water (of the oxygen atoms) an average over 4000 steps and a correlation of 2000 steps, 200K.
- 3.7 $g(r)$ obtained by Ewald method for CF water with 216 molecules, 322K.
- 3.8 VACF obtained by Ewald method for CF water (of the oxygen atoms) an average over 4000 steps and a correlation of 2000 steps, 322K.
- 4.1 A pictorial representation of the computational box. The dashed lines denote image cells. The shaded regions represent the crystal; the rest is vacuum. Origin (0,0,0) is at the centre of the cell.
- 4.2 Density profile, $\rho(z)$, for Na^+ at 300K, two thirds of the computational cell occupied by crystal and the rest by vacuum. $\rho(z)\Delta Z =$ no. of particles between z and ΔZ . $\Delta Z = 0.085\text{\AA}$.

- 4.3 Density profile for Cl^- at 300K, two thirds of the computational cell occupied by crystal and the rest vacuum, $\Delta Z = 0.085\text{\AA}$.
- 4.4 Density profile for Na^+ and Cl^- at 900K, two thirds of the computational cell occupied by crystal and the rest vacuum, $\Delta Z = 0.085\text{\AA}$.
- 4.5 Density profile for Na^+ at 300K, half the computational cell occupied by crystal and the rest vacuum, $\Delta Z = 0.085\text{\AA}$.
- 4.6 Density profile for Cl^- at 300K, half the computational cell occupied by crystal and the rest vacuum, $\Delta Z = 0.085\text{\AA}$.
- 4.7 Density profile for Na^+ and Cl^- at 900K, half the computational cell occupied by crystal and the rest vacuum, $\Delta Z = 0.085\text{\AA}$.
- 4.8 Density profile, $\rho(z)$, $\Delta Z = 0.1\text{\AA}$, for;
- (a) Bulk NaCl, $r_0 = 2.86\text{\AA}$, $T = 298\text{K}$.
 - (b) Lamina NaCl, $r_0 = 2.86\text{\AA}$, $T = 302\text{K}$.
 - (c) Lamina NaCl, $r_0 = 2.91\text{\AA}$, $T = 658\text{K}$.
 - (d) Lamina NaCl, $r_0 = 2.97\text{\AA}$, $T = 1034\text{K}$.
- dots: representing lamina method, Na^+ .
- solid lines: representing isolated lamina method, Na^+ .
- 5.1 Computer generated snapshot of a (001) NaCl crystal plane, thickness $\Delta Z = 1.8\text{\AA}$, the xy plane viewed from the Z direction.
- 5.2 Density profile, $\rho(z)$, at $t = 0$, of Na^+ , Cl^- and H_2O (represented by the O atoms). Histogram thickness $\Delta Z = 0.176\text{\AA}$.
- 5.3 Density profile, of O and H, after equilibration period.
- 5.4 Computer generated snapshot of the crystal surface with the first layer of water molecules, thickness $\Delta Z = 3\text{\AA}$. Na^+ and Cl^- ions drawn to scale, H_2O reduced for clarity. xy plane viewed from z direction, 300K.

- 5.5 As Fig. 5.4 but after 0.1ps.
- 5.6 As Fig. 5.4 but after 0.5ps.
- 5.7 As Fig. 5.4 but after 1ps.
- 5.8 As Fig. 5.4 but after 2ps.
- 5.9 Density profile, of Na^+ , Cl^- and H_2O (represented by O atoms) after 0.5ps, 300K.
- 5.10 As Fig. 5.4 but after 1ps.
- 5.11 As Fig. 5.4 but after 2ps.
- 5.12 Density profile, $\rho(z)$, at $t = 0.2\text{ps}$ of Na^+ , Cl^- and H_2O (represented by the O atoms), histogram thickness $\Delta Z = 0.176\text{\AA}$, $T = 480\text{K}$.
- 5.13 Computer generated snapshot of the interfaced region of thickness. $\Delta Z = 4.4\text{\AA}$ at 0.5ps. The Na^+ and Cl^- are drawn to scale, H_2O reduced for clarity. The xy plane viewed from the z direction, $T = 480\text{K}$.
- 5.14 As Fig. 5.12 but at 0.5ps.
- 5.15 As Fig. 5.13 but at 1.6ps.
- 5.16 As Fig. 5.12 but at 2.35ps.
- 5.17 The history of the water molecule that has penetrated the crystal the furthest at the end of the simulation, viewed in the XZ plane.
- 6.1 $\rho(z)$ for oxygen and hydrogen next to a fixed NaCl crystal, $\Delta Z = 0.176\text{\AA}$, hydrogen $\rho(z)$ divided by two.
- 6.2 Computer generated snapshot of the interfacial region, $\Delta Z = 3.5\text{\AA}$, xy plane viewed in the z direction.
- 6.3 $\rho(x)$ and $\rho(y)$ of oxygen at one crystal surface, $\Delta Z = 0.176\text{\AA}$.
- 6.4 As Fig. 6.3 at the other crystal surface.
- 6.5 $\langle \cos\theta \rangle$ of the water molecules, where θ is the angle between the dipole moment vector and the outward normal to the crystal plane, $\Delta Z = 0.085\text{\AA}$.

- 6.6 Comparison of diffusion of water at the surface (full line), and the bulk (dashed line), by accumulation of mean square displacements, $\Delta Z \approx 4.4\text{\AA}$.
- 6.7 Diffusion of water at the surface, in the x,y and z direction, by accumulation of mean square displacements, $\Delta Z \approx 4.4\text{\AA}$.
- 6.8 Comparison of angular momentum correlation function between surface (full line), bulk (dashed line) and pure water (dotted line), $\Delta Z \approx 4.4\text{\AA}$.
- 6.9 Comparison of $\langle \underline{J}e_1(0) \cdot \underline{J}e_1(t) \rangle$ between surface (full line), bulk (dashed) and pure water (dotted), $\Delta Z \approx 4.4\text{\AA}$. $\underline{J}e$ represents the scalar produce of $\underline{J} \cdot \underline{e}$.
- 6.10 As Fig. 6.9 but for $\langle \underline{J}e_2(0) \cdot \underline{J}e_2(t) \rangle$.
- 6.11 As Fig. 6.10 but for $\langle \underline{J}e_3(0) \cdot \underline{J}e_3(t) \rangle$.
- 6.12 Indicates the directions of the axes of inertia of the water molecule.
- 6.13 Comparison of $\langle \underline{e}_1(0) \cdot \underline{e}_1(t) \rangle$ for surface (full line), bulk (dashed line) and pure water (dotted line), $\Delta Z \approx 4.4\text{\AA}$.
- 6.14 As Fig. 6.13 but for $\langle \underline{e}_2(0) \cdot \underline{e}_2(t) \rangle$.
- 6.15 As Fig. 6.13 but for $\langle \underline{e}_3(0) \cdot \underline{e}_3(t) \rangle$.
- 6.16 Density profile for water next to a fixed crystal $\Delta Z = 0.176\text{\AA}$. (a) O (b) H (c) O¹⁸, 480K.
- 6.17 Computer generated snapshot of the interfac water next to a fixed crystal, 480K, $\Delta Z = 3.5\text{\AA}$.
- 6.18 $\rho(x)$ and $\rho(y)$ of oxygen at one crystal surface, $\Delta Z = 0.085\text{\AA}$, T = 480K.
- 6.19 As Fig. 6.18 but at the other crystal surface.
- 6.20 $\langle \cos\theta \rangle$ of the water molecules, $\Delta Z = 0.085\text{\AA}$, T = 480K.
- 6.21 Comparison of diffusion of water at the surface (full line), and the bulk (dashed line) by accumulation of mean square displacements, $\Delta Z \approx 4.4\text{\AA}$, T = 480K.

- 6.22 Comparison of angular momentum correlation function between surface (full line), bulk (dashed line) and H_2O^{318} (dotted line), $\Delta Z \approx 4.4\text{\AA}$.
- 6.23 Comparison of $\langle \underline{J}_{e_1}(0) \cdot \underline{J}_{e_1}(t) \rangle$ between surface (full line), bulk (dashed line), and H_2O^{318} (dotted), $\Delta Z \approx 4.4\text{\AA}$.
- 6.24 As Fig. 6.23 but for $\langle \underline{J}_{e_2}(0) \cdot \underline{J}_{e_2}(t) \rangle$.
- 6.25 As Fig. 6.23 but for $\langle \underline{J}_{e_3}(0) \cdot \underline{J}_{e_3}(t) \rangle$.
- 6.26 As Fig. 6.23 but for $\langle \underline{e}_1(0) \cdot \underline{e}_1(t) \rangle$.
- 6.27 As Fig. 6.23 but for $\langle \underline{e}_2(0) \cdot \underline{e}_2(t) \rangle$.
- 6.28 As Fig. 6.23 but for $\langle \underline{e}_3(0) \cdot \underline{e}_3(t) \rangle$.
- 6.29 $\langle \cos\theta \rangle$ for H_2O^{318} over 4ps, $T = 480K$, water next to a fixed crystal.
- 6.30 Diffusion of water at the surface, in the x,y and z directions, by accumulation of mean square displacements, $\Delta Z \approx 4.4\text{\AA}$, $T = 480K$.
- 6.31 Angular momentum correlation function for H_2O^{318} , $T = 480K$.
- 6.32 $\langle \underline{J}_{e_1}(0) \cdot \underline{J}_{e_1}(t) \rangle$ for H_2O^{318} , $T = 480K$.
- 6.33 As Fig. 6.32 for $\langle \underline{J}_{e_2}(0) \cdot \underline{J}_{e_2}(t) \rangle$.
- 6.34 As Fig. 6.32 for $\langle \underline{J}_{e_3}(0) \cdot \underline{J}_{e_3}(t) \rangle$.
- 6.35 $\langle \underline{e}_1(0) \cdot \underline{e}_1(t) \rangle$ full line, $\langle \underline{e}_2(0) \cdot \underline{e}_2(t) \rangle$ dashed line, $\langle \underline{e}_3(0) \cdot \underline{e}_3(t) \rangle$ dotted line.

CHAPTER 1

THE METHOD

1.1 Introduction

The computer is now an important tool of science, it serves in a plethora of disciplines; ones as diverse as astrophysics and crystallography. In theoretical chemistry computer simulation techniques are used to investigate the properties of fluids and solids. In the work presented here we show an example illustrating the scope of computer simulation in chemistry.

In this method $\sim 10^2 - 10^3$ particles are confined within a model cell and the particles allowed to interact. The behaviour of such a system is simulated on a computer. The techniques of computer simulation are known as the Monte Carlo [1,2] method and the method of molecular dynamics [3].

The Monte Carlo method was devised originally by Metropolis [4]. In this method a Boltzmann weighted set of configurations is generated by a suitable stochastic process. Wood [5,6] later extended the method and applied it to Lennard-Jones (LJ) fluids.

In the method of molecular dynamics developed by Alder and Wainright [7] the equations of motion of the particles are solved by numerical integration. Alder and Wainright first studied a system of hard spheres by molecular dynamics. Rahman [8] then applied the method to simulate the properties of liquid argon, the particles interacting through the more realistic LJ potential.

A good approximation to the intermolecular pair potential in real liquids is given by the LJ potential

$$\phi(r) = 4\epsilon \left[\left(\frac{\sigma}{r}\right)^{12} - \left(\frac{\sigma}{r}\right)^6 \right]$$

which has an attractive part varying as r^{-6} and a repulsive part varying as r^{-12} ; σ is the collision diameter and ϵ the maximum depth of the potential well. The equilibrium properties of the LJ fluid have been very extensively studied both by molecular dynamics and the Monte Carlo method [9-13], and it has been found that the thermodynamic behaviour of liquid argon is accurately reproduced by the potential with values of ϵ and σ taken from high temperature second virial coefficient measurements. However the success of this potential serves better as an effective pair potential rather than an exact pair potential between argon atoms [14], the omitted many body effects appear to be compensated by the LJ potential. The potential is nevertheless a good effective model for argon and also for other simple liquids [15].

Only a limited number of liquid mixtures exist in which the molecules may be expected to interact according to the 12-6 potential. These are mixtures of rare gases and of substances obeying the law of corresponding states. Lack of reliable experimental data has in addition hampered the development of satisfactory theories of mixtures. In the case of a mixture of two 12-6 liquids, A and B, with interaction parameters ϵ_{AA} , σ_{AA} and ϵ_{BB} , σ_{BB} it is often assumed that the potential between A-B pairs is described by a 12-6 function with parameters defined by the Lorentz-Berthelot rules:

$$\epsilon_{AB} = (\epsilon_{AA}\epsilon_{BB})^{\frac{1}{2}} \quad \sigma_{AB} = \frac{1}{2}(\sigma_{AA} + \sigma_{BB}).$$

The Monte Carlo method has been used to calculate thermodynamic properties of such mixtures over an arbitrary range of potential parameters. The comparison of computer results with measured values of the properties of mixtures serves as a method for obtaining ϵ_{AB} and σ_{AB} of real systems. Application of computer simulation to the calculation of excess thermodynamic properties of simple liquid mixtures is useful in testing theories of liquid mixtures [16-19].

Berne and Harp [20,21] were the first to apply molecular dynamic calculations to a molecular liquid, they simulated CO by a Stockmayer potential, i.e. a LJ potential plus a point dipole (and a quadrupole) moment; time-dependent properties which characterize rotational motion were investigated. Calculations on liquid N₂ simulated by 2-LJ centres at a fixed distance apart have since been extensively studied by Barojas et al. [22] and by Cheung and Powles [23]. The thermodynamic and structural properties and some of the dynamic properties were found to be in good agreement with experiment. Singer et al. [24,25] carried out further calculations for F₂, Cl₂, Br₂ and CO₂. Murthy et al. [26,27] have shown that simple 2 or 3 centre models with a quadrupole moment can adequately describe the properties of N₂ and CO₂ in the solid, liquid and gas phases.

Rahman and Stillinger's remarkable paper on water [28] showed that a great deal of insight into the nature of more complicated liquids such as water can be obtained by molecular dynamics. A further discussion on the simulation of water and also aqueous solutions follows in Chapter 3.

Woodcock and Singer [29] were the first to study the computer simulation of ionic systems with the long range coulombic forces included. Chapter 2 gives more details on the simulation of ionic systems.

With advances in computing power, interfaces have recently received a great deal of attention. There have been computer simulation studies on liquid-gas systems of both monatomic [30-34] and molecular systems [35]. Heyes et al. [36-38] have studied the ionic crystal-vacuum interface of various alkali halides. Lately there has also been a lot of interest in simulating the solid-liquid interface [39-43] of LJ systems. More recent work is by Christou et al. [44] who have simulated water in contact with a structureless wall.

The computer simulation study of this project is of the more realistic ionic crystal-water interface. The importance of crystallisation in a wide variety of industries and the difficulty in obtaining experimental information on interfaces [45] suggests that computer simulation can provide results on the molecular level to give an insight into what is happening at this interface.

1.2 Computational Details

In both Monte Carlo and molecular dynamics the same basic computer model is used. A system of N particles is confined within a cell, usually a cube of volume $V = L^3$.

$$\underline{r}_{ij} = \underline{r}_i - \underline{r}_j$$

$$r_{ij} = |\underline{r}_{ij}|$$

$$\alpha = x, y, z$$

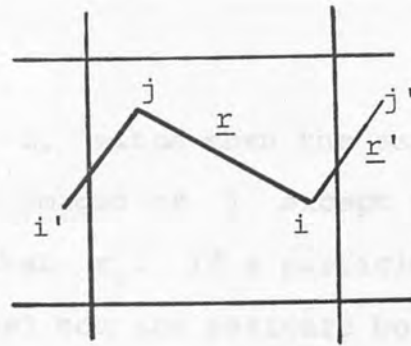


Figure 1.1. Nearest image convention. In evaluating pair interactions \underline{r}_{ij} is replaced by \underline{r}'_{ij} whenever $|\underline{r}'_{ij}| < |\underline{r}_{ij}|$.

The particles are assumed to interact via a pair potential $u(r_{ij})$ within a cut-off r_c (usually half the box length L). The potential energy ϕ is obtained by

$$\phi = \sum_{i=1}^N \sum_{j>i}^N u(r_{ij})$$

and the virial ψ by

$$\psi = \sum_{i=1}^N \sum_{j>i}^N r_{ij} \frac{du}{dr_{ij}}$$

The coordinates which define the positions of each particle within the cell are stored in the computer. In order to simulate as closely as possible the behaviour of a macroscopic system periodic boundary conditions are used in the three Cartesian coordinates. This is achieved by the nearest image conversion see Fig. 1.1. In evaluating the interaction on particle i due to particle j the image of j which is nearest to i is taken. This is achieved by the transformation

$$\text{if } r_{ija} > \frac{L}{2} \quad r_{ija} \leftarrow r_{ija} - L$$

$$\text{if } r_{ija} < -\frac{L}{2} \quad r_{ija} \leftarrow r_{ija} + L.$$

This is consistent with the cut-off criterion provided that the cut-off radius r_c is not greater than half the side

of the calculation box L , since then the separation between i and all the images of j except the nearest image must be greater than r_c . If a particle is displaced outside the computational box the periodic boundary conditions are applied to bring it back into the box. Due to the cut-off it is necessary to apply a long range correction for $r > r_c$. This can be done by the assumption [46] of a uniform average density at distances greater than r_c . These corrections are

$$\phi_{lrc} = \frac{1}{2} \frac{N^2}{V} \int_{r_c}^{\infty} u(r_{ij}) 4\pi r_{ij}^2 dr_{ij}$$

$$\psi_{lrc} = \frac{1}{2} \frac{N^2}{V} \int_{r_c}^{\infty} r_{ij} \frac{du}{dr_{ij}} 4\pi r_{ij}^2 dr_{ij}.$$

The initial positions of the particles are set out as far as possible so as to closely resemble the system wished to be studied.

1.3 The Monte Carlo Method

The total potential energy ϕ and total virial ψ are calculated as a sum of pair terms. A particle of the system of N particles in the computational box of volume V is chosen, either serially or at random, and given a random displacement. The change in total potential energy ϕ of the system is $\Delta\phi$. If $\Delta\phi$ is negative the move is accepted with a probability $\exp(-\beta\Delta\phi)$ where $\beta = 1/k_B T$, k_B is the Boltzmann constant and T the temperature.

This procedure is repeated generating a chain of configurations proportional to the Boltzmann factor $\exp(-\beta\phi)$. If a move is rejected the previous configuration is counted

again. The overall chain average of any configurational property converges to the canonical ensemble average as the chain length increases, giving e.g. $\langle\phi\rangle$ and $\langle\psi\rangle$. The pressure P is calculated from the average virial ψ by means of the virial theorem $P = (N_0 k_B T - (N_0/3N) \langle\psi\rangle) / V$ where $N_0 =$ Avogadro's number.

The procedure described here is for the NVT ensemble though it is also possible to work with the NPT ensemble. In this method in addition to a change in the position of a particle at each step the box length L is changed by a small amount as well. A configuration is then accepted with a probability W

$$W = \left(\frac{V'}{V}\right)^N \exp(-\beta\Delta H)$$

where V' and V are the volume of the new and old configurations respectively and $\Delta H = \Delta\phi + P\Delta V$ is the increase in enthalpy. The molar volume of the system at pressure P is proportional to the average volume $\langle V \rangle$ of the box.

1.4 The Method of Molecular Dynamics

In this method the particles are given initial velocities and the trajectories of the particles are determined by numerical integration of the classical equations of motion. The equations of motion are solved in a series of time steps.

Equilibrium properties such as $\langle\phi\rangle$ and $\langle\psi\rangle$ of the system are now calculated as an average over time. Also, since a dynamical sequence of states of the system is generated, time-dependent phenomena can be studied and transport coefficients can be calculated.

In this method the equations of motion are solved in a series of time steps, at each of which all the pair forces are calculated

$$\underline{f}_{ij} = - \frac{du}{dr_{ij}} \frac{\underline{r}_{ij}}{r_{ij}}$$

At each time step the potential energy and virial terms are also obtained. The total force on each particle

$$\underline{F}_i = \sum_{j \neq i} \underline{f}_{ij}$$

is found and its equations of motion are integrated, between times $n\Delta t$ and $(n+1)\Delta t$, where Δt is the time step using the leapfrog algorithm [4]:

$$F(x) = m\ddot{x} \quad a = F/m$$

where m is the mass a the acceleration and x the position then $\frac{dv}{dt} = a$ and $\frac{dx}{dt} = v$ where v is the velocity. At time $n\Delta t$ have position x^n since $v = \frac{dx}{dt}$ a good approximation is

$$v^{n+\frac{1}{2}} = \frac{x^{n+1} - x^n}{\Delta t}$$

and since $a = \frac{dv}{dt}$ a good approximation is

$$a^n = \frac{v^{n+\frac{1}{2}} - v^{n-\frac{1}{2}}}{\Delta t}$$

giving the leapfrog algorithm

$$v^{n+\frac{1}{2}} = v^{n-\frac{1}{2}} + \Delta t a^n$$

$$\underline{r}^{n+1} = \underline{r}^n + \Delta t v^{n+\frac{1}{2}}$$

and the velocity at step n is calculated as

$$\underline{v}^n = \frac{1}{2}(\underline{v}^{n+\frac{1}{2}} + \underline{v}^{n-\frac{1}{2}})$$

The algorithm is algebraically equivalent to the Verlet [48] algorithm that was initially used.

The velocities \underline{v}^n are used to calculate the kinetic energy K

$$K = \sum \frac{1}{2} m |v^n|^2 \quad \text{summing over all particles,}$$

and hence pressure

$$P = \left(\frac{2}{3} K - \frac{1}{3} \psi \right) / V$$

and temperature

$$T = 2K / 3Nk_B.$$

1.5 Equilibrium Properties

In the Monte Carlo method it is only possible to obtain equilibrium properties. We have seen that an average value may be obtained over a whole set of configurations for $\langle \phi \rangle$ and $\langle \psi \rangle$. The pressure $P(V, T)$ is obtained from the virial. Since the temperature is fixed in this method, it is suitable for the study of isothermal processes. It can also be used for isothermal-isobaric work by the NPT-ensemble.

In molecular dynamics the thermodynamic averages $\langle \phi \rangle$, $\langle P \rangle$ and $\langle T \rangle$ are obtained as averages over the time steps of the simulation.

In both Monte Carlo and molecular dynamics useful information can also be obtained from the fluctuations in the system [49]. We can obtain the following estimates by molecular dynamics, specific heat:

$$C^* = C_V / R = \frac{3}{2} \left\{ 1 - \frac{3N}{2} \frac{\langle \delta K^2 \rangle}{\langle K \rangle^2} \right\}^{-1}$$

thermal pressure coefficient:

$$\left(\frac{\partial P}{\partial T}\right)_V = \frac{2}{3} \frac{N}{V} k_B C^* \left\{ 1 - N \left(\frac{3}{2}\right)^2 \frac{\langle \delta K \delta \Gamma \rangle}{\langle K \rangle^2} \right\}$$

and adiabatic compressibility:

$$\frac{1}{V} \left(\frac{\partial V}{\partial P}\right)_S = V \left\{ \frac{2}{3} \langle \Gamma \rangle + \frac{2}{3} \langle K \rangle + \frac{1}{9} \langle \Omega \rangle - N \left(\frac{3}{2}\right) \frac{\langle \delta \Gamma^2 \rangle}{\langle K \rangle} \right\}^{-1}$$

where for example, $\langle \delta K^2 \rangle$ means $\langle K^2 \rangle - \langle K \rangle^2$; $\Gamma = VP$ and

$$\Omega = \sum_{i=1}^N \sum_{j>1}^N r_{ij}^2 \frac{d^2 u}{dr_{ij}^2}.$$

The equilibrium structure is normally discussed in terms of equilibrium distribution functions. The n-particle distribution function is defined as

$$g_N^{(n)}(\underline{r}_1, \dots, \underline{r}_n) = \frac{P_N^{(n)}(\underline{r}_1, \dots, \underline{r}_n)}{\prod_{i=1}^n P_N^{(1)}(\underline{r}_i)}$$

where $P_N^{(n)}(\underline{r}_1, \dots, \underline{r}_n)$ is the probability of simultaneously finding particle 1 in a volume $d\underline{r}_1$ around \underline{r}_1 , particle 2 in $d\underline{r}_2$ around \underline{r}_2 etc.

The most important distribution functions are the single-particle and pair functions

$$P_N^{(1)}(\underline{r}_1) = \frac{\int \dots \int \exp[-\beta V_N(\underline{r}^N)] d\underline{r}_2 \dots d\underline{r}_N}{\int \dots \int \exp[-\beta V_N(\underline{r}^N)] d\underline{r}_1 d\underline{r}_2 \dots d\underline{r}_N} \\ = \frac{1}{V}$$

and therefore $g_N^{(n)}(\underline{r}^n) = V^n P_N^{(n)}(\underline{r}^n)$

and in particular

$$g_N^{(2)}(\underline{r}_1, \underline{r}_2) = V^2 P_N^{(2)}(\underline{r}_1, \underline{r}_2).$$

If the system is isotropic

$$g_N^{(2)}(\underline{r}_1, \underline{r}_2) = g(|\underline{r}_1 - \underline{r}_2|)$$

The quantity $g(r)$ is called the radial distribution function and $g(r) \rightarrow 1$ as $r \rightarrow \infty$.

The structure of a molecular fluid, in so far as pair correlations are concerned, is described by the total pair correlation $g^{(2)}(\underline{R}, \underline{\Omega}_1, \underline{\Omega}_2)$ which is the probability of finding two molecules with a centre-centre vector separation \underline{R} and the orientations $\underline{\Omega}_1$ and $\underline{\Omega}_2$ relative to a space fixed axis. Alternatively, it is possible to study the structure of a molecular fluid by the site-site correlation functions. In the case of water for example we have $g_{OH}(r)$, $g_{HH}(r)$ and $g_{OO}(r)$. The distribution function $g_{\alpha\beta}(r)$ is defined by the relation

$$4\pi r^2 \rho_\beta g_{\alpha\beta}(r) dr = n_\beta(r)$$

where ρ_β is the density of species β and $n_\beta(r)$ is the average number of particles β in a spherical shell of radius r and thickness dr around a particle of species α .

1.6 Time-dependent Phenomena

Molecular dynamics gives information on time dependent properties in addition to equilibrium properties. A transport coefficient can be calculated as an integral over a time correlation function of the appropriate dynamical variable. The correlation function is

$$C_{\alpha\beta}(t) = \langle \alpha(0) \cdot \beta(t) \rangle$$

where the bracket indicates an equilibrium ensemble average of initial conditions. When α and β are the same property it is called an autocorrelation function. Each system in the ensemble is in an initial state characterised by a point in phase space. As time progresses each system traverses a $6N$ dimensional trajectory in phase which is uniquely determined by its initial state and by canonical equations of motion. The function β varies on each trajectory due to its dependence on the phase. Thus corresponding to each replica system there is an initial point in phase space, a corresponding trajectory and a corresponding time variation of the property β . Thus for each replica system the product $\alpha(0)\beta(t)$ depends only on the initial state of the system and time.

The easiest transport property to be computed is that of self diffusion. If a particle at time $t = 0$ is located at a position $\underline{r}_i(0)$ and has a velocity $\underline{v}_i(0)$. The mean square displacement (msd) at time t is

$$\text{msd} = \frac{1}{N} \left\langle \sum_{i=1}^N |\underline{r}_i(t) - \underline{r}_i(0)|^2 \right\rangle.$$

Both the msd and the velocity autocorrelation function (vacf) are related to the process of diffusion

$$\lim_{t \rightarrow \infty} \text{msd} = 6Dt$$

where D is the coefficient of self-diffusion.

D is related to the vacf by:

$$\langle |\underline{r}(t) - \underline{r}(0)|^2 \rangle = \left\langle \int_0^t \underline{v}(t') dt' \cdot \int_0^t \underline{v}(t'') dt'' \right\rangle.$$

Using the fact that $\langle \underline{v}(t+s) \cdot \underline{v}(s) \rangle$ is independent of s leads to

$$\langle |\underline{r}(t)|^2 \rangle = 2t \left\{ \int_0^t \langle \underline{V}(s) \cdot \underline{V}(0) \rangle ds - \frac{1}{t} \int_0^t \langle \underline{V}(s) \cdot \underline{V}(0) \rangle s ds \right\}.$$

This relates $\langle \underline{r}^2 \rangle$ to the vacf. At long times the second term is negligible, and

$$\langle r^2 \rangle = 2t \int_0^t \langle \underline{V}(s) \cdot \underline{V}(0) \rangle ds.$$

Also, if t is large enough for the vacf to have fallen to zero, the integral is constant

i.e.
$$\lim_{t \rightarrow \infty} \langle |\underline{r}(t) - \underline{r}(0)|^2 \rangle = 2t \int_0^\infty \langle \underline{V}(s) \cdot \underline{V}(0) \rangle ds$$

$$\lim_{t \rightarrow \infty} \langle |\underline{r}(t) - \underline{r}(0)|^2 \rangle = 6Dt$$

therefore
$$D = \frac{1}{3} \int_0^\infty \langle \underline{V}(s) \cdot \underline{V}(0) \rangle ds$$

$$D = \frac{k_B T}{m} \int_0^\infty Z(t) dt$$

where $Z(t)$ is the normalised vacf

$$Z(t) = \frac{1}{N} \langle \underline{V}(t) \cdot \underline{V}(0) \rangle / \langle \underline{V}^2 \rangle.$$

At $t = 0$ $Z(t)$ is equal to one and decays to zero as time advances and memory of the initial conditions is lost.

Other transport properties can also be calculated such as the electrical conductivity σ

$$\sigma = \frac{e^2}{3V k_B T} \int_0^\infty J(t) dt \quad \text{where } e \text{ is the electronic charge.}$$

This can be calculated from the autocorrelation function of the electrical current $M(t)$

$$M(t) = \left\langle \sum_i q_i \underline{V}_i(t) \cdot \sum_j q_j \underline{V}_j(0) \right\rangle$$

where q is the ratio of the charge to e . In the case of shear viscosity η

$$\eta = \frac{1}{V k_B T} \int_0^\infty \langle J_{\alpha\beta}(t) \cdot J_{\alpha\beta}(0) \rangle dt \quad v = \text{volume}$$

where $J_{\alpha\beta}$ is any off diagonal element of the microscopic stress tensor

$$J_{\alpha\beta} = \sum_{i=1}^N \left(\frac{P_{i\alpha} P_{i\beta}}{m_i} + r_{i\alpha} F_{i\beta} \right)$$

where the α th Cartesian component of the position of the i th particle is $r_{i\alpha}$, the corresponding component of momentum is $P_{i\alpha}$, the α th component of total force on the i th particle is $F_{i\alpha}$.

Another correlation function of interest is the force autocorrelation function $C_F(t)$

$$C_F(t) = \frac{1}{N} \langle \underline{F}(t) \cdot \underline{F}(0) \rangle / \langle \underline{F}^2 \rangle$$

in its normalised form. This differs markedly from the vacf in that the correlation decays to zero more rapidly and it is more oscillatory, i.e. less damped.

Correlation functions which characterize rotational motion in molecular liquids are also studied. The normalised angular momentum autocorrelation function $A_J(t)$ is defined by

$$A_J(t) = \frac{\langle \underline{J}(0) \cdot \underline{J}(t) \rangle}{\langle \underline{J}^2 \rangle}$$

where \underline{J} is the angular momentum of the molecular

$$\underline{J} = \sum_a m_a \underline{r}_a \times \underline{V}_a$$

m_a , \underline{r}_a and \underline{V}_a are the mass, position and velocity of the a th atom relative to those of the centre of mass. The angular momentum autocorrelation function is sensitive to the magnitude of the anisotropy and density. Thus for the nearly spherical nitrogen molecule, the decay is monotonic at all densities [22]. Where the anisotropy is larger, the curve passes through a negative minimum indicating a high probability of reversal

of the angular momentum [50]. It has been shown that the shape of the angular momentum autocorrelation function is largely due to its change in direction rather than magnitude [50].

In the study of orientational properties the physically important first and second Legendre functions are computed through the following correlation functions:

$$C_1(t) = \langle \underline{u}_i(0) \cdot \underline{u}_i(t) \rangle$$

$$C_2(t) = \frac{3}{2} \langle | \underline{u}_i(0) \cdot \underline{u}_i(t) |^2 \rangle - \frac{1}{2}$$

where \underline{u} is a unit vector in a particular inertial axis.

A general discussion of time correlations is given by Berne and Harp [21].

A more simple though still very informative way of studying time-dependent phenomena, as shown in Chapter 5, is following the trajectories of individual particles in the computational cell.

1.7 The Aim of the Work

In the last decade the Monte Carlo and molecular techniques have provided information on the structure and dynamics of water and aqueous solutions. More recently computer simulation has been shown to be a valuable tool in the study of interfaces. In this project we adopt the molecular dynamics technique to investigate the ionic crystal-water interface so as to be able to obtain equilibrium and dynamic properties of the system.

A further understanding of hydration and solubility is of great technological importance. This interface is difficult to study experimentally due to the small number

of particles involved. It would be impossible to observe the behaviour of water molecules next to an ionic crystal at such short times by any other method than computer simulation.

The sodium chloride-water interface was simulated and changes of the lattice structure and the mechanism of the dissolution were studied.

In addition the behaviour of water next to a crystal in which the ions were not allowed to move was investigated. The structure and orientation of water at the crystal surface was looked at, and also the diffusion and other time-dependent properties of the water at this surface were calculated.

with ρ_{+} , ρ_{-} and ρ_{\pm} , the partial radial distribution functions. In ionic liquids the distance of closest approach of \pm pairs is the only important size parameter. The structure of the structure is determined by the electrostatic forces producing a charge ordering effect predicted on theoretical grounds some years ago [51]. In ionic liquids the dominant role of repulsion. At short distances is modified by the tendency to local electrical neutrality. The tendency to retain the balance of electrical neutrality makes the partial radial distribution functions persist over a much longer range than those of ρ_{\pm} . The maxima and minima of ρ_{+} and ρ_{-} coincide and are out of phase relative to ρ_{\pm} . An example of a computer species simulation of NaCl is that of Levine et al. They studied the melt at three temperatures. This work also shows that the corresponding mean square displacements of the ions $\langle r^2(t) \rangle_{+}$ and $\langle r^2(t) \rangle_{-}$ give the self-diffusion coefficients D_{+} and D_{-} . Levine and Sengers [50] also

CHAPTER 2

IONIC SIMULATION

2.1 Introduction

Woodcock and Singer [29] first applied computer simulation to the study of ionic system with the long range coulombic forces included; the Monte Carlo method was adopted to calculate the thermodynamic properties of KCl. These calculations which used a non-polarizable rigid ion model gave satisfactory predictions to these properties. This encouraged further work on simulation of ionic liquids [51-60]. Of particular interest is the resolution of $g(r)$ into g_{++} , g_{+-} and g_{--} , the partial radial distribution functions. In ionic liquids the distance of closest approach of $+-$ pairs is the only important size parameter. The remainder of the structure is determined by the electrostatic forces producing a charge ordering effect predicted on theoretical grounds some years ago [61]. In ionic liquids the dominant role of repulsion at short distances is modified by the tendency to local electrical neutrality. The tendency to attain the maximum of electrical neutrality makes the partial radial distribution functions persist over a much longer range than those of $g(r)$. The maxima and minima of g_{++} and g_{--} coincide and are out of phase relative to g_{+-} . An example of a molecular dynamics simulation of NaCl is that of Lantelme et al. They studied the melt at three temperatures. This work also shows that the corresponding mean square displacements of the ions $\langle r^2(t) \rangle_+$ and $\langle r^2(t) \rangle_-$ give the self diffusion coefficients D_+ and D_- . Lewis and Singer [60] also

calculated diffusion constants for NaCl over 22 VT points.

In the ionic simulations described above non-polarizable rigid ion models were used. The main deficiency of such work particularly for dynamical properties is the neglect of polarization. The effects of polarization are included by picturing each ion as being made up of a core connected by a spring to a shell of negative charge and zero mass. The short range potentials are taken to act between shells, to incorporate these potentials into molecular dynamics simulations. The method adopted is that for a given configuration the force on every core and shell is known from the potentials and shell parameters and hence the equations of motion can be followed. In molecular dynamics simulations the equations of motion for the cores are integrated over the time step and then shells are then allowed to relax to positions of zero force while the cores are held fixed in their new positions. Since the force on any shell depends on the positions of all the other shells the relaxation procedure must be carried out consistently, and this introduces a time-consuming inner cycle in the calculation. By allowing the shells to relax about fixed core positions non-conservation of both momentum and total energy is introduced, and in order to keep the variations in these quantities as fluctuations about steady mean values rather than drifts a time step which is slightly shorter than that used in rigid ion simulations is necessary. The procedures for relaxing the shells are by Jacucci et al. [62] and Dixon and Sangster [63]

2.2 Interionic Pair Potential

To simulate the NaCl crystal we use pairwise additive Born-Mayer-Huggins potential represented by:

$$\phi_{ij}(r) = \frac{q_i q_j}{r} + A_{ij} \exp(B_{ij}(\sigma_{ij} - r)) - \frac{C_{ij}}{r^6} - \frac{D_{ij}}{r^8}$$

with the Tosi-Fumi [64] parameters. The pair potential, $\phi_{ij}(r)$ consists of a Coulomb, short range repulsion and two dispersion terms. The full ionic values ± 1 for the charges q_i, q_j are taken and the Mayer [65] values for C_{ij}, D_{ij} the coefficients of the dipole-dipole and dipole-quadrupole dispersion energy terms. $A_{ij} = \beta_{ij}^b$ where β_{ij} are the Pauling [66,67] factors which are defined by

$$\beta_{ij} = 1 + \frac{q_i}{n_i} + \frac{q_j}{n_j}$$

where n_i, n_j are the number of electrons in the outer shell. b is a constant for all crystals and interaction types.

$B_{ij} = \frac{1}{\rho}$ where ρ is a hardness parameter which varies from crystal to crystal. σ_{ij} is the sum of the ionic radii of the particular interaction type.

Table 2.1 Parameters in the NaCl interaction potential

Inter action	σ_{ij}/m	A_{ij}/J	B_{ij}/m^{-1}	C_{ij}/Jm^6	D_{ij}/Jm^8
++	0.236×10^{-9}	42.25×10^{-21}	31.545×10^9	0.168×10^{-78}	0.8×10^{-99}
+-	0.2755×10^{-9}	33.80×10^{-21}	31.545×10^9	1.120×10^{-78}	13.9×10^{-99}
--	0.3170×10^{-9}	25.35×10^{-21}	31.545×10^9	11.600×10^{-79}	233.0×10^{-99}

In an ionic system the coulombic potential is slowly convergent, and can not be evaluated directly, it is traditionally

evaluated using an Ewald [68] summation, though it is also possible to use the P^3M method [69]. The computer program MDIONS [70] was written here, it is a rigid ion Ewald sum program for the dynamic simulation of particles. This chapter relates to MDIONS, though the P^3M program [71] which is considered computationally more economical for a large number of particles which was also used here is also discussed.

2.3 Non-Coulomb Force, Potential Energy and Virial

The non-Coulomb part of the interaction between a pair of ions belonging to species α and β respectively is represented by the pair potential

$$u_{\alpha\beta}(r) = A_{\alpha\beta} \exp[B_{\alpha\beta}(\sigma_{\alpha\beta} - r)] - C_{\alpha\beta}/r^6 - D_{\alpha\beta}/r^8.$$

In MDIONS [70] the interactions in the non-Coulomb part are considered till the cut off r_c . To make the system pseudo-infinite the simulation cube is surrounded by periodic replicas of itself. A particular particle is assumed to interact only with the nearest image of another particle, as discussed in Chapter 1.

For each pair of particles in the computational box we find \underline{r} , the vector separating the particles, apply the nearest-image transformation and evaluate the pair potential energy $u(r)$, the pair virial $r(du/dr)$ and the pair force $\underline{f} = (-du/dr)\underline{r}/r$. These terms are accumulated to give the total energy ϕ and the total virial ψ , and the force \underline{F} on each particle.

Correction terms to the total energy and virial are

added to compensate for the omitted interactions for $r > r_c$. The terms are obtained by the assumption of uniform average density at distances greater than r_c from a typical particle. If N_α is the number of particles of species α in the computational box of volume V these long range interactions are

$$\phi_{lrc} = \sum_{\alpha \leq \beta} \frac{N_\alpha N_\beta}{V} (1 - \frac{1}{2} \delta_{\alpha\beta}) \int_{r_c}^{\infty} u_{\alpha\beta}(r) 4\pi r^2 dr$$

$$\psi_{lrc} = \sum_{\alpha \leq \beta} \frac{N_\alpha N_\beta}{V} (1 - \frac{1}{2} \delta_{\alpha\beta}) \int_{r_c}^{\infty} r \frac{du_{\alpha\beta}}{dr} 4\pi r^2 dr .$$

In evaluating these expressions only the attractive r^{-6} and r^{-8} are taken into account as the exponential repulsive term is negligible except at small distances.

2.4 Coulomb Force and Energy

To take account of the Coulomb forces in the system we use techniques developed for performing lattice sums in ionic crystals, the computational box of the simulation corresponding to the unit cell of the lattice. The value of the electrostatic potential in such an infinite point charge lattice is not unique; the intrinsic potential $V_i(\underline{r}_i)$ at the position \underline{r}_i of a charge i is

$$V_i(\underline{r}_i) = V_d(\underline{r}_i) - V_e(\underline{r}_i) \\ = \sum_{\underline{h}}' \sum_j \frac{1}{|\underline{r}_i - \underline{r}_j + \underline{h}|} - \frac{2\pi}{3L^3} \left(\sum_j q_j \underline{r}_j \right)^2 \quad (1)$$

where the first term $V_d(\underline{r}_i)$ is the lattice site energy obtained by directly summing the terms this is called the direct energy. The sum over \underline{h} is over images of the

unit cell

$$\underline{h} = (-l\underline{L} + m\underline{M} + n\underline{N})$$

where (l,m,n) are integers and $\underline{L},\underline{M},\underline{N}$ are vectors defining the sides of the computational cell. The sum over j is over all particles in the cell, and $j = i$ is excluded when $\underline{h} = \underline{0}$. Because of the long range nature of the Coulomb forces the sum over \underline{h} is conditionally convergent so that the order of summation is important; the lattice is assembled in units of spherical cells of image cells, as in the case of de Leeuw, Perram and Smith [72]. Each cell has an instantaneous dipole and the expanding sphere is polarised. The term V_e , the extrinsic potential, acts as a depolarisation correction to V_d to give V_i , the latter being independent of the choice of unit cell. This makes V_i a more reasonable choice than V_d for the simulation of liquids where in reality there is no long range periodicity, and hence no polarisation. de Leeuw, et al. [72] have shown how to use the direct potential but add on a term corresponding to a dielectric continuum ϵ' surrounding the sphere of repeated unit cells, where ideally ϵ' should be chosen to match the actual dielectric constant of the simulated system. This gives the potential

$$V_{LPS} = V_i + \frac{2\pi}{3L^3} \left(\frac{3}{2\epsilon'+1} \right) \left(\sum_j q_i \underline{r}_j \right)^2.$$

The use of V_i hence corresponds to the choice of $\epsilon' = \infty$, i.e. the sphere of unit cells is surrounded by a perfect conductor. The use of V_{LPS} instead of V_i does not effect the structural and local dynamical properties of the system [73]. For example the use of V_{LPS} with $\epsilon' = 1$, corresponds to surrounding the system with a

vacuum, and hence leads to a zero conductivity. MDIONS uses the conventional choice of V_i , see below, but could easily be modified to use V_{LPS} to give further study to these effects.

In the conventional Ewald method, which we use in MDIONS, V_i is not calculated from equation (1) because of the slow convergence of the direct sum. Instead the following method is used. We imagine the system of point charges in the cell specified by the charge density

$$\rho(\underline{r}) = \sum_i q_i \delta(\underline{r} - \underline{r}_i)$$

to be replaced by two distributions

$$\rho_1(\underline{r}) = \sum_i q_i [\delta(\underline{r} - \underline{r}_i) - d(\underline{r} - \underline{r}_i)]$$

$$\rho_2(\underline{r}) = \sum_i q_i (d(\underline{r}_1 - \underline{r}_1) - L^{-3})$$

where $d(\underline{r})$ is some spherical distribution of non-zero but limited range whose integral is equal to one over all space. Taking a Gaussian representation for $d(r)$

$$d(r) = \alpha^3 \pi^{-3/2} \exp(-\alpha^2 r^2)$$

leads to the conventional Ewald sum [29]. This is a mathematical transformation which is equivalent to the addition of mutually cancelling charge distributions, whereby the non-convergent Coulomb sum is converted into two rapidly convergent sums.

In $\rho_1(\underline{r})$ the second term is now a Gaussian charge distribution of half width α^{-1} and of opposite sign, centred on each ion. $\rho_2(\underline{r})$ consists of an identical Gaussian charge distribution of the same sign as the ion, and of a uniform normalised charge distribution of opposite sign.

The Gaussian distributions are $\rho_1(\underline{r})$ and $\rho_2(\underline{r})$ cancel each other, as do the uniform distributions corresponding to equal numbers of positive and negative ions. The potentials of $\rho_1(\underline{r})$ and $\rho_2(\underline{r})$, however, converge rapidly: the former because the potentials of the point charge and the Gaussian cancel each other at large distances; the latter, because the integration of the Poisson equation for $\rho_2(\underline{r})$ leads to a convergent Fourier series. Thus the potential due to ρ_1 is evaluated in a direct, real space, sum and the potential due to the ρ_2 distribution is evaluated as a sum in reciprocal space.

The potential for the real space part of the total energy is

$$\phi^{RL} = \frac{1}{2} \sum_i q_i \sum_j q_j \left[\sum_{\underline{h}} \frac{\text{erfc}(\alpha r)}{r} - \frac{2q_i \alpha}{\sqrt{\pi}} \right]; \text{ where } \text{erfc}(x) = \frac{2}{\pi} \int_x^\infty e^{-t^2} dt$$

$r = |\underline{r}_i - \underline{r}_j + \underline{h}|$, and $i = j$ is excluded when $\underline{h} = \underline{0}$. We choose the parameter α so that the complementary error-function term $\text{erfc}(\alpha r)$ decreases rapidly enough with r to make it a good approximation to take only nearest images in the sum over \underline{h} and for values of r greater than r_c to be neglected. The sum then becomes

$$\phi^{RL} = \sum_{j \neq i} q_i q_j \frac{\text{erfc}(\alpha r)}{r} - \sum_i q_i^2 \frac{\alpha}{\sqrt{\pi}}$$

where now $r = |\underline{r}_i - \underline{r}_j|$ but with the application of the nearest image transformation and cut-off so that the pair sum in the first term, and the corresponding pair forces, can be evaluated along with the non-Coulomb interactions. The second term is just an additive constant, the self energy of the charge distributions of ρ_1 . Computationally we evaluate the error-function complement by means of a polynomial exponential approximation [74].

The reciprocal-space part of the energy of the system is

$$\phi^{RC} = \sum_{\underline{k} \neq \underline{0}} A(\underline{k}) \sum_i q_i \sum_j q_j \cos |\underline{k} \cdot (\underline{r}_i - \underline{r}_j)| \quad (2)$$

where $\underline{k} = 2\pi(l/L, m/M, n/N)$

and

$$A(\underline{k}) = \frac{2\pi}{LMN} \frac{\exp(-|\underline{k}|^2/4\alpha^2)}{|\underline{k}|^2}$$

In the case of the cubic box $L = M = N$ but the equations are kept general so that it is easy to adapt to a non-cubic system, see Chapter 4.

The double sum over ij in (2) can be converted to a single sum, which written in complex notation is

$$\phi^{RC} = \sum_{\underline{k}} A(\underline{k}) \left| \sum_i q_i e^{i\underline{k} \cdot \underline{r}_i} \right|^2.$$

The corresponding force in particle i is

$$\underline{F}_i^{RC} = -q_i \sum_{\underline{k} \neq \underline{0}} \underline{k} A(\underline{k}) 2\text{Im}\{e^{-i\underline{k} \cdot \underline{r}_i} \sum_j q_j e^{i\underline{k} \cdot \underline{r}_j}\}.$$

The reciprocal space sums are rapidly convergent, and a spherical cut off in k space is applied, so that a sum over \underline{k} becomes a sum over l, m, n with $(l^2 + m^2 + n^2) \leq k_{\text{max}}^2$. The computing time is halved by the use of the inversion symmetry of ϕ_{RC} and \underline{F}_i under $\underline{k} \rightarrow -\underline{k}$. The balance between accuracy and computing time of the Coulomb calculation is controlled by the parameter α and k_{max}^2 . A larger value of α means that the real space sum is more rapidly convergent. In practise we choose α to give good convergence at the cut-off radius r_c determined by the requirements of the non-Coulomb calculation. The value of k_{max}^2 is

then chosen to optimise the reciprocal space calculation.

There is no separate calculation of the Coulomb virial in MDIONS [70] because this is just the negative of the Coulomb potential energy: for Coulomb forces we have

$$u(r) = \frac{q_i q_j}{r}$$

$$f(r) = - \frac{du}{dr} = \frac{q_i q_j}{r^2}$$

and therefore the Coulomb virial is equal to the negative

$$\psi(r) = \frac{rd u}{dr} = - u(r)$$

of the Coulomb potential energy.

2.5 The P³M Method

There is an alternative method of evaluating the Coulomb sums, the P³M method [69]. This is a combination of traditional particle-particle, PP, methods and also particle-mesh, PM, methods. The P³M program [71] was used to simulate central-force water [75] using the IBM 360/195 computer this will be discussed in Chapter 3.

In the P³M program the total force \underline{F}_i , on a particle i is calculated in two parts

$$\underline{F}_i = \underline{F}_m + \underline{F}_{sr}$$

The mesh part of the force \underline{F}_m , is long range and smoothly varying. It can be approximated by a particle-mesh force calculations. The short range \underline{F}_{sr} is rapidly varying, having non-zero contributions only from those particles within a radius r_c of particle i . It is calculated by

summing over the particles within a sphere of radius r_c surrounding particle i . To calculate the short range part of the force efficiently the program employs a linked list [76] technique.

In the P^3M method the charges are assigned to a charge/potential mesh. The charge/potential mesh is a regular lattice of $m \times m \times m$ mesh points covering the whole of the volume of the calculation box. For this assignment a triangular shaped cloud charge assignment scheme [77] is used. The electrostatic potential on each mesh point is found rapidly by a numerical solution of Poisson's equations, with periodic boundary conditions using a Green's function approach and Fourier transform techniques [69,78] and a fast Fourier transform algorithm [79]. The potential obtained in this way is that due to all the charges and their images. These features lead to an execution time proportional to N compared with N^2 in conventional molecular dynamics.

2.6 MDIONS on the Cray-1

The work we have done with MDIONS has been mainly on the Cray-1 computer [80]. The Cray-1 is a vector processing computer. A vector processor differs from a conventional serial computer such as the CDC 7600 or IBM 360/195 by processing a set of operations called vectors, with one instruction.

To take full advantage of the Cray-1 in molecular dynamics there are a few changes [81] that need to be made to the conventional molecular dynamics program. The force calculation takes up to 98% of the computing time in

molecular dynamics. It can be regarded as an operation which obtains a vector of forces $\underline{F}(i)$ from a vector of positions $\underline{r}(i)$, this is amenable to vectorisation. In the Fortran program this would be represented by three arrays (vectors) FX, FY, FZ .

Pair forces \underline{f}_{ij} are vectorised in a double loop over i and j particles. The nearest image transformation ensures interactions with j particles are taken within a cube centred on the current particle i . The pair force is evaluated if the separation between i and the nearest image j is within the cut-off distance. The effect of the nearest image transformation together with the cut-off is to take interactions within a sphere centred on the cut-off. In molecular dynamics we exclude interactions outside the cut-off with a "If..... go to" statement but this statement would inhibit vectorisation, so it is left out, and for cubic computational box we are therefore using a cubic cut-off.

A further inhibition to vectorisation in the force loop is provided the accumulation

$$\underline{F}(i) = \underline{F}(i) + \underline{f}_{ij}$$

in the double loop $\underline{F}(i)$ would be treated as a scalar quantity by the inner loop. To overcome this, the pair forces are stored in an auxiliary array $FI(i)$. The array is summed and the total added to $\underline{F}(i)$ in a separate operation outside the inner loop using the `SSUM` function. This is a Cray-1 Fortran compiler (CFT) library function which sums the elements of an array.

The accumulation of potential energy and virial terms also uses the SSUM function. Also, in order to get accurate results for the potential energy and virial long range corrections are added for the short range interactions, due to the use of a cut-off. These corrections are easily calculated for the case of a spherical cut-off. On the Cray, it is convenient to set the pair interactions to zero for pairs separated by distances outside the cut-off. This is done by using the CFT utility function (called a vector-merge function) CVMGP. This does not inhibit vectorisation and does not increase the execution time. All that is required to perform this operation is the instruction:

```
RSQR = CVMGP(RSQR,0.0,RSQR-RCSQR)
```

where $RSQR = 1./(\text{RX}*\text{RX} + \text{RY}*\text{RY} + \text{RZ}*\text{RZ})$ as defined by the separation of particles and the nearest image convention and $RCSQR = 1./\text{RCUTSD}$ where RCUTSD is the square of the dimensionless cut-off, as in a conventional molecular dynamics force routine.

Another useful point is the application of the nearest image transformation. Normally we use internal units between -1 and +1 for the particles in the box. So in Fortran language the nearest image transformation is programmed as

```
RX = X(I) - X(J) - 2*INT(X(I) - X(J))
```

with similar expressions for the y and z components. This holds no problem for vectorisation but the Cray cannot yet perform such integer multiplications. The CFT compiler would perform this as a floating point multiplication which is a slow operation. It is therefore

presently faster to write the above Fortran statement as

$$RX = X(I) - X(J) - INT(X(I) - X(J)) - INT(X(I) - X(J)).$$

These changes make the program faster by a factor of more than two than the unvectorised version on the Cray-1, which is already much faster than on the most powerful of the previous generation of computers. In a system of 108 NaCl molecules the short range part of the force routine when vectorised executes at 0.074s per step compared with 0.394s on the CDC 7600, an improvement factor of about five and a half. The long range part of the Coulomb interaction executes at 0.041s compared with 0.370s on the CDC 7600.

2.7 Applications of MDIONS

The MDIONS [70] program applies the molecular dynamics method to ionic liquids or solids. We mentioned above that it has been used in the simulation of NaCl. In Chapter 3 we apply the program to simulate liquid water and also compare the Ewald and P^3M methods for this system. Chapter 4 describes how MDIONS has been adopted to the study of non-cubic systems and we give results for an ionic crystal-vacuo interface simulation. Chapter 5 and Chapter 6 uses MDIONS in the simulation of the ionic crystal-water interface.

CHAPTER 3

COMPUTER SIMULATION OF WATER

AND AQUEOUS SOLUTIONS

3.1 Introduction

Since the proposal of a three-charge model by Bernal and Fowler [82] fifty years ago, the representation of water molecule interactions by point-charge attractions and repulsions has provided a flexible framework for the theoretical study of water. Neutron diffraction studies on ice [83] confirmed Bernal and Fowler's and also Pauling's [84] beliefs that water molecules maintain their identity in condensed phases with very little distortion of their molecular geometry. Other point-charge models that have figured in the development of a statistical mechanical theory of water are the ones of Verwey [85], Rowlinson [86] and Bjerrum [87]. In 1969 Barker and Watts [88] showed the feasibility of computer simulation in the study of water by a Monte Carlo simulation with the four-point-charge model derived by Rowlinson. In 1971 Rahman and Stillinger [28] produced their remarkable paper on water; applying the molecular dynamics method they obtained detailed results of the structure and dynamics of liquid water. They used the Ben-Naim Stillinger (BNS) model [89] in their work. The BNS model is an effective pair potential for water i.e. terms higher than pair interactions are incorporated in an approximate manner into the pair potential. Section 3.2 describes a few of the important models that have evolved since the BNS model.

3.2 Water Models

3.2.1 ST2 Water

The ST2 model [90] is essentially a revised version of the BNS model, in which there are four centres, see Fig. 3.1. The potentials for the BNS and ST2 models consist of a LJ component plus a modulated Coulomb term for the 16 pairs of point-charges, the pair potentials for the atom-atom portions are:

BNS:

$$V_{OO} = 4.87230 \times 10^{-4} \left[(5.32903/R_{OO})^{12} - (5.32903/R_{OO})^6 \right]$$

$$V_{OH} = V_{HH} = 0.0.$$

ST2:

$$V_{OO} = 4.826364 \times 10^{-4} \left[(5.85815/R_{OO})^{12} - (5.85815/R_{OO})^6 \right]$$

$$V_{OH} = V_{HH} = 0.0$$

where energies are given in Hartree and distances in bohr.

Charges interacting through Coulomb's law:

BNS $1 = 1\text{\AA}$

ST2 $1 = 0.8\text{\AA}$

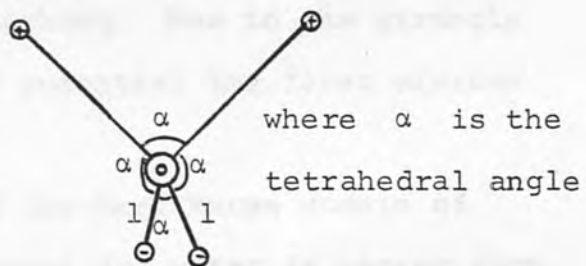


Figure 3.1 The point-charge models employed for the BNS and ST2 models.

The major difference between the models is that in the ST2 model charge assymetry has been introduced by changing 1 to 0.8\AA . The BNS model consists of a LJ function between oxygen pairs with the constant for neon (water and

neon are isoelectronic closed-shell systems) and a modulated four-point-charge model in which the two positive charges (+0.19e) represent the hydrogen atoms and the two negative charges (-0.19e) represent the lone-pair positions. The charge interaction term also has a switch function

$$S(R_{OO}) = 0 \quad 0 > R_{OO} > R_L$$

$$S(R_{OO}) = (R_{OO} - R_L)^2 (3R_u - R_L - 2R_{OO}) / (R_u - R_L)^3 \quad R_L > R_{OO} > R_u$$

$$S(R_{OO}) = 1 \quad R_u > R_{OO}$$

BNS: $R_u = 6.02388$ bohr $R_L = 3.85107$ bohr

ST2: $R_u = 5.91239$ bohr $R_L = 3.80969$ bohr

which switches it out on close approach of the charges to prevent an electrostatic catastrophe when opposite charges come into coincidence.

The defects of the BNS potential are principally that $g_{HH}(r)$ shows appreciable amplitude at distances less than the intramolecular H-H separation and that structure in $g_{OO}(r)$ around 3.5\AA is lacking. Due to the strongly tetrahedral nature of the BNS potential the first minimum in $g_{OO}(r)$ is too deep.

The ST2 model is one of the best known models of water. The structure it predicts for water is better than the BNS model but it still predicts an enhanced tetrahedral nature when compared to experiment [91]. The ST2 model does not predict the second virial coefficient of steam well over a range of temperatures [92]. The model interestingly predicts a density maximum at $\sim 20^\circ\text{C}$ (c.f. reality 4°C). A nice picture of water molecules continually breaking and

remaking highly strained hydrogen bonds which themselves form a roughly tetrahedral network is presented in an early paper with ST2 water [93].

3.2.2 CI Model

Popkie et al. [94] obtained the Hartree-Fock energies and the pair interaction energies for a discrete set of configurations, they used 190 configurations of the water dimer. In addition 26 points close to the absolute minimum energy configurations were calculated with a larger basis set yielding energies close to the Hartree-Fock limit. They then put forward an analytical expression for the pair potential by numerically fitting the 216 points to a four-centre point-charge model of the molecule. The results obtained were improved by a configuration interaction (CI) method [95] giving a more accurate representation of the quantum mechanical potential surface.

The interaction potentials for the atom-atom portions:

$$V_{OO} = 1864.27 \exp(-2.75311 R_{OO})$$

$$V_{OH} = 2.68445 \exp(-1.43979 R_{OH}) - 0.675342 \exp(-1.14149 R_{OH})$$

$$V_{HH} = 0.662712 \exp(-1.29998 R_{HH})$$

charges interacting through Coulomb's law

$$q = 0.7175e \quad \text{on each H atom}$$

$$q = 1.435e \quad \text{on H-O-H bisector } 0.4869862 \text{ bohr from the O atom}$$

Energies are given in Hartree and distances in Bohr.

The CI model gives very good agreement between $g_{OO}(r)$ and the distribution obtained by x-ray work [91] (the oxygen

being the main contributors to x-ray scattering patterns). The agreement is a bit surprising, as many-body forces which are important in water [96] are neglected and there is not a very good agreement with the only dimer property with which it has been tested [97] the second virial coefficient of steam.

3.2.3 Watt's Model

Watt's model [98] is an empirical atom-atom potential with point-charges placed on the atoms to reproduce the observed dipole moment. The molecules are non-rigid, the vibrationally energy described in terms of an harmonic potential function. Values for the ground state vibrational energy and the other coefficients in this potential function were obtained from spectroscopic data. The intermolecular terms consist of a Born-Mayer repulsion term and the Coulombic terms obtained by fitting the dipole moment of the model to that of the isolated molecule. V_{OO} also has a switch function and V_{OH} has a Morse potential term added to it in an attempt to give some short range character to the hydrogen bond. The parameters of this model were constrained roughly to fit the lattice energy of ice and the second virial coefficient of steam.

Interaction potentials for the atom-atom part

$$V_{OO} = 2.53708 \times 10^3 \exp(-2.55593R_{OO}) - \exp\{-[(8.86896/R_{OO}) - 1]^2\} \times \\ (45.3913/R_{OO}^6 + 680.774/R_{OO}^8 + 16610.4/R_{OO}^{10})$$

$$V_{OH} = 3.28924 \times 10^{-3} \exp[-4.63030(R_{OH}/3.30702 - 1)] \times \{-4.63030(R_{OH}/ \\ 3.30702 - 1)\}^{-2}$$

$$V_{HH} = 0.489136 \exp(-1.76703 R_{HH})$$

charges interacting through Coulomb's law

$$q = 0.329447e \quad \text{on each H atom}$$

$$q = -0.658894e \quad \text{on the O atom}$$

energies in Hartree and distances in bohr.

The model does then give a very good fit to the second virial coefficient of steam. It also gives good agreement with the differential cross section for crossed molecular beams of water, even though it was not fitted to this quantity. Molecular dynamics simulation [99] has been carried out on this model with the water molecules kept rigid. The model though does not give a good $g_{OO}(r)$ when compared to the CI model, the second $g_{OO}(r)$ peak (the indication of a well defined hydrogen bounded structure) is missing. Also, $g_{HH}(r)$ shows appreciable amplitude even for r less than the intramolecular H-H distance.

3.2.4. Polarisable Electropole Model (PE)

In this model [92] the electronic charge distribution of an isolated water molecule is represented by a multiple expansion [100] using the known dipole and quadrupole moments plus a spherically symmetric LJ function. The non-pair additivity is handled by means of a classical polarisability tensor [101]. In performing the polarisation calculations, the resultant electric field acting on a given molecule was considered; this induces an electron cloud distortion quantified by the product of the field and polarisability. This polarisation gives rise to

corrections to the previously calculated fields and hence to a further change in the actual polarisation, and so on. The total polarisation is hence determined in an iterative fashion, 2-5, iterations are typically necessary to achieve the required accuracy. Once this is completed electropolar energy is evaluated over all pairs using a multipole expansion. A polarisation energy term [101] and a LJ term are added to this to obtain the total energy.

This model is computationally expensive and the $g_{OO}(r)$ shows it to give a less structured water when compared with experiment [91]. It does not, unlike the effective pair potentials, give a reasonable value for the internal energy $-6.8 \text{ Kcal mole}^{-1}$ compared to the experimental value $-9.9 \text{ Kcal mole}^{-1}$ [102], though it does give good second virial coefficients for steam for a range of temperatures.

3.2.5. Central-Force (CF) Model

In this model [75] water is treated as a simple mixture of interacting atoms. Whether the atoms combine to form molecules depends on the atom-atom interactions involved. The potential energy function describes intramolecular interactions as well as leads to the formation of the correct stable molecular species. In addition to its simplicity the model allows inclusion of vibrational modes and the possibility of ionic dissociation. The equilibrium geometry of the single molecule is both density and temperature dependent, the nuclear distortions that occur as the molecules interact provides a source of nonadditive interactions between the molecules.

The water molecule consists of three point-charges, with the centres of mass and charge coinciding. Each molecule is composed of two charges $+q$ located at the equilibrium position of the hydrogens and one charge $-2q$ located at the equilibrium position of oxygen as shown in Fig. 3.2.

$$r_{\text{OH}} = 0.9584 \text{ \AA}$$

$$\theta_{\text{HOH}} = 104.45^\circ$$

$$q = 0.32983e$$

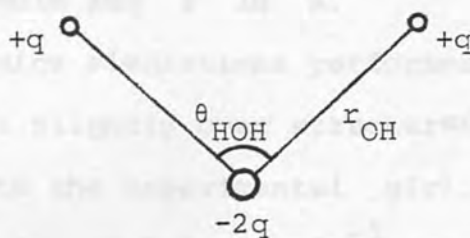


Figure 3.2 Point-charge representation of the water molecule in the central-force model.

The charge q is determined using the experimental dipole moment. The oxygen-hydrogen potential is such as to exhibit an attractive well with $V_{\text{OH}}(0.9584 \text{ \AA})$ being the absolute minimum. Short range repulsive forces and long range attractive contributions are incorporated in $V_{\text{OH}}(r)$. $V_{\text{HH}}(r)$ is chosen to consist of a Coulombic term and a term corresponding to a local minimum at $V_{\text{HH}}(1.5151 \text{ \AA})$ and also to prevent the opening for $\theta_{\text{HOH}} \rightarrow 180^\circ$. $V_{\text{OH}}(r)$ and $V_{\text{HH}}(r)$ finally incorporate the experimental modes of vibration of a water molecule. $V_{\text{OO}}(r)$ is chosen to be repulsive preventing the formation of an OH bond with the hydrogens of another molecule, but also includes forces to favour hydrogen bonding between neighbouring molecules.

The model is defined by the interactions:

$$V_{OO} = 144.538/r + 26758.2/r^{8.8591} - 0.25 \exp[-4(r-3.4)^2] - 0.25 \exp[-1.5(r-4.5)^2]$$

$$V_{OH} = -72.269/r + 6.23403/r^{9.19912} - 10/1 + \exp 40(r-1.05) - 4/1 + \exp [5.49305(r-2.2)]$$

$$V_{HH} = 36.1345 + 18/1 + \exp [40(r-2.05)] - 17 \exp [-7.62177(r-1.45251)^2]$$

where energy is in Kcal/mole and r in Å.

The molecular dynamics simulations performed show the $g_{OO}(r)$ to predict a slightly over structured nature for water when compared to the experimental $g(r)$. The total energy it predicts is -9.2 Kcal/mole⁻¹ compared to the experimental value 9.9 -Kcal/mole⁻¹, it does not though predict the second virial coefficient of steam well over the range of temperatures it has been tested with [98].

3.3 Choice of Water Model

The water models that we thought would be most useful in our study of the ionic crystal-water interface were the point-charge ST2, CF and CI models. The Watts model though attractively simple, does not reproduce the structure of water well enough and the PE model is computationally too expensive to be considered. ST2, CF and CI all reproduce the structure and properties of water well with the CI model giving the best structure. The CI model takes no account of non-pair-addictivity and is a four-centre model which makes it computationally more expensive than a three-centre model. The ST2 and CF models are effective potential models and hence many-body interactions are taken

into account. The ST2 model is also a four-centre model and hence computationally more expensive than the CF model. The CF model was eventually chosen as our model for water as it is fairly realistic and it is a three-centre model which makes it computationally relatively economical. The other advantage of this model is that it is unlike the ST2 and CI models a non-rigid model permitting the study of bending and stretching distortions in the strong field of the crystal ions.

A recent paper [103] has substantiated our choice of water model. In this work eight models of water were tested against the stability of various forms of ice and the CF model was found to be among the three best models, the other two were the ST2 and CI models.

3.4 Comparison of P³M and Ewald Methods

The CF model is a three-centre model with partial charges on each of the centres. The long range interaction due to the Coulombic force can be accounted for either by the Ewald summation [29] or by the P³M method [69]. In the study of the ionic crystal-water interface it is necessary to use a large number of particles in order to correctly model an interface of the salt and water and also have a sufficient bulk part to these. The P³M method has the advantage that the cycle time scales linearly with particle number N compared with N^2 in conventional simulation using an Ewald summation. The P³M program is considered more economical for large systems ($N \geq 10^3$); though this is certainly true for a constant mesh size, for a larger number of particles more mesh points would be required.

CF water was set up on the IBM 360/195 using the P^3M program. The program is at its most efficient with a cut-off $\frac{1}{4}L$ or less in the short range part of the force; a cut-off of 6\AA was applied. This cut-off is adequate since, the second $g_{OO}(r)$ peak is only at $\sim 4.5\text{\AA}$. Moreover we calculated the contribution outside this cut-off to be only 0.11KJ/mol . We therefore had a box length of 24\AA and since the P^3M is considered economical for large systems, for a unit mass density we had 462 water molecules.

It was attempted to start the simulation from a random configuration; this was also how Rahman and Stillinger had started their equilibration [28]. We found that it was impossible to equilibrate from this configuration because the strong forces present in the system led to dissociation of some of the water molecules.

In polyatomic molecules such as H_2O the fast internal vibrations are usually decoupled from the rotational and translational motions and can therefore be frozen out by introducing rigid bonds. This can be done by means of a method [104] in which the equations of motion for the individual atoms are solved subject to constraints imposed on the molecule. Initially undetermined constraint forces are added to maintain the shape of the water molecules. In water this is conveniently achieved by applying the constraints along the bond vectors. For each water molecule, labelling the atoms 1,2 and 3 we have the equations of motion plus the unknown forces

$$\underline{r}_1^{n+1} = \underline{r}_1^n + \underline{v}_1^{n+\frac{1}{2}} + \underline{F}_1/m_1 + \frac{1}{m_1} \lambda_{12} (\underline{r}_1^n - \underline{r}_2^n) + \frac{1}{m_1} \lambda_{13} (\underline{r}_1^n - \underline{r}_3^n)$$

$$\underline{r}_2^{n+1} = \underline{r}_2^n + \underline{v}_2^{n+\frac{1}{2}} \Delta t + \left(\frac{F_2}{m_2} + \frac{1}{m_2} \lambda_{21} (\underline{r}_2^n - \underline{r}_1^n) + \frac{1}{m_2} \lambda_{23} (\underline{r}_2^n - \underline{r}_3^n) \right) \Delta t^2$$

$$\underline{r}_3^{n+1} = \underline{r}_3^n + \underline{v}_3^{n+\frac{1}{2}} \Delta t + \left(\frac{F_3}{m_3} + \frac{1}{m_3} \lambda_{31} (\underline{r}_3^n - \underline{r}_1^n) + \frac{1}{m_3} \lambda_{32} (\underline{r}_3^n - \underline{r}_2^n) \right) \Delta t^2$$

where the λ 's are unknown. To constrain we use

$$(\underline{r}_j - \underline{r}_i)^2 = d_{ij}^2 \quad \text{where } d_{ij} \text{ is the constrained distance.}$$

This leads to three simultaneous quadratic equations for three unknown λ values necessary for the imposed constraints along the bonds. These equations are then solved simultaneously by a method of linearising and iterating. An alternative method [105] is also available using a program called SHAKE, this is an iterative method that considers all constraints in succession. This requires more iterations for triatomic systems and is more suitable for larger systems.

With the constraints present the system equilibrates quite easily, and there are no additional problems when the constraints are removed. In the simulations with CF water we use a timestep of 0.25Fs to avoid a drift in the total energy. The time for each step on the IBM 360/195 using the P³M method for 462 water molecules was 2.4s.

We compared the potential energy obtained using the P³M with 462 molecules with the published results for 216 molecules with an Ewald summation [75], both simulations were at unit mass density and 300K, see Table 3.1. The potential energy by the P³M method we found to be 3% higher than the published result. This difference is significant considering the same interaction potentials were used.

The next simulation we set up with the P^3M was for CF water with now 216 molecules to see if there was a size effect present as has previously been suggested [106]. The box length was 18.62\AA and a cut-off of 6\AA was again applied and the simulation at the same density and temperature. The potential energy was very similar to the 462 molecules simulation, indicating no size effect, but still different to the published result. The $g(r)$ results, see Figs. 3.3 and 3.4 by the P^3M method for the 462 and 216 water simulations were in good agreement but they showed differences to the published $g(r)$'s. In particular the second peak for $g_{OO}(r)$ is not reproduced well compared to the published, and also the second $g_{HH}(r)$ peak is not exactly the same.

At this time the Cray-1 computer became available to us and we had by now implemented the MDIONS program [70], which has the Ewald routine, onto the Cray. It had not really been possible previously to set up CF water on a conventional computer like the CDC 7600 or IBM 360/195 with the standard Ewald routine because of the large cycle time. Simulating CF water with the MDIONS program we could now make a comparison of the P^3M and Ewald methods.

The time for each step for 216 water molecules on the Cray-1 was 0.96s. The simulation initially performed was for supercooled water at 200K, with the same box length 18.62\AA , at the same density and with a cut-off of half the box length. The agreement for the potential energy with the published results at 300K, see Table 3.1 and for the $g(r)$ see Fig. 3.5 was now good. The diffusion constant D $1.51 \times 10^{-9} \text{m}^2 \text{s}^{-1}$ was obtained both by the velocity

Fig 33

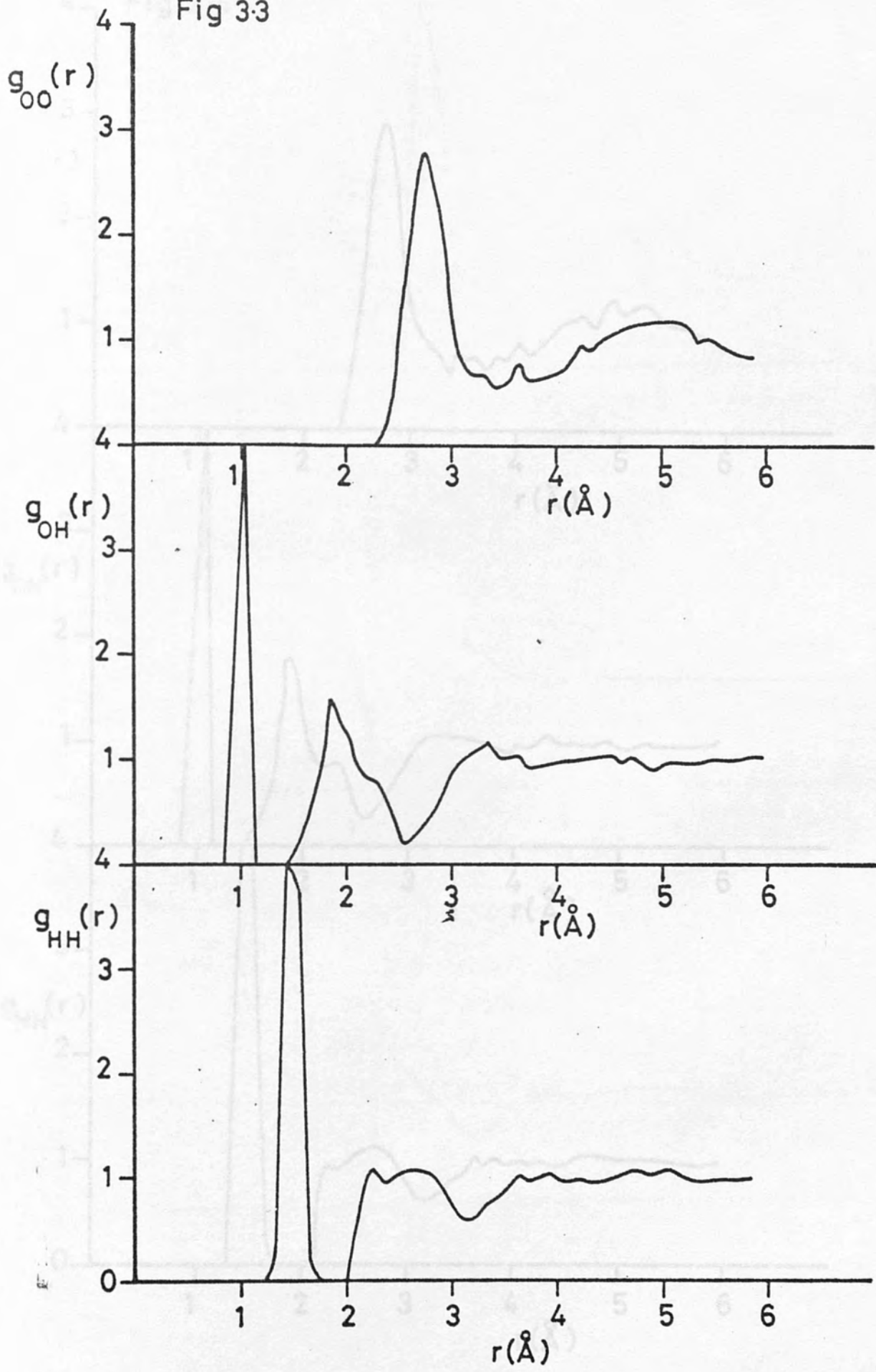


Fig. 3-4

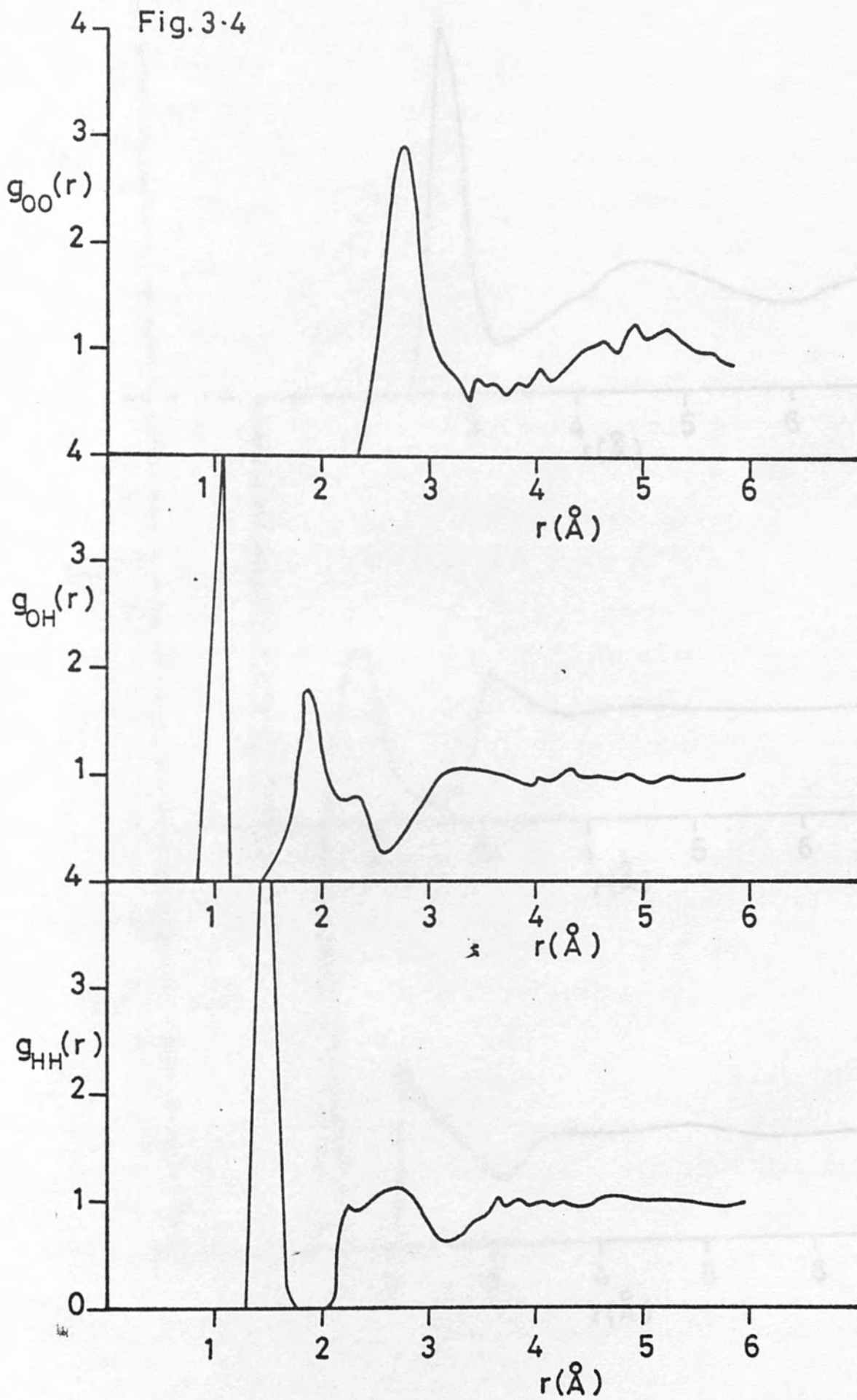
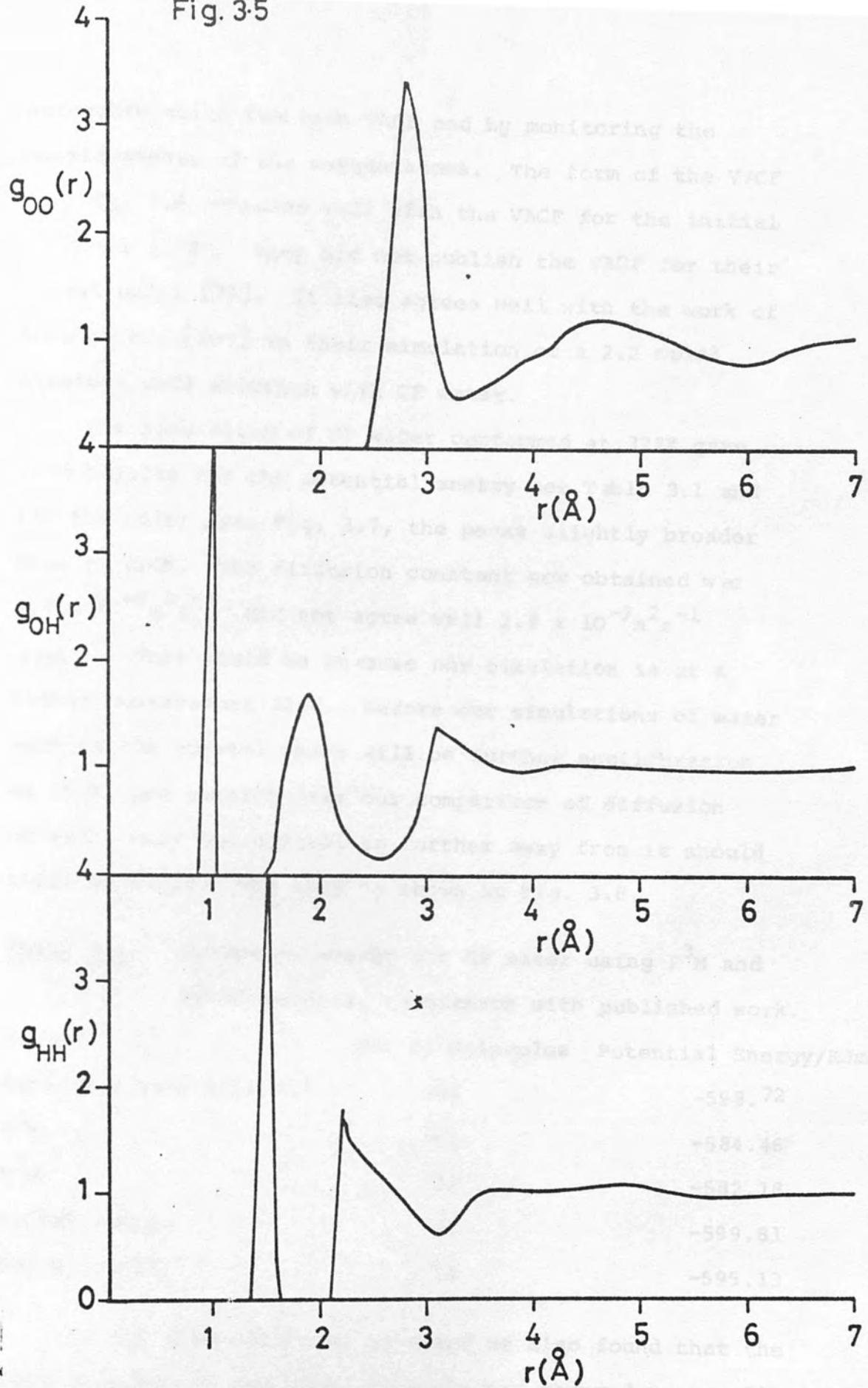


Fig. 3.5



autocorrelation function VACF and by monitoring the displacements of the oxygen atoms. The form of the VACF see Fig. 3.6 compares well with the VACF for the initial CF model [108], they did not publish the VACF for their latest model [75]. It also agrees well with the work of Bopp et al. [107] in their simulation of a 2.2 molal aqueous NaCl solution with CF water.

The simulation of CF water performed at 322K gave good results for the potential energy see Table 3.1 and for the $g(r)$, see Fig. 3.7, the peaks slightly broader than at 200K. The diffusion constant now obtained was $6.7 \times 10^{-9} \text{ m}^2 \text{ s}^{-1}$ did not agree well $2.4 \times 10^{-9} \text{ m}^2 \text{ s}^{-1}$ (75). This could be because our simulation is at a higher temperature 322K. Before our simulations of water next to the crystal there will be further equilibration at 300K, and nevertheless our comparison of diffusion of water near the crystal to further away from it should still be valid. The VACF is shown in Fig. 3.8.

TABLE 3.1 Potential energy for CF water using P^3M and Ewald methods, comparison with published work.

Method	No. of Molecules	Potential Energy/KJmol ⁻¹
Published result (Ewald)	216	-598.72
P^3M	462	-584.46
P^3M	216	-582.18
MDIONS (200K)	216	-599.81
MDIONS (300K)	216	-595.13

In our simulations of CF water we also found that the mean geometry of the water molecule had changed on equilibration from their initial values; as given in Table 3.2.

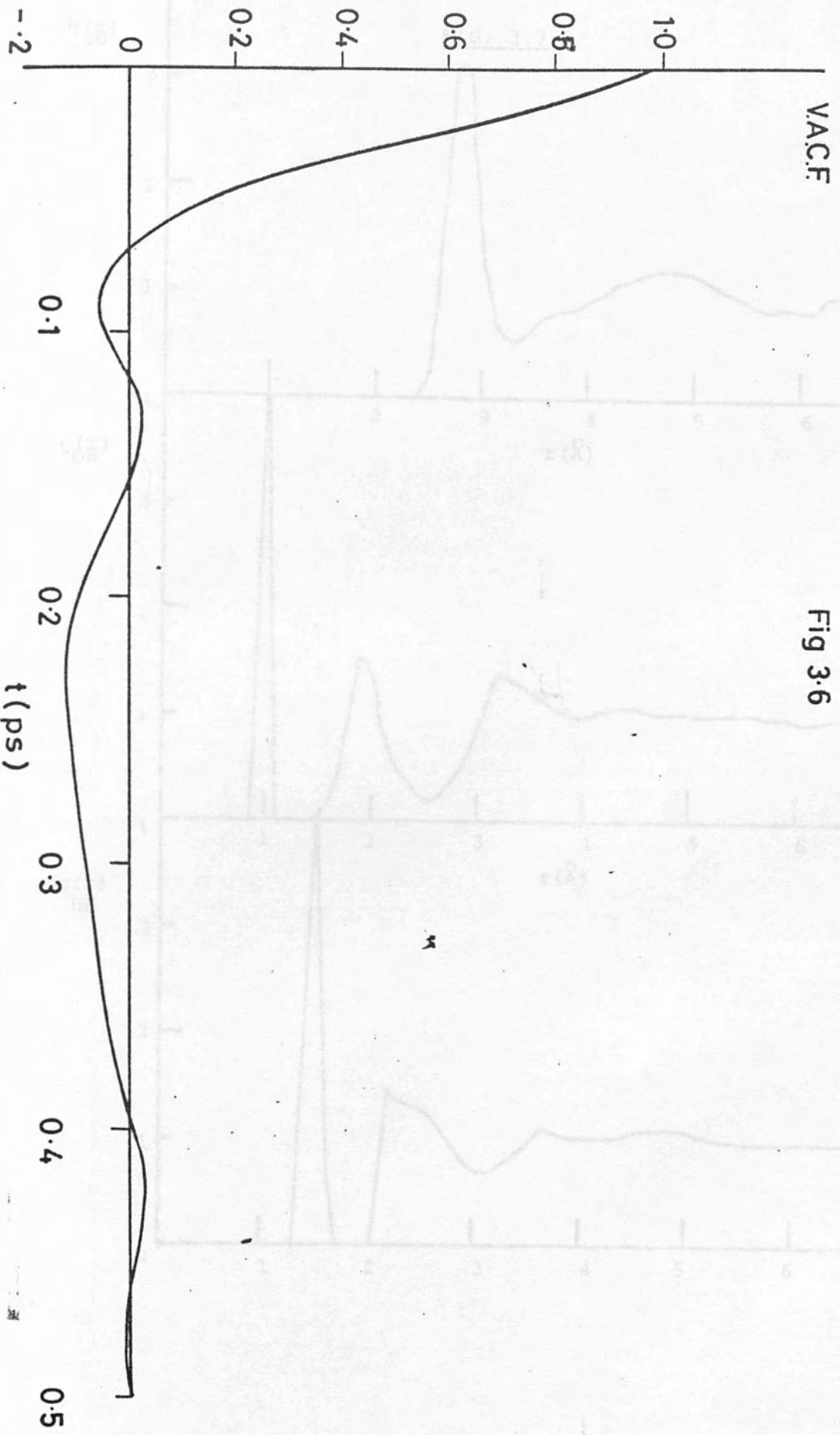
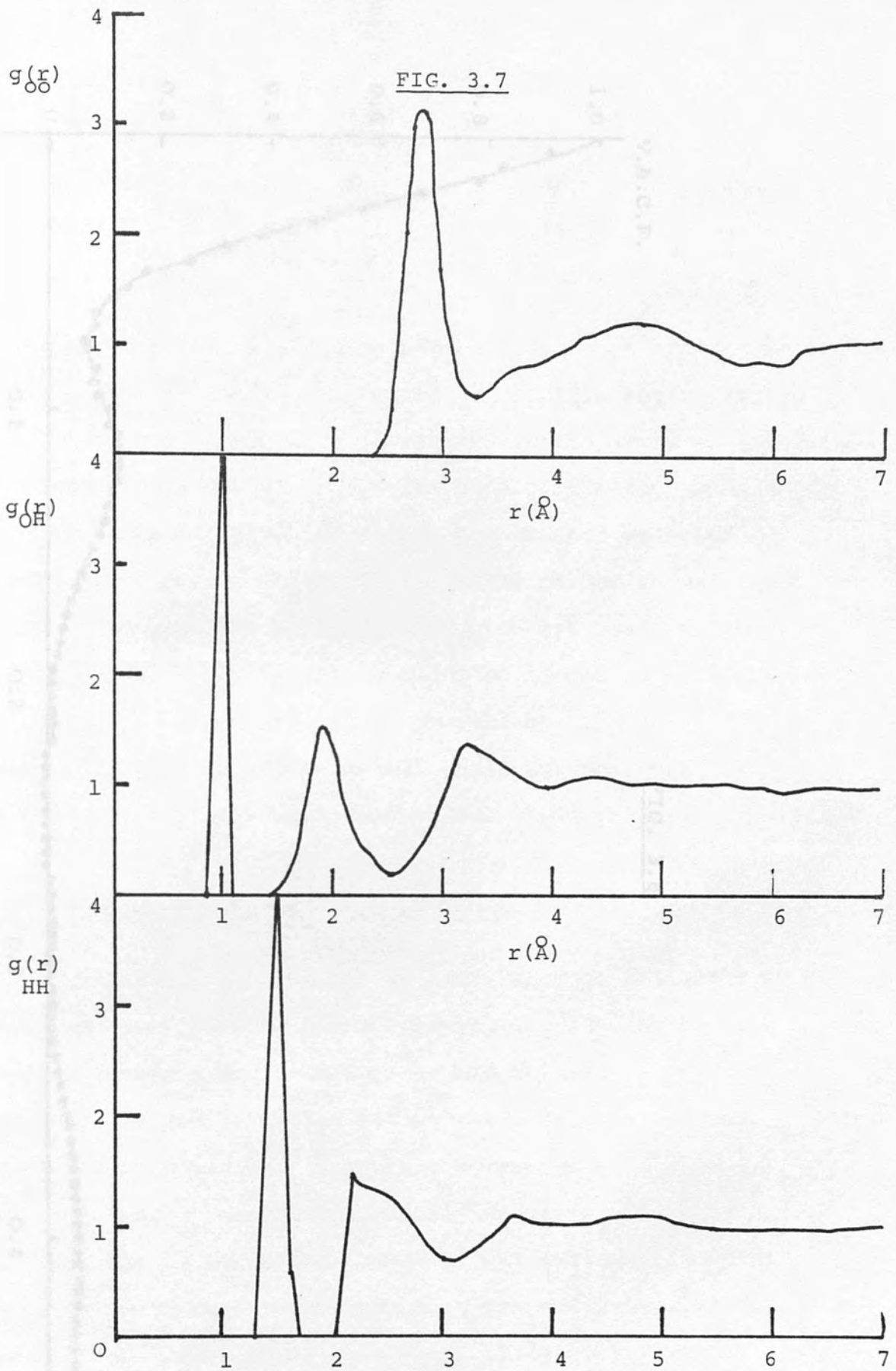


Fig 3.6



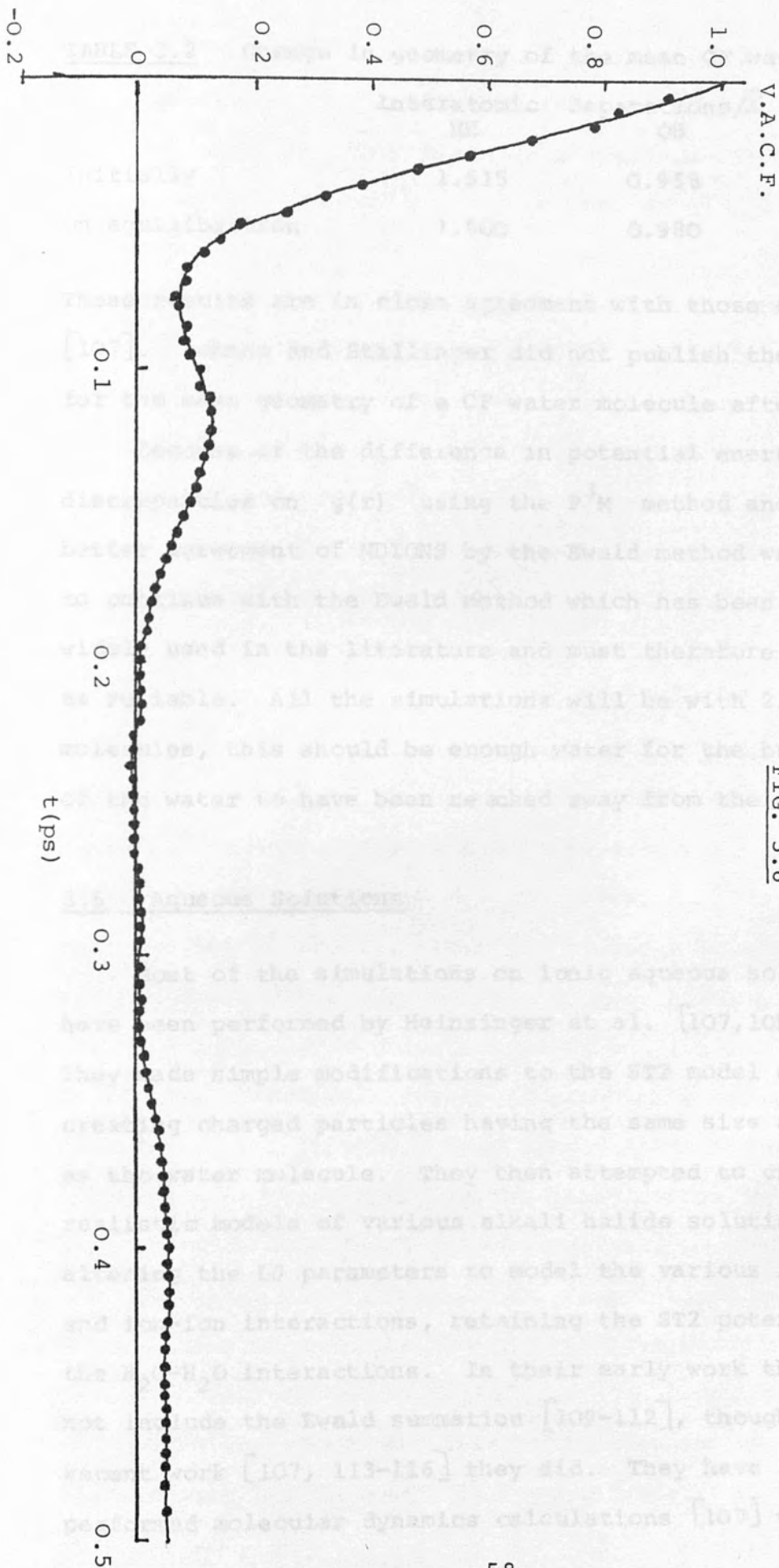


FIG. 3.8

TABLE 3.2 Change in geometry of the mean CF water molecule

	Interatomic HH	Separations/ \AA OH	Bond Angle HOH
Initially	1.515	0.958	104.45 $^{\circ}$
On equilibration	1.500	0.980	99.45 $^{\circ}$

These results are in close agreement with those of Bopp et al. [107]. Rahman and Stillinger did not publish their results for the mean geometry of a CF water molecule after equilibration.

Because of the difference in potential energy and discrepancies on $g(r)$ using the P^3M method and the better agreement of MDIONS by the Ewald method we decided to continue with the Ewald method which has been much more widely used in the literature and must therefore be regarded as reliable. All the simulations will be with 216 water molecules, this should be enough water for the bulk part of the water to have been reached away from the crystal surface.

3.5 Aqueous Solutions

Most of the simulations on ionic aqueous solutions by MD have been performed by Heinzinger et al. [107,109-116]. They made simple modifications to the ST2 model of water creating charged particles having the same size and mass as the water molecule. They then attempted to create realistic models of various alkali halide solutions by altering the LJ parameters to model the various ion-water and ion-ion interactions, retaining the ST2 potential for the H_2O-H_2O interactions. In their early work they did not include the Ewald summation [109-112], though in their recent work [107, 113-116] they did. They have also performed molecular dynamics calculations [107] with the

central force model of water with potentials for the ion-H and ion-O which were assumed to have certain form and the parameters then fixed by comparison with the ab-initio calculations of Kistenmacher et al. [117-119] see below.

In the work of Heinzinger et al. the aqueous solution of LiI, LiCl, NaCl, CsCl, CsF and NH_4Cl were simulated. Their results included the radial distribution functions for all these. Second hydration shells are reported for the lighter ions but this feature disappears for the heavier ions. Various dynamical properties were also calculated.

Extensive ab-initio Hartree-Fock SCF calculations of the ground state energies and interaction energies between a water molecule and the ions Li^+ , Na^+ , K^+ , F^- and Cl^- were undertaken by Kistenmacher et al. [117-121]. They then fitted potentials to these results. Mezei and Beveridge [122-123] have performed Monte Carlo calculations with these interaction potentials. In one study [122] they analyzed the nature and extent of hydrogen bonding for water and aqueous solutions. In another paper [123] they did Monte Carlo calculations of one ion in 215 water molecules, effectively considering infinite dilution. Clementi et al. [124-127] have also fitted interaction potentials to quantum mechanical calculations in a water molecule with complex organic molecules.

Ab-initio quantum mechanical calculations on a model system of a single ion and a single water molecule have also been carried out [128].

There have also been interesting studies on ion-ion correlations for solutions of ions in water. One is

the study of the hydrophobic bond by the simulation of the pair interactions for two non-polar solute particles in water- two Ne atoms in one case [129]; two Xe atoms in ST2 in a second [130]- and two methane molecules in CI water in a third [131]. Other examples are the simulations of the ion-ion potential for two oppositely charged hard sphere ions in a solvent made up of dipolar hard spheres [132], and the simulations of the average interionic force for two opposite charges embedded in LJ molecules and dissolved in a solvent of Stockmayer molecules [133,134]. Gosling and Singer [135] also performed molecular dynamics calculations of an ion in a dipolar (two LJ centres) solution.

The ion-water interaction potentials we have used in this project are the ones used by Bopp et al. [107] in their simulation of aqueous NaCl in CF water. The interaction potentials are :

$$V_{\text{NaO}}(r) = -15.22/r - 2.55/r^2 + 8125 \exp(-4.526r)$$

$$V_{\text{NaH}}(r) = 7.61/r + 0.52/r^2 + 6921 \exp(-7.07r)$$

$$V_{\text{ClO}}(r) = 15.22/r - 1.81 \times 10^{-2}/r^2 + 6230 \exp(-3.28r)$$

$$V_{\text{ClH}}(r) = -7.61/r - 0.28/r^2 + 181.9 \exp(-3.314r)$$

r in Å and V in units of 10^{-12} ergs. MDIONS is used with a full Ewald summation in all the work.

CHAPTER 4

COMPUTER SIMULATION OF IONIC CRYSTAL SLABS

4.1 Introduction

It is now widely accepted that processes which involve a phase change such as melting [136,137] and crystal nucleation [138] are to a large extent controlled by the behaviour of the molecules at the boundary between the two phases. It has also been suggested that electrical conductivity in alkali halides exhibits an enhancement in the surface region just below the melting temperature [139]. The thickness of the interfacial region and the time scales of the phenomena make them particularly well suited to study by the techniques of computer simulation.

In the study of surfaces the methods of Monte Carlo and molecular dynamics have largely superseded the lattice dynamics approach [140] which incorporates molecular motion by using a harmonic potential. Lattice dynamics is not suitable for surface study because of the larger amplitudes of vibration present especially at higher temperatures when the potential field is no longer harmonic. Thermal expansion and the significant anharmonicity of the molecular interactions and the appearance of defects in the interfacial region are automatically accounted for in molecular dynamics.

Previous molecular dynamics simulations of the (001) crystal-vacuum properties of LiCl, NaCl, KCl and RbCl at temperatures between room temperature and their melting points have been reported [37]. The surface properties

of the crystals were studied by two methods, firstly by coupling one side of an ionic lamina to a static ionic crystal and secondly by the use of isolated laminae, with periodic boundary conditions only in directions parallel to the surface, the x and y directions. It was found that at least ten layers were necessary to simulate an ionic surface with a sufficient amount of bulk crystal. It was also found that the static lattice method was not as good statistically as the isolated lamina method and it appeared to have a distorting effect on some of the surface properties. In addition [38] the (011) crystal-vacuum interface using isolated laminae for NaCl and KCl was examined. These were stable at room temperature contrary to previous predictions [141]. With increase in temperature the surface properties depart markedly from those of the innermost layers, and a ten layer NaCl lamina became unstable near the melting point. In addition the isolated lamina method was used to simulate molten KCl and LiCl the density of the central region of their lamina was seen to be different to that of the bulk liquid [142]. There have been several computer simulation studies on liquid-gas systems of noble gas-liquids with LJ potentials [30-33] in which layering has been reported in the liquid near the interface. To achieve smooth density profile, long simulations are required [31] as discussed in a review by Croxton [143]. The molecular dynamics method has been used to study the liquid-gas interface of molecular fluids of N_2 and Cl_2 [35] the results indicated alignment of the molecules perpendicular to the surface.

Lately there has been a growing interest in solid-

liquid interface. Toxvaerd [39] performed two sets of molecular dynamics calculations of a LJ fluid next to a surface with and without lattice structure. The lattice structure is taken to be a (111) surface of a face centred cubic crystal. The interface was found to consist of 4-5 layers, its thickness increasing continuously with pressure and its profile found to be insensitive to the structure of the solid surface. Monte Carlo calculations by Snook and van Megen [40] of a dense liquid at a solid interface also showed pronounced structuring of the fluid next to the wall. Cape and Woodcock [41] have used molecular dynamics to study the crystal-liquid interface. Other work on the crystal-melt is by Ladd and Woodcock [137] who simulated the LJ face centred cubic (001) interface at the triple point. Toxvaerd and Praestgaard [42] examined the (111) orientation at a higher temperature and pressure. Broughton et al. [43] compared the face centred cubic (111) and (001) crystal-melt interfaces. They found that for the (111) system, the density decreases, in traversing the interface, from that of the crystal to that of the liquid by reducing the number of particles per layer. The interlayer spacing remains constant throughout the interface. The same density decrease is accomplished by the (001) system in a different manner; here the number of particles per layer remains constant through the interface, but the interlayer spacing changes. The crystal layers relax in the direction perpendicular to the surface when approaching the interface.

The aim of the present project is to report a molecular dynamics simulation of an ionic crystal-water interface. Firstly though we describe in this Chapter

results for a (001) ionic crystal-vacuum interface. To simulate the crystal surface there are certain requirements that must be satisfied in order to ensure a reliable and realistic simulation of surface properties. In our simulation of the NaCl-H₂O interface periodic boundary conditions were used in all three perpendicular directions to avoid having a water-vacuum interface, as would have been necessary had we only used periodic boundary conditions in two dimensions c.f. Heyes et al. [37]. The method we have used as shown in this chapter for a crystal-vacuum interface gives results in very good agreement with those of Heyes et al. For the crystal-vacuum interface the model creates an infinite series of ionic slabs which are parallel in the xy plane but separated by vacuum gaps. Simulations have also been carried out here in which the thickness of the vacuum was doubled to show that our ionic slabs do not significantly interact across the vacuum.

4.2 Computational Details

The method of molecular dynamics is applied to a (001) NaCl-vacuum simulation. Twelve layers of 36 (6 x 6) ions (18Na⁺, 18Cl⁻ ions), giving a total of 432 ions, with free space on either side of the crystal were simulated with periodic boundary conditions in all three perpendicular directions. A Born-Mayer-Huggins potential was used with the parameters given in Chapter 2.

In bulk simulations the computational cell is usually cubic, the sides of the cell $L = M = N$ (see Chapter 2) are equal. However, for ionic slabs it is convenient to work with an orthorhombic computational box. We now have

a situation in which $L = M \neq N$, this effects the Ewald summation in particular the cubic symmetry of the coefficient $A(\underline{k})$, see Chapter 2, is lost. The program MDIONS [70] is easily adapted to this situation, as it is not written just for the cubic case but for the general case. The dimension of the side N is increased so that $N = \eta L = \eta M$, η being the factor by which the side of the computational cell is increased. In a cubic cell simulation $\alpha L = 5.6$ and $l_{\max} = m_{\max} = n_{\max} = 5$ are the maximum integer values in the reciprocal lattice sum and $k_{\max}^2 = 27$ are used, as discussed in Chapter 2. αL is chosen to give good convergence at the cut-off radius r_c . In the non-cubic case αL is maintained at 5.6. It is necessary to increase the number of reciprocal lattice vectors in the z direction, however, so as to retain equal weighting for the x, y and z reciprocal lattice components, see below.

Surfaces were introduced into the system by replacing a portion of the crystal by another phase at opposite ends of the computational cell in the z direction. In this chapter the other phase is vacuum in Chapter 5 and 6 it is replaced by water. The computational cell is shown in Fig. 4.1. This creates an infinite series of laminae which are parallel in the xy plane but separated by vacuum gaps. The computational cell as seen in Fig. 4.1 has two interfaces.

We perform simulations at 300K and 900K which is below the melting point for NaCl. In this simulation $\eta = 3$ i.e. $L = M = N = 1:1:3$. The crystal contained 12 (001) layers of 36 NaCl ions in the computational cell with a nearest neighbour distance of 2.82\AA . The slab occupied two thirds of the computational cell with surfaces disposed symmetrically about the centre of the cell, the rest of

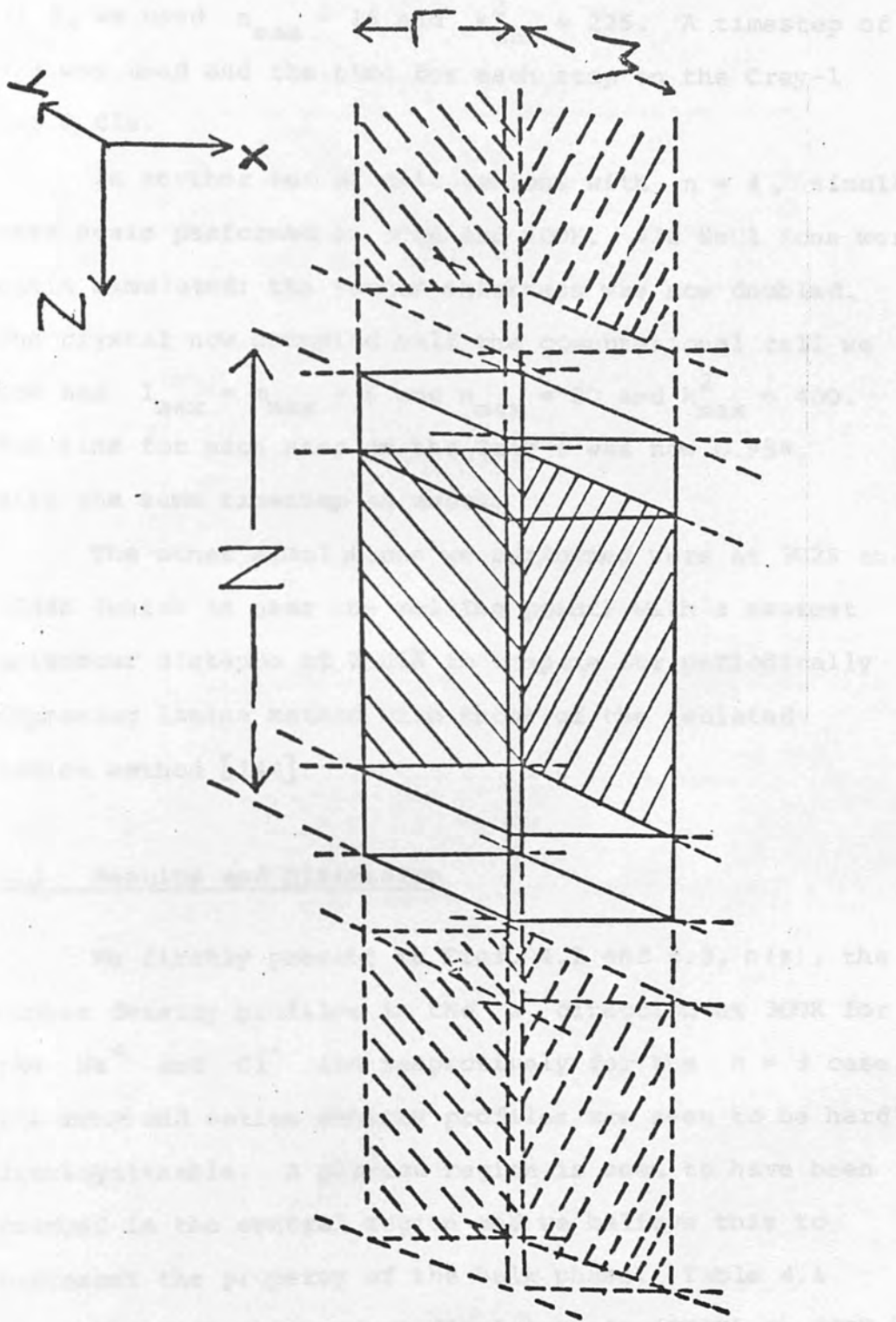


FIG. 4.1

the cell was free space. We had $l_{\max} = m_{\max} = 5$ and since the N side of the cell was increased by a factor of 3, we used $n_{\max} = 15$ and $k_{\max}^2 = 225$. A timestep of 8Fs was used and the time for each step on the Cray-1 was 0.81s.

In another set of calculations with $\eta = 4$, simulations were again performed at 300K and 900K. 432 NaCl ions were again simulated; the vacuum thickness was now doubled. The crystal now occupied half the computational cell we now had $l_{\max} = m_{\max} = 5$ and $n_{\max} = 20$ and $k_{\max}^2 = 400$. The time for each step on the Cray-1 was now 0.95s, with the same timestep as above.

The other simulations we performed were at 302K and 1034K (which is near the melting point) with a nearest neighbour distance of 2.86\AA to compare our periodically repeating lamina method with those of the isolated lamina method [144].

4.3 Results and Discussion

We firstly present in Figs. 4.2 and 4.3, $\rho(z)$, the number density profiles in the z direction at 300K for the Na^+ and Cl^- ion respectively for the $\eta = 3$ case. The anion and cation density profiles are seen to be hardly distinguishable. A plateau region is seen to have been reached in the central region and we believe this to represent the property of the bulk phase. Table 4.1 shows the root mean square displacements (RMSD) at 300K in the x, y and z directions, layers 1 and 12 are the surface layers. The RMSD in the x and y directions in which the crystal is infinite are consistent for all layers and

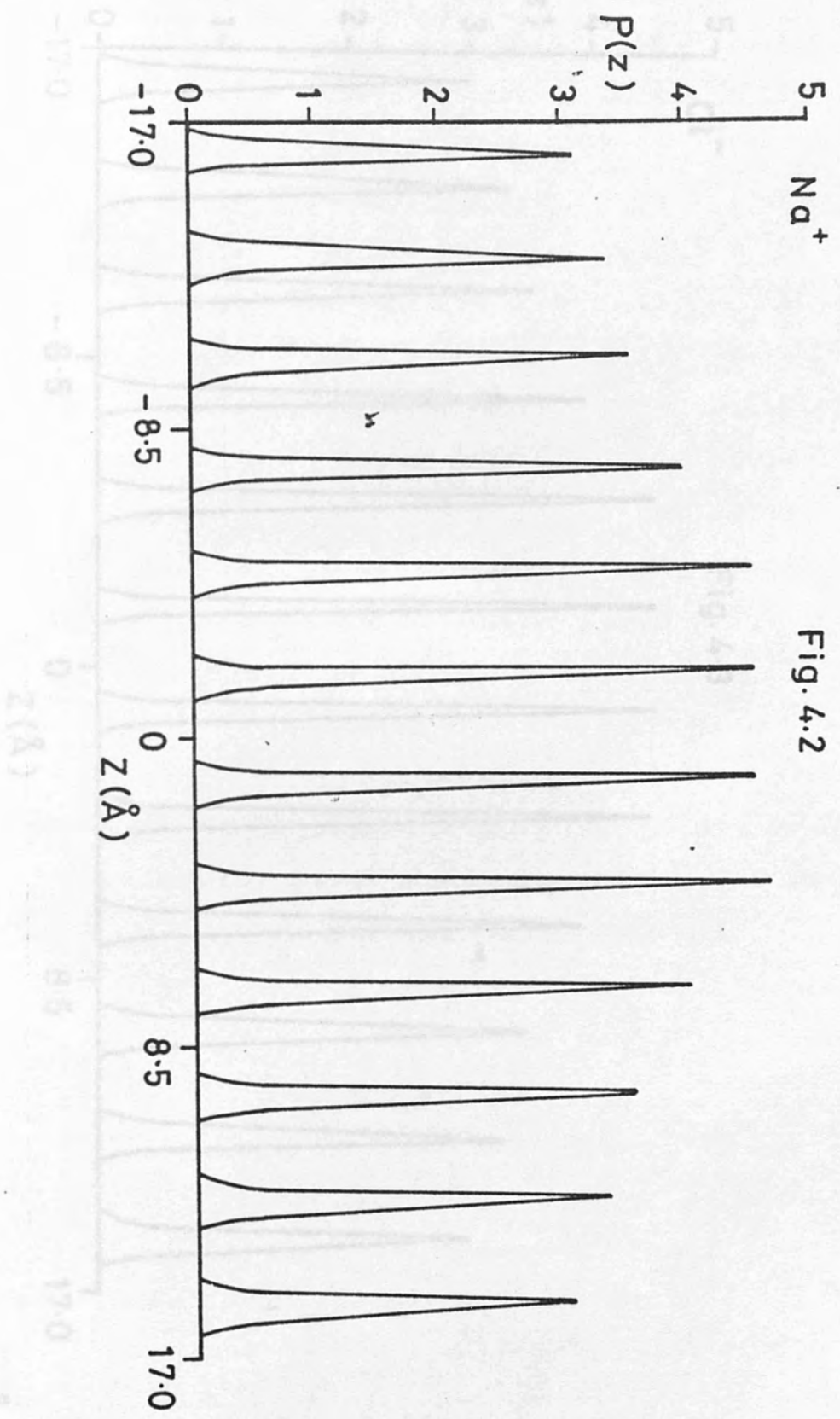


Fig. 4.2

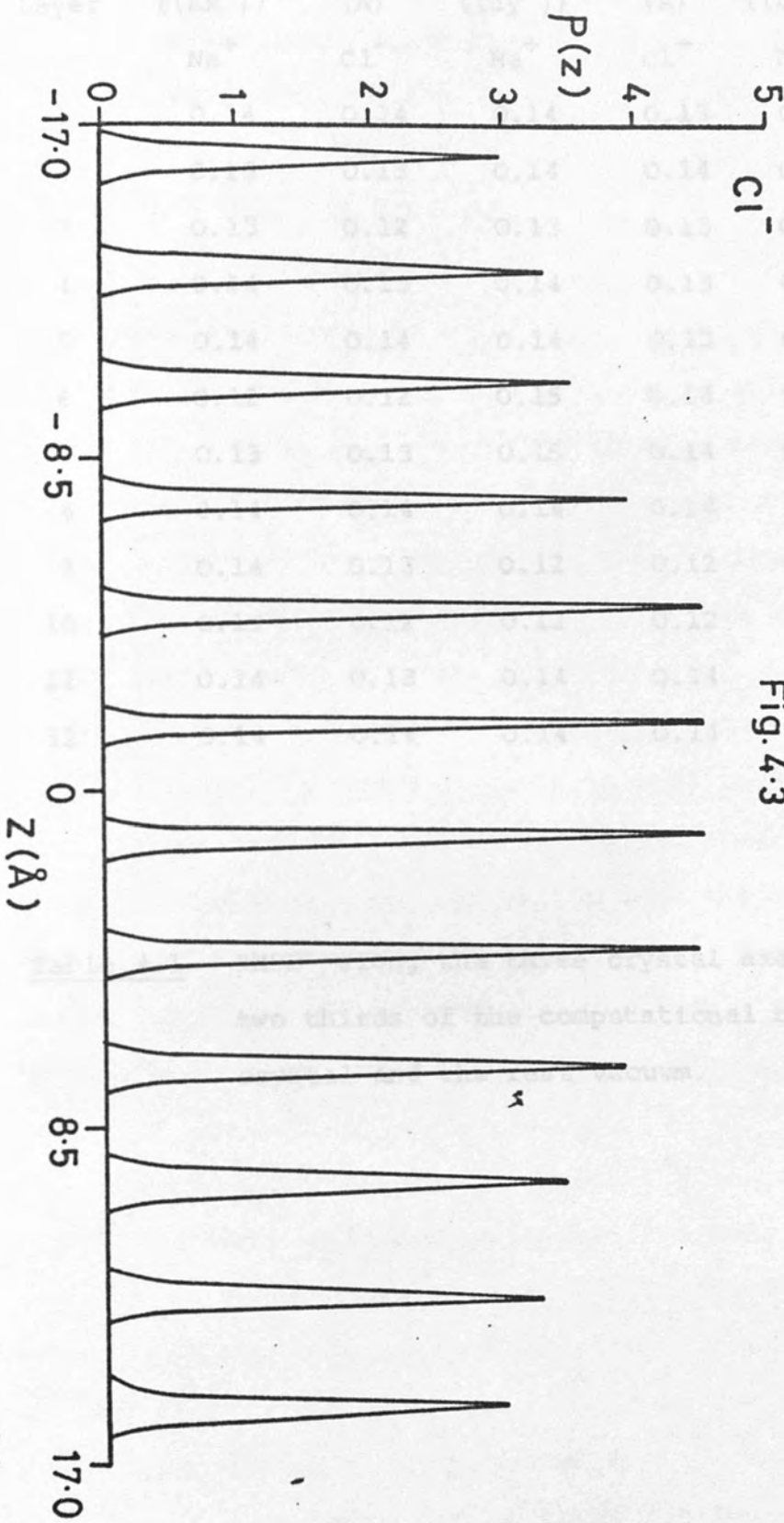


Fig. 4.3

Layer	$\overline{(\Delta x^2)}^{\frac{1}{2}}$	(Å)	$\overline{(\Delta y^2)}^{\frac{1}{2}}$	(Å)	$\overline{(\Delta z^2)}^{\frac{1}{2}}$	(Å)
	Na ⁺	Cl ⁻	Na ⁺	Cl ⁻	Na ⁺	Cl ⁻
1	0.14	0.14	0.14	0.15	0.21	0.22
2	0.13	0.13	0.14	0.14	0.19	0.19
3	0.13	0.12	0.13	0.13	0.18	0.18
4	0.14	0.13	0.14	0.13	0.16	0.15
5	0.14	0.14	0.14	0.13	0.14	0.14
6	0.12	0.12	0.15	0.14	0.14	0.14
7	0.13	0.13	0.15	0.14	0.14	0.14
8	0.14	0.14	0.14	0.14	0.16	0.15
9	0.14	0.13	0.12	0.12	0.16	0.17
10	0.13	0.12	0.12	0.12	0.18	0.17
11	0.14	0.13	0.14	0.14	0.19	0.19
12	0.14	0.14	0.14	0.14	0.22	0.21

Table 4.1 RMSD along the three crystal axes at 300K, two thirds of the computational box occupied by crystal and the rest vacuum.

the RMSD for the bulk z layers are also very similar to the x and y results showing there is a fairly uniform bulk region at the centre of the crystal. The RMSD at the surface in the z direction are about a factor of 0.5 greater than these in the bulk.

Fig. 4.4. shows, $\rho(z)$, for the Na^+ and Cl^- at 900K, again their density profiles are seen to be quite similar. The peaks in the density profile are now much more spread out than at 300K due to the greater amplitude of the oscillations of the ions at higher temperature. We again appear to have reached the uniform plateau region at the centre of the crystal. The RMSD results are about a factor of two greater than at 300K, see Table 4.2. Against the x and y RMSD values are in close agreement with those of the bulk z values, though not quite as good as the 300K results, the surface RMSD are about 0.5 times greater than the bulk once more. We also notice that the RMSD results at 900K are slightly smaller for the Cl^- ion compared to the Na^+ ion due to their heavier mass. This is not obvious from $\rho(z)$ especially at 300K where there is less motion of the ions.

In Figs. 4.5 and 4.6 we present, $\rho(z)$, at 300K for the $\eta = 4$ case and Table 4.3 shows the RMSD results. The results are in very good agreement with those for $\eta = 3$. Fig. 4.7 shows $\rho(z)$ at 900K for the $\eta = 4$ case and Table 4.4 gives the RMSD results. Again the results are in quite good agreement as those for $\eta = 3$. These results show that for our periodically repeating laminae the ionic surfaces do not interact across the vacuum, this is encouraging for our ionic crystal-water project, see Chapters 5 and 6,

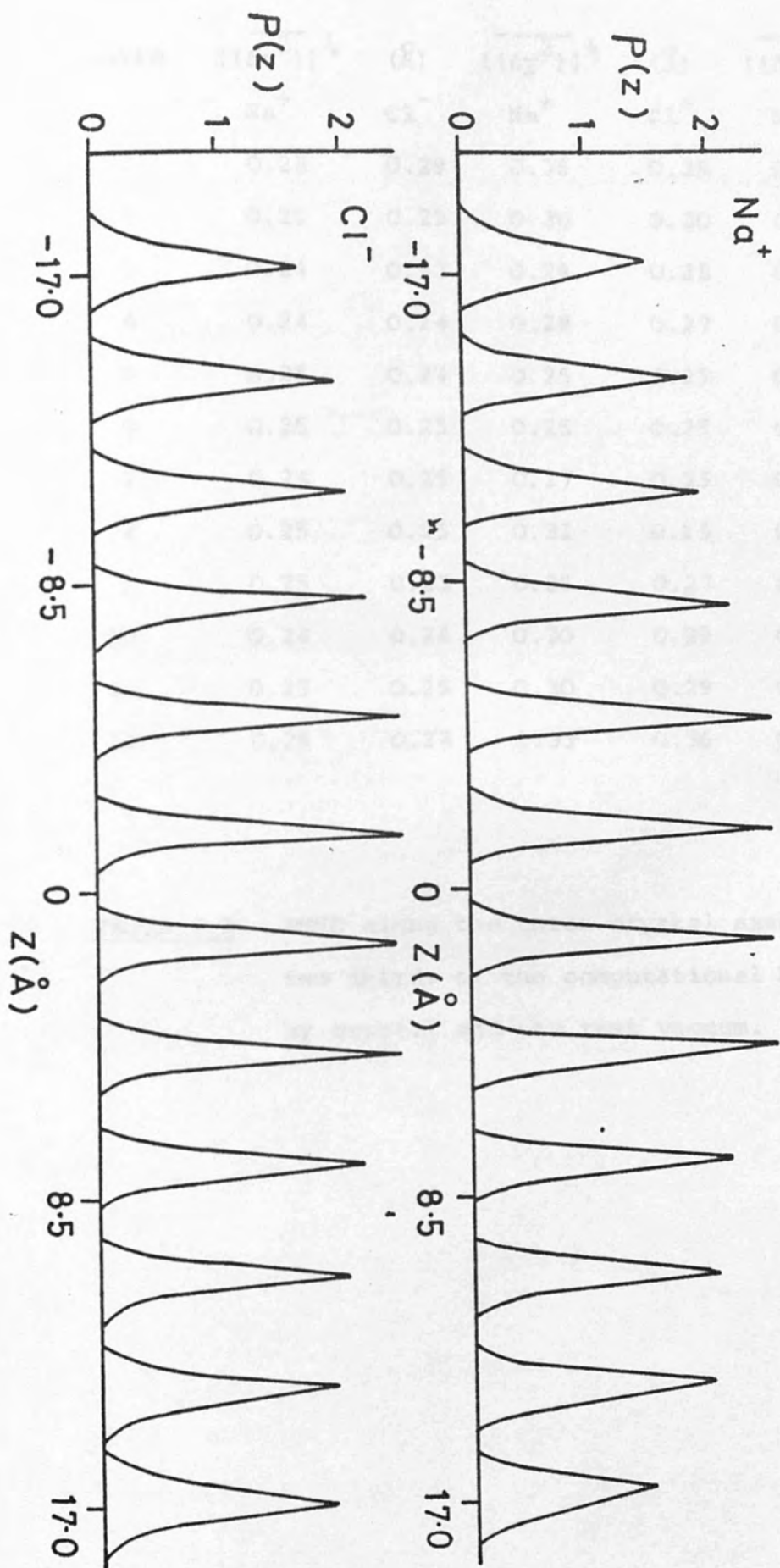


Fig. 4.4

LAYER	$\overline{((\Delta x^2))}^{\frac{1}{2}}$	(Å)	$\overline{((\Delta y^2))}^{\frac{1}{2}}$	(Å)	$\overline{((\Delta z^2))}^{\frac{1}{2}}$	(Å)
	Na ⁺	Cl ⁻	Na ⁺	Cl ⁻	Na ⁺	Cl ⁻
1	0.28	0.29	0.36	0.35	0.47	0.46
2	0.25	0.25	0.30	0.30	0.40	0.38
3	0.24	0.23	0.29	0.28	0.37	0.37
4	0.24	0.24	0.28	0.27	0.36	0.36
5	0.25	0.24	0.25	0.25	0.34	0.35
6	0.25	0.25	0.25	0.25	0.32	0.31
7	0.25	0.25	0.27	0.25	0.33	0.31
8	0.25	0.25	0.31	0.25	0.35	0.34
9	0.25	0.23	0.29	0.27	0.36	0.36
10	0.24	0.24	0.30	0.29	0.39	0.38
11	0.25	0.25	0.30	0.29	0.42	0.41
12	0.29	0.28	0.33	0.36	0.49	0.48

Table 4.2 RMSD along the three crystal axes at 900K,
two thirds of the computational box occupied
by crystal and the rest vacuum.

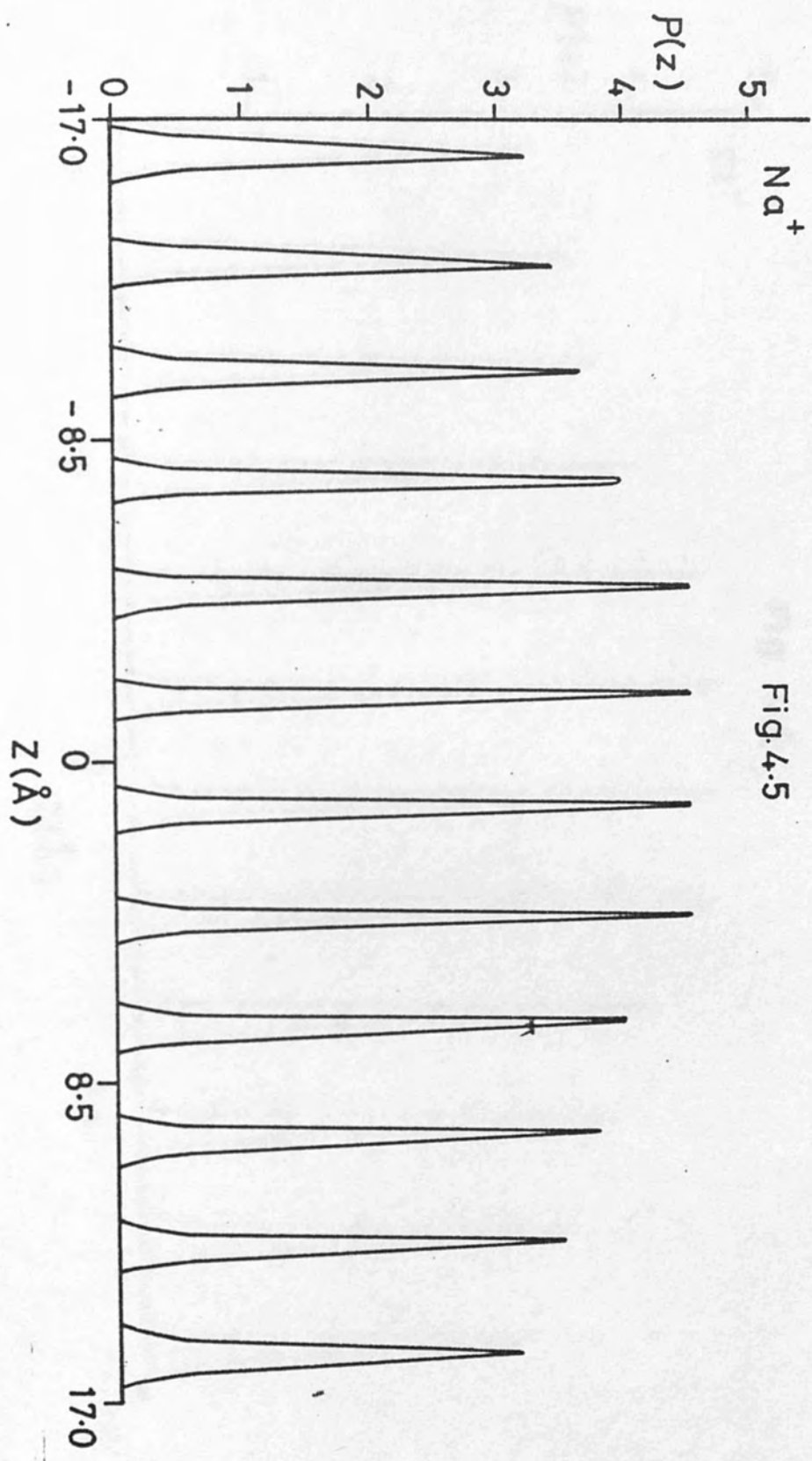


Fig. 4.5

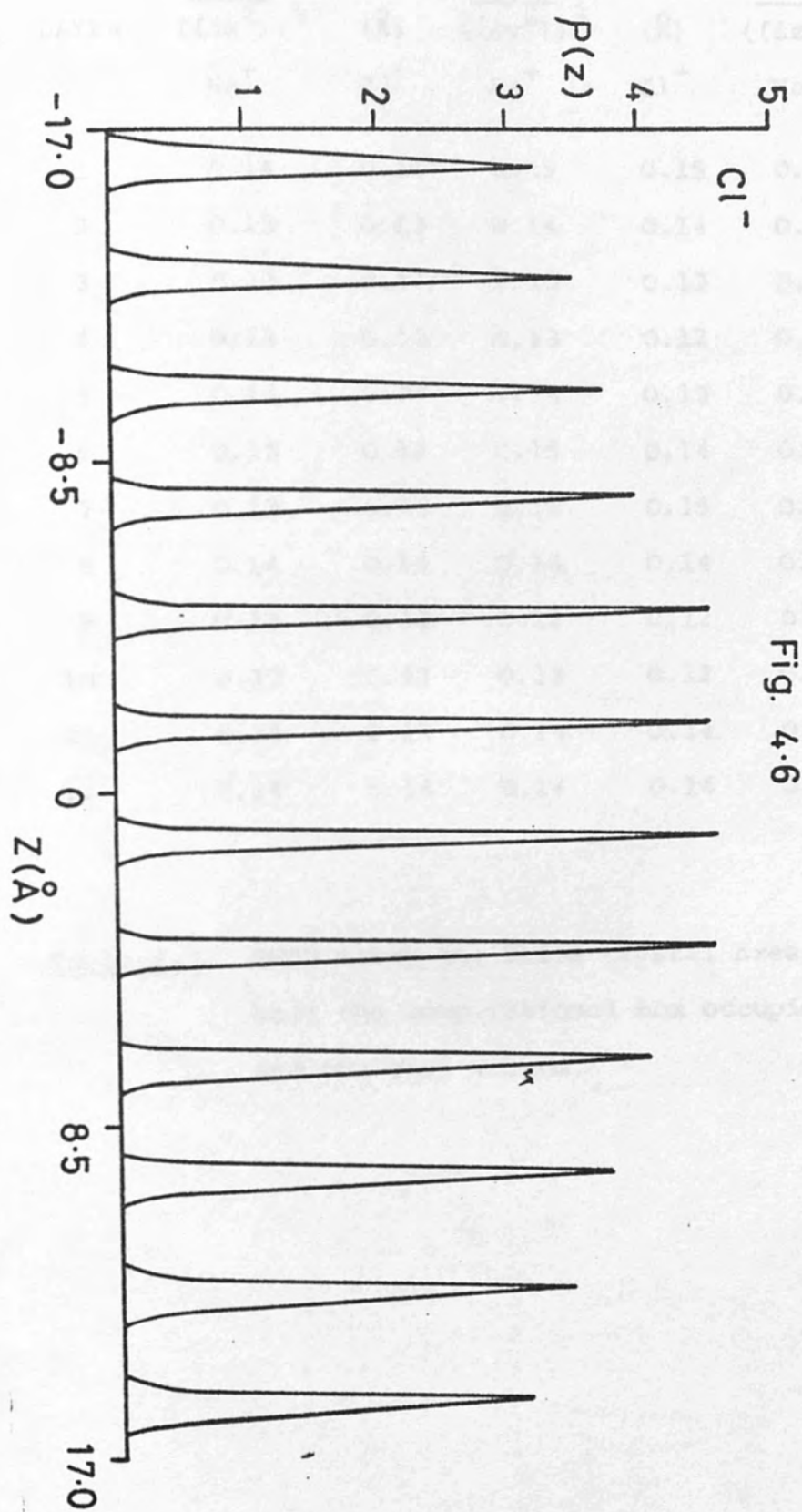


Fig. 4.6

LAYER	$\overline{((\Delta x^2))}^{\frac{1}{2}}$	(Å)	$\overline{((\Delta y^2))}^{\frac{1}{2}}$	(Å)	$\overline{((\Delta z^2)^{\frac{1}{8}})^{\frac{1}{2}}}$	(Å)
	Na ⁺	Cl ⁻	Na ⁺	Cl ⁻	Na ⁺	Cl ⁻
1	0.14	0.14	0.15	0.15	0.21	0.22
2	0.13	0.13	0.14	0.14	0.19	0.19
3	0.13	0.12	0.13	0.13	0.18	0.18
4	0.14	0.13	0.13	0.12	0.16	0.15
5	0.14	0.14	0.14	0.13	0.14	0.14
6	0.13	0.12	0.15	0.14	0.14	0.14
7	0.13	0.13	0.15	0.15	0.14	0.14
8	0.14	0.14	0.14	0.14	0.16	0.15
9	0.14	0.13	0.12	0.12	0.17	0.17
10	0.13	0.12	0.13	0.12	0.18	0.18
11	0.14	0.13	0.14	0.14	0.19	0.19
12	0.14	0.14	0.14	0.14	0.22	0.21

Table 4.3 RMSD along the three crystal axes at 300k, half the computational box occupied by crystal and the rest vacuum.

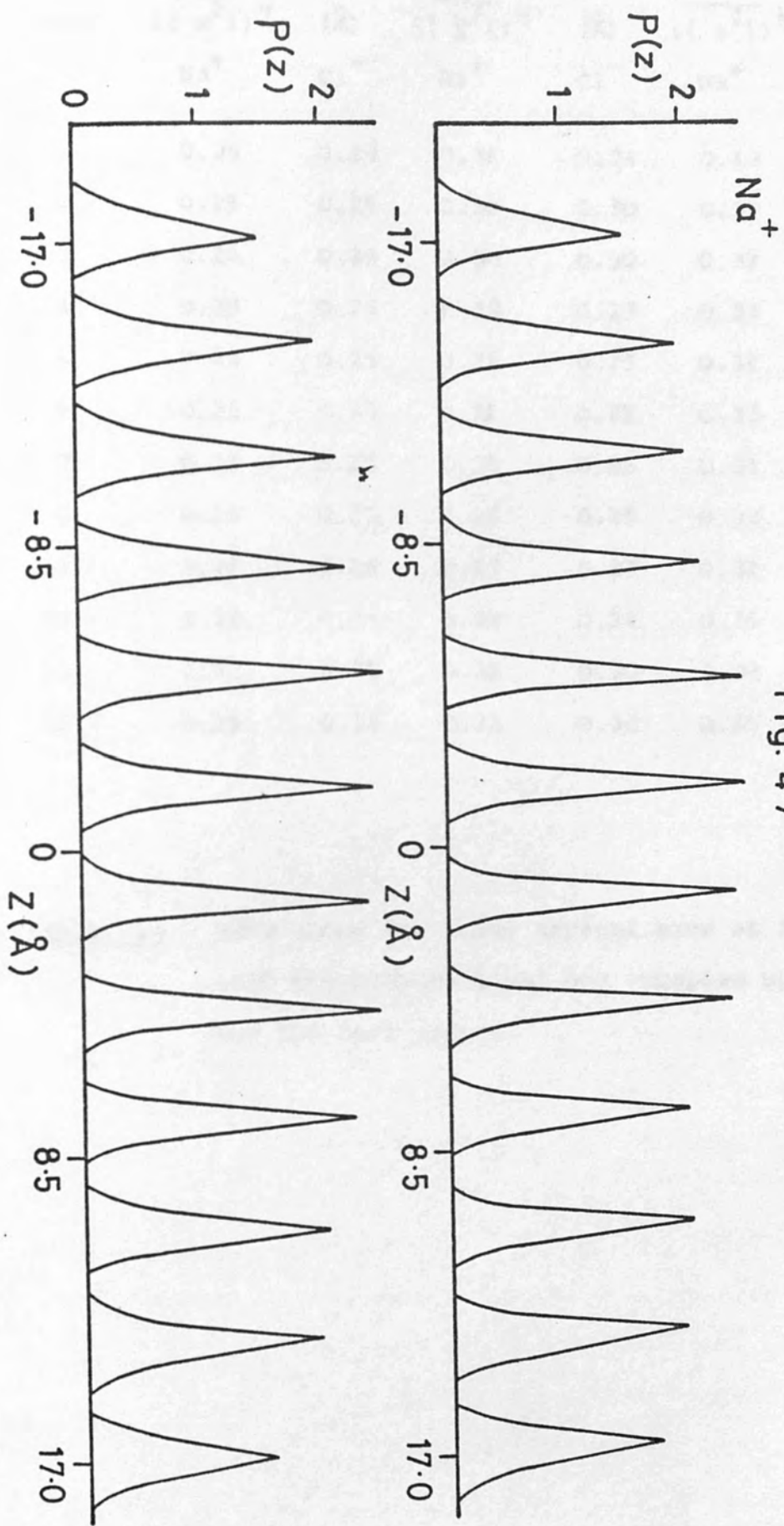


Fig. 4.7

LAYER	$\overline{((x^2))}^{\frac{1}{2}}$ Na ⁺	$\overline{((y^2))}^{\frac{1}{2}}$ Cl ⁻	$\overline{((x^2))}^{\frac{1}{2}}$ Na ⁺	$\overline{((y^2))}^{\frac{1}{2}}$ Cl ⁻	$\overline{((z^2))}^{\frac{1}{2}}$ Na ⁺	$\overline{((z^2))}^{\frac{1}{2}}$ Cl ⁻
1	0.36	0.28	0.36	0.34	0.43	0.44
2	0.26	0.25	0.30	0.30	0.39	0.38
3	0.25	0.25	0.30	0.30	0.39	0.36
4	0.25	0.25	0.28	0.27	0.34	0.30
5	0.24	0.25	0.25	0.25	0.31	0.30
6	0.25	0.25	0.25	0.25	0.33	0.30
7	0.25	0.25	0.25	0.25	0.31	0.30
8	0.25	0.25	0.26	0.25	0.33	0.30
9	0.25	0.24	0.27	0.27	0.32	0.31
10	0.25	0.24	0.29	0.24	0.36	0.36
11	0.25	0.25	0.31	0.30	0.38	0.38
12	0.29	0.28	0.32	0.33	0.46	0.46

Table 4.4 RMSD along the three crystal axes at 900K, half the computational box occupied by crystal and the rest vacuum.

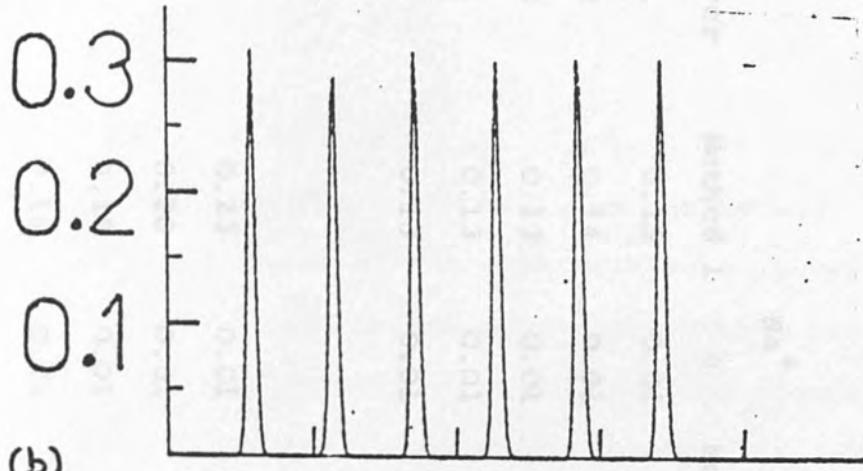
when the vacuum replaced is by water (which has a large dielectric constant) the ion-ion interaction across the water are therefore likely to be quite negligible.

We then thought it would be useful to compare our model with that of the isolated lamina of Heyes [144]. We have used a nearest neighbour distance r_0 of 2.82\AA which is the experimental value at 300K. A slightly larger value r_0 of 2.86 which gave zero pressure at the centre of the computational cell was used by Heyes. This difference in r_0 does not significantly effect the results for either $\rho(z)$ or RMSD. Also we had used a histogram separation in $\rho(z)$ of 0.085\AA as compared with theirs of 0.1\AA . Fig. 4.8(b) compares $\rho(z)$ of our periodically repeating lamina method with their isolated lamina method, with $r_0 = 2.86\text{\AA}$ and a histogram separation of 0.1\AA . The comparison is with the two innermost layers of our twelve larger crystal excluded, as their simulation had been with ten layers. This must be valid if we have reached the bulk region of the crystal. The results for one species only is shown and are now normalised to one by dividing by 18. The agreement is very satisfactory. Fig. 4.8(a) also shows $\rho(z)$ for a bulk NaCl simulation [144]; the peaks at the centre of our ionic slab compare very well with those of the bulk crystal.

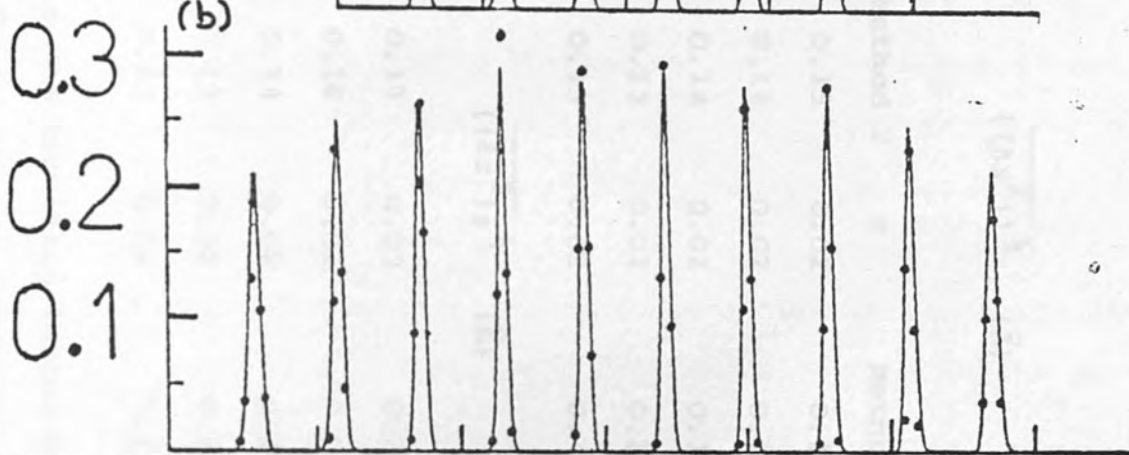
We have also compared our results at 1034K near the melting point ($r_0 = 2.97\text{\AA}$), where again good agreement is obtained see Fig. 4.8(d). Fig. 4.8(c) [144] is by isolated lamina method at an intermediate temperature. Table 4.5 compares the RMSD results at 302K, the agreement is again good. We see that the RMSD's at 1034K are slightly

FIG. 4.8

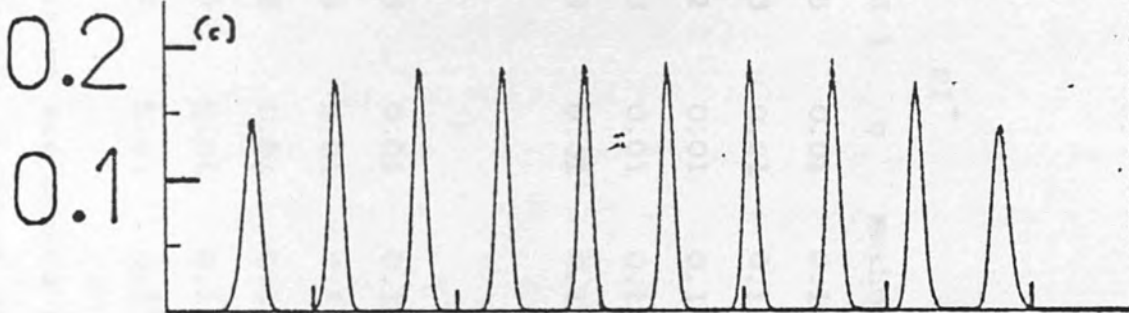
(a)



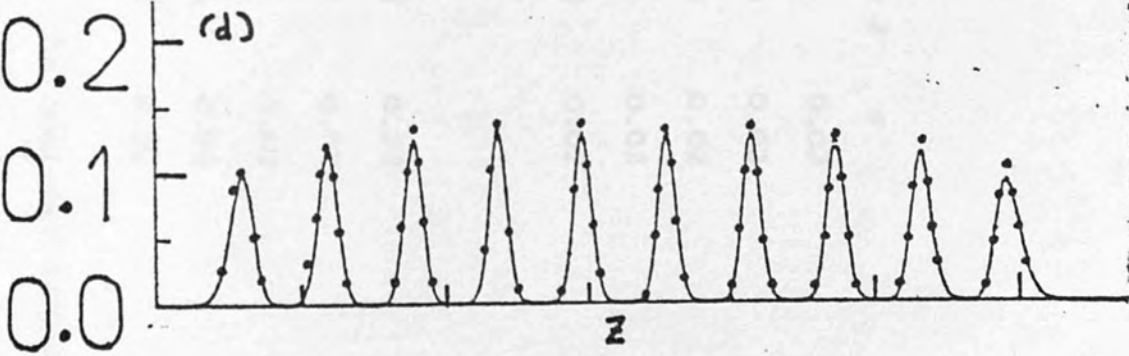
(b)



(c)



(d)



Layer	Na^+				Cl^-			
	Method 1	σ	Method 2	σ	Method 1	σ	Method 2	σ
1	0.15	0.01	0.15	0.02	0.15	0.01	0.14	0.02
2	0.14	0.01	0.14	0.02	0.13	0.01	0.13	0.02
3	0.13	0.01	0.14	0.02	0.12	0.01	0.13	0.02
4	0.13	0.01	0.13	0.02	0.13	0.01	0.13	0.02
5	0.13	0.01	0.13	0.02	0.13	0.01	0.13	0.02

$$\frac{((\Delta x^2))^{\frac{1}{2}}}{(\text{\AA})}$$

$$\frac{((\Delta z^2))^{\frac{1}{2}}}{(\text{\AA})}$$

1	0.23	0.01	0.19	0.03	0.23	0.01	0.18	0.03
2	0.20	0.01	0.16	0.02	0.20	0.01	0.15	0.02
3	0.18	0.01	0.14	0.02	0.18	0.01	0.14	0.02
4	0.16	0.01	0.13	0.02	0.15	0.01	0.13	0.02
5	0.14	0.01	0.13	0.02	0.14	0.01	0.13	0.02

Table 4.5

RMSD, method 1 is the repeating lamina method and method 2 the isolated lamina method at 302K. The RMSD in the x (parallel to the surface) direction and z (perpendicular to the surface) direction are given. The average on either side of the slab is taken.

smaller for the Cl^- ion than for the Na^+ ions, see Table 4.6, this is again not obvious from $\rho(z)$ alone.

4.4 Conclusion

We find that an ionic slab of twelve layers is adequate in the study of surfaces since the central layers describe the properties of the bulk crystal quite well. We have also found that these ionic slabs with a separation distance in the z direction of one periodic distance (16.91\AA) of the x and y distance is adequate for them not to interact across the vacuum i.e. one surface is not influenced by the other's image in the neighbouring replica cell. This is in agreement with previous calculations [36] in which it was demonstrated that the electric field above a static point charge film dies away rapidly to insignificance at a perpendicular distance from the surface which is equal to the periodicity length along the lamina.

The method of periodically repeating layers shown to be equivalent to the isolated lamina method is of important use in solid-liquid interfaces since it avoids liquid-vacuum interfaces when not required. An example of such an application is given in Chapters 5 and 6 of the ionic crystal-water interface.

Layer	Na ⁺				Cl ⁻			
	Method 1	σ	Method 2	σ	Method 1	σ	Method 2	σ
1	0.54	0.14	0.39	0.07	0.46	0.08	0.41	0.08
2	0.39	0.03	0.34	0.07	0.39	0.08	0.32	0.04
3	0.37	0.05	0.32	0.04	0.36	0.06	0.31	0.04
4	0.34	0.03	0.31	0.04	0.33	0.03	0.30	0.04
5	0.32	0.01	0.32	0.04	0.32	0.02	0.31	0.04

$\left(\frac{\overline{(\Delta z^2)}}{2}\right)^{\frac{1}{2}}$ (Å)

Table 4.6

RMSD, method 1 is the repeating lamina method and method 2 the isolated lamina method at 1034K. The RMSD in the x (parallel to the surface) direction and z (perpendicular to the surface) direction are given. The average on either side of the slab is taken. σ is the standard error.

CHAPTER 5

THE SODIUM CHLORIDE-WATER INTERFACE

5.1 Introduction

Molecular dynamics and Monte Carlo studies have lately proved to be powerful tools in the study of interfaces [145]. Of particular relevance to this work is the simulation of solid-liquid interfaces [39-43], discussed in Ch. 4; this work is mainly concerned with LJ systems. There has been though little work on solid-water interfaces. A Monte Carlo study is reported of water in contact with structureless walls by Christou et al [44]. The simulation was performed with Rowlinson water [86] in contact with a structureless wall which exerts a 9-3 potential on the water molecules. The Rowlinson model of water is an early simple model which consists of a LJ function together with the electrostatic interactions arising from the presence of four-point-charges on each molecule. This potential has been used in computer simulations at the experimental density at 25°C [88,146]. The structure it predicts for water does not compare well with experiment [91]. In particular $g_{oc}(r)$ peaks at too small a value of r and lacks detailed structure in the 3.5-5.0Å range. In the study of Christou et al. the density profile of the water molecules away from the walls showed considerable oscillations. Another simulation [147] in which CI water [95] is placed between two hard walls has been performed. In this work oscillations extending several molecular diameters out have also been reported.

In this project we have studied the more realistic

ionic crystal-water interface. The availability of ion-water potentials is limited to alkali halide-water potentials and this study concerns the NaCl-H₂O interface. Our objective was a close examination of phenomena occurring near the crystal-water interface.

5.2 Computational Details

The Born-Mayer Huggins interaction potential with Tosi-Fumi [64] parameters, as previously given in Ch. 2, is used to simulate NaCl. For water we have the central-force model [75] (see Ch.3) which besides being fairly realistic is a three-centre model and hence computationally more economical than the other good models such as ST2 and CI. Its non-rigidity is also an advantage as it may show any distortion of the water molecule at the crystal surface. The ion-water interaction potentials we use are the ones fitted by Bopp et al. [107] to the ab-initio calculations of Kisternacher et al. [117-119], see Ch 3.

The computer program MDIONS [70] is adapted to an orthorhombic computational box with sides in the ratio $x:y:z = 1:1:3$ approximately two thirds of the z-axis occupied by crystal and the rest by water. The computational box is as Fig. 4.1 but instead of vacuum we now have 108 water molecules on either side of the crystal. As described in Ch.4 there are two interfaces in the computational box. A full Ewald summation with the parameters $\alpha_1 = 5.6$, $l_{\max} = m_{\max} = 5$, $n_{\max} = 15$ and $k_{\max}^2 = 225$ are used as discussed in Ch.4. The system is made fully periodic in all three directions so that it consists of alternating slabs of crystal and water. 216 Na⁺ and 216 Cl⁻ ions form twelve

crystal planes; we have shown in Ch.4 that twelve layers are adequate for a realistic surface simulation of the crystal-vacuum system. The total number of ions in the computational cell is 1080 (216 Na⁺, 216 Cl⁻, 216 O, 432 H), giving a box volume = $1.634 \times 10^{-26} \text{ m}^3$. A time step of 0.25 Fs is used to avoid a drift in the total energy.

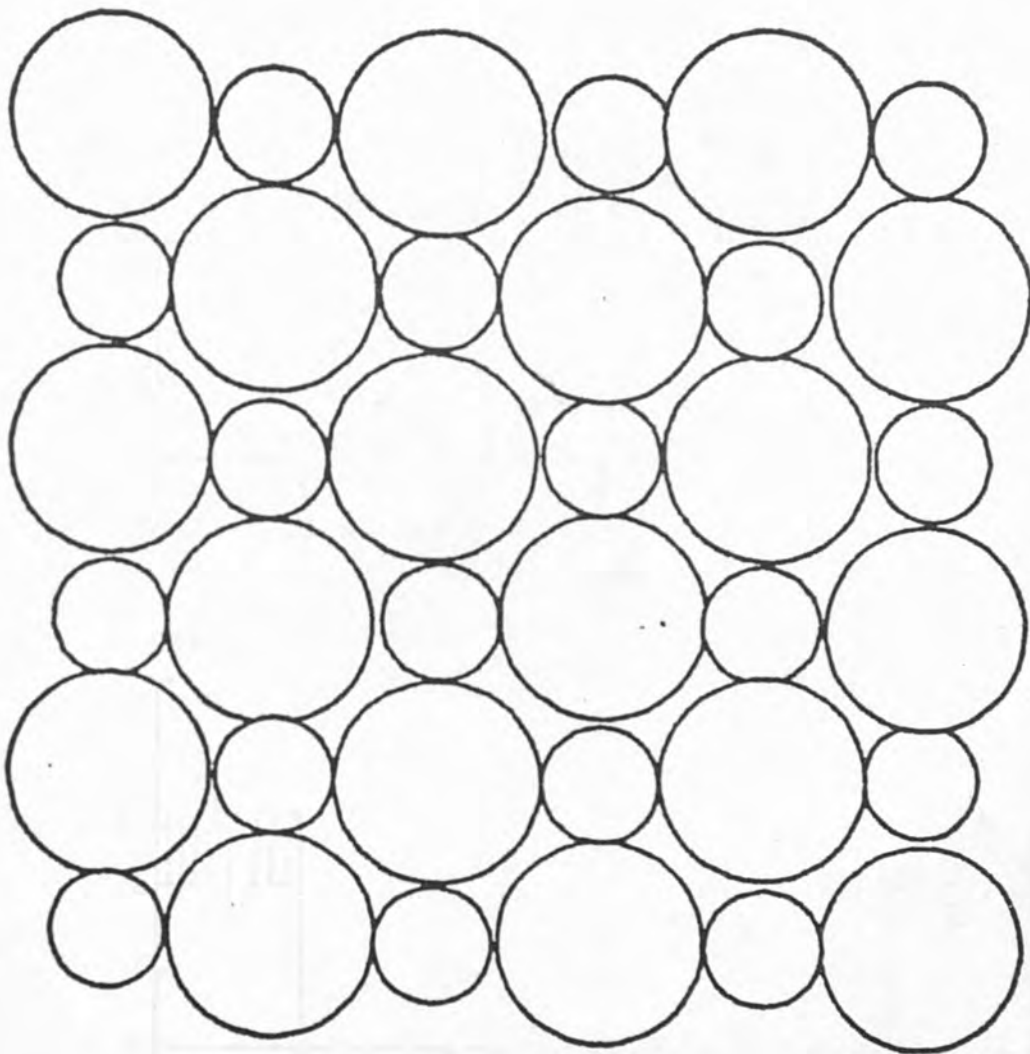
In the crystal-water simulations the configurations taken were the equilibrated configuration of water (Ch.3), and for the crystal the configuration from the crystal-vacuum simulation (Ch.4). They were combined to form the crystal-water system.

Two simulations were performed (a) at 300K as described in section 5.3 and (b) at 480K as described in section 5.4. The simulation at 480K was carried out because initially we thought we had been working at 300K but not all degrees of freedom were taken so the temperature of the system was at 480K. The simulation at 480K is still of interest as will be discussed later.

The system was followed in time by viewing the displacements of the average positions of the crystal layers, the density profile in the z direction, $\rho(z) \Delta z (\Delta z = 0.176 \text{ \AA})$, the direction perpendicular to the crystal surface, and by computer generated snapshots at different times t . The integration time step on the Cray⁻¹ was 2.7s.

At the outset, $t = 0$, before the crystal and water have interacted the picture of the crystal is shown by Fig. 5.1. Fig. 5.1 shows a computer generated picture of a (001) crystal plane (the xy plane viewed from the z direction). It shows an almost perfectly ordered 6×6 arrangement of Na⁺ (small circles) and Cl⁻ (large circles) ions. On either side of the two crystal surfaces is the water and Fig. 5.2

FIG. 5.1



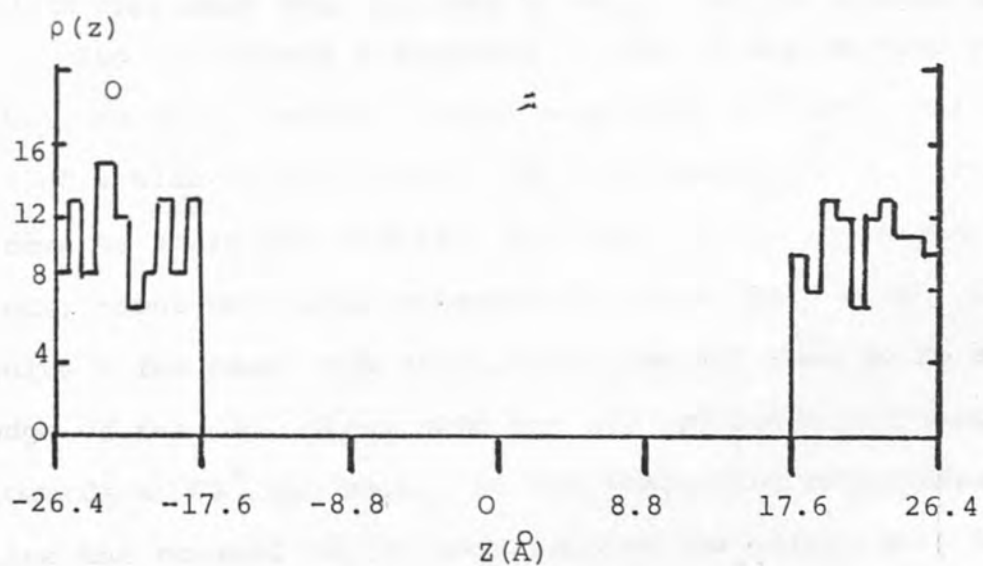
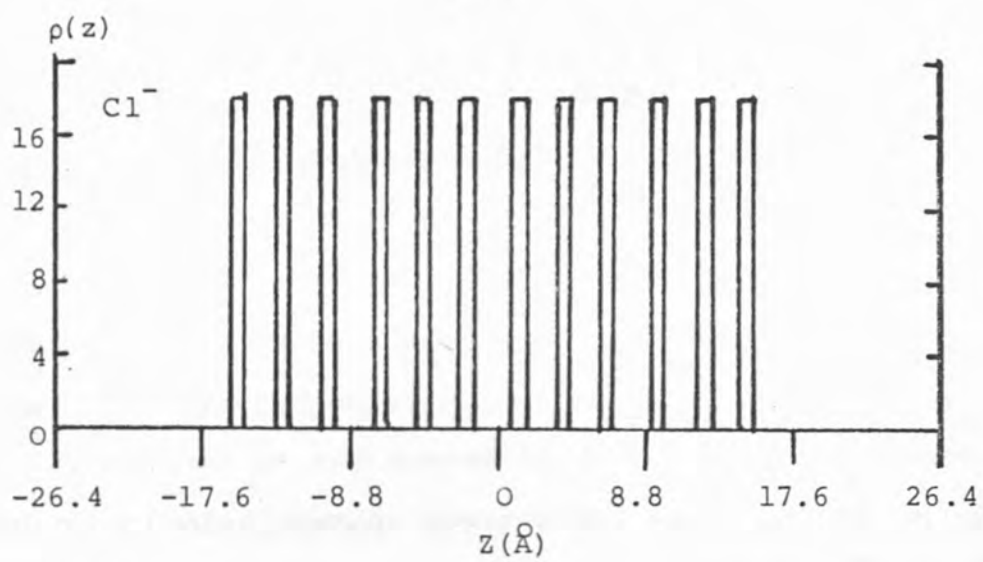
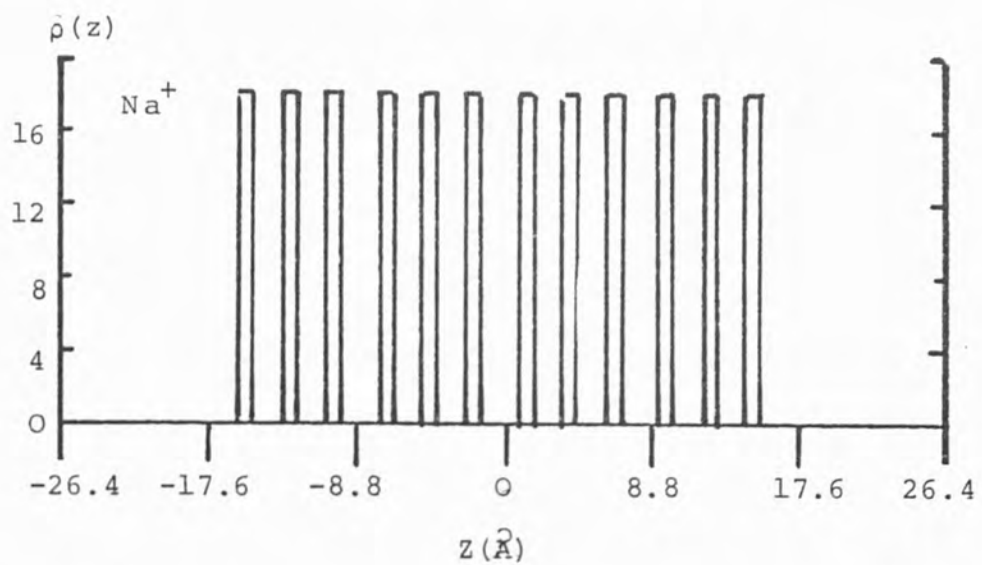


FIG. 5.2

shows the density profile, $\rho(z)$, at $t = 0$ for Na^+ , Cl^- and H_2O (represented by the O atoms).

5.3 Simulation at 300K.

In the equilibration process at 300K the crystal was kept rigid and the water allowed to move, full ion water interactions were still taken. The temperature of the water was then scaled to 300K. After this equilibration Fig. 5.3 shows the density profile of the O and H. It is seen that the density of the water near the crystal surface has increased compared to the bulk and also when compared to Fig. 5.2, the density profile at $t = 0$, before the crystal and water have been allowed to interact. From Fig. 5.3 it is also seen that the oxygens are slightly closer to the crystal surface than the hydrogens. After this time the water is not allowed to move but the crystal is, and the crystal is now scaled to 300K. The Na^+ ions show a very slight displacement towards the water at the two surfaces. Both phases were then allowed to move, and the simulation followed.

Fig. 5.4 shows a snapshot of one of the crystal surfaces with the first layer of water molecules included, the picture is of a slab of thickness $\sim 3\text{\AA}$. The water molecules (not drawn to scale for clarity) are seen to lie above the Na^+ ions, about one water molecule for each Na^+ site. In quite a few cases the water molecules are seen to be at the edge of the Na^+ ions with the two hydrogens pointing towards a Cl^- ion each. As the simulation progresses with time the crystal layers move towards the water, with the Na^+ ions further out. After 0.1ps the Na^+ ions are seen from Fig. 5.5, a snapshot of the same layer, to have moved

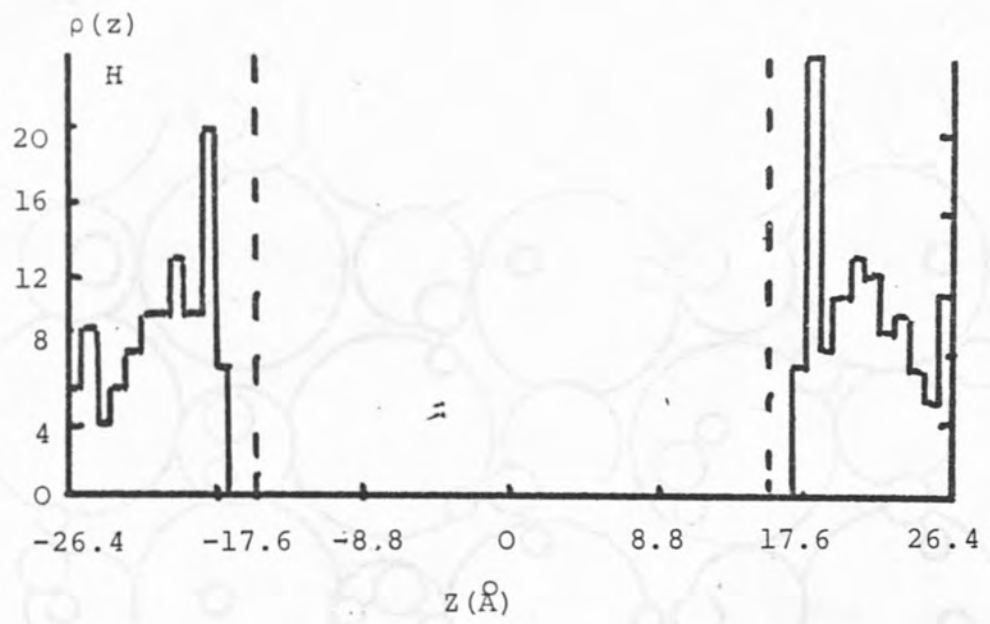
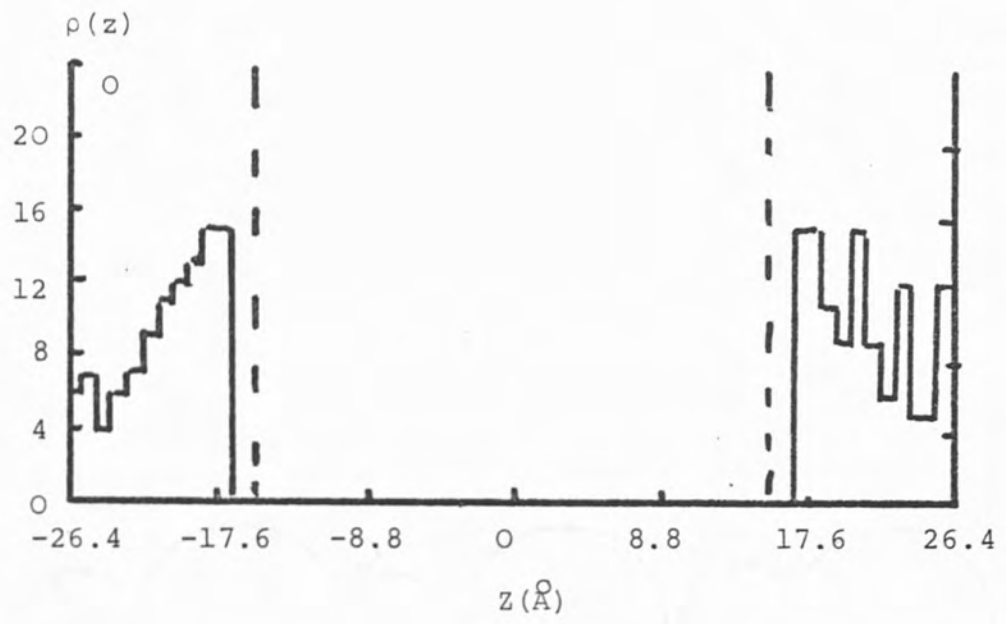


FIG. 5.3

FIG. 5.4

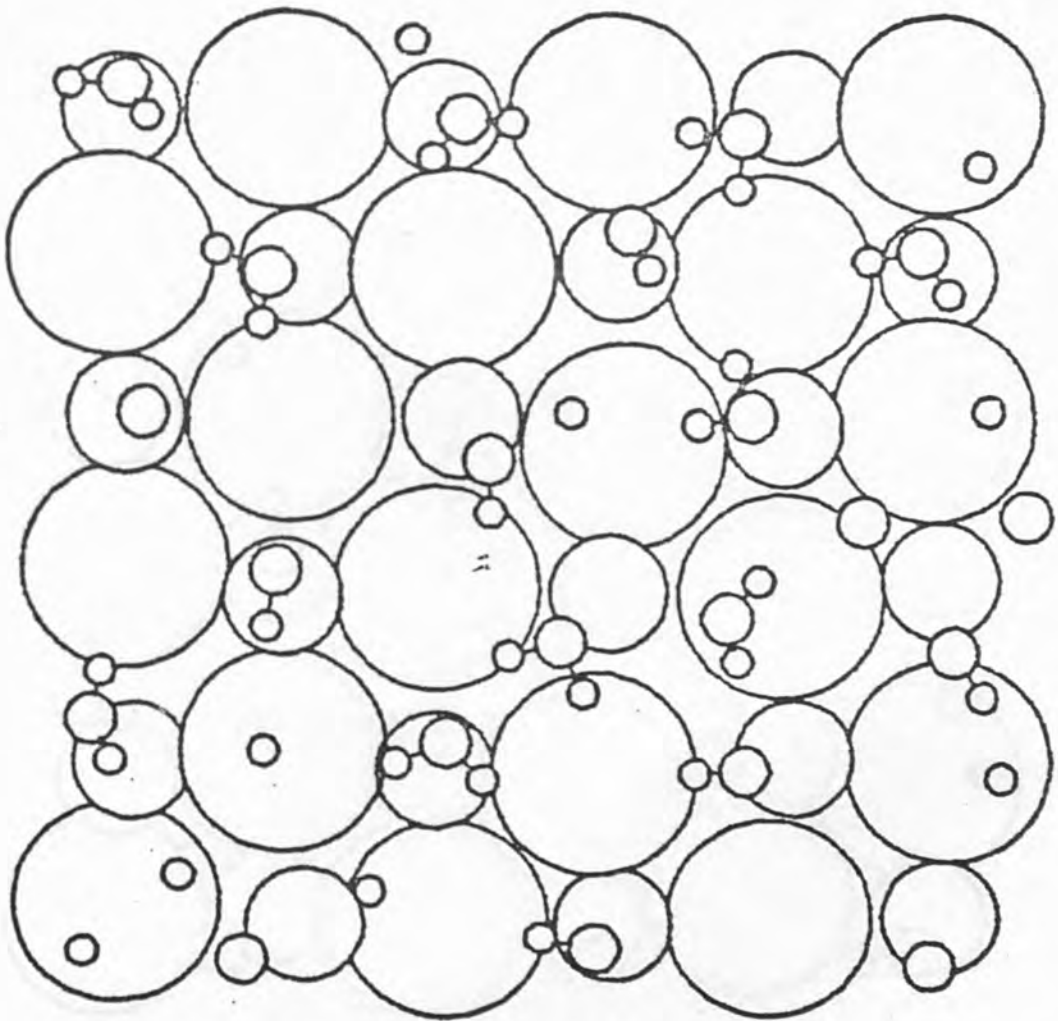
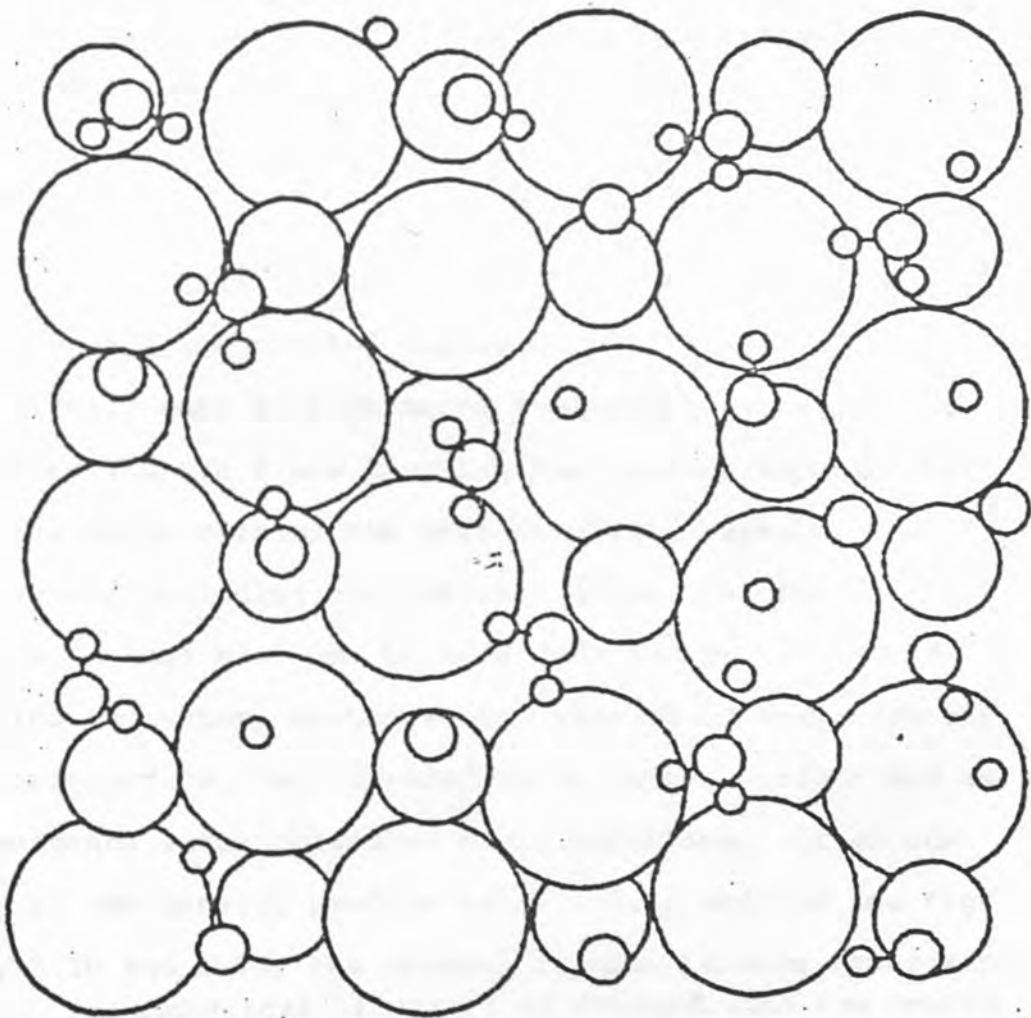


FIG. 5.5



further out towards the water, and also some of the water molecules moved slightly parallel to the crystal surface and are in some cases lying over the gaps left by the Na^+ as they move out. Fig. 5.6 shows the same layer after 0.5ps and the crystal is seen to be disturbed when compared with Fig. 5.1, with the crystal layers having moved further towards the water, the Na^+ was still displaced further out. Figs. 5.7 and 5.8 show the same layer after 1ps and 2ps. At these stages the crystal layers are seen to have also pushed the water further out, with a consequence of the water density increasing. After 1ps some water molecules have now penetrated the first crystal layer, after 2ps about 5 water molecules have entered the voids left by the Na^+ as they move more nearer to the water.

Table 5.1 shows the mean displacements of the crystal layers from their initial position after 0.05 and 2ps. After 0.05ps the crystal layers in particular the Na^+ ions are already seen to have moved towards the water at both surfaces (layers 1 and 12 being the surface layers), after 2ps the whole crystal has been displaced outwards towards the water, including the central layers. At the surface the Na^+ ions are seen to have been further attracted towards the water, as these ions have moved away from the crystal surface, this created voids on the surface and as a consequence water molecules could penetrate. If we now look at the density profile after 0.5, 1 and 2ps see Figs. 5.9, 5.10 and 5.11, the crystal is seen to move towards the water. An unphysical situation is created with the centre of crystal almost void, and also water molecules are seen to have penetrated the crystal surface, 1-2 water molecules are approaching

FIG. 5.6

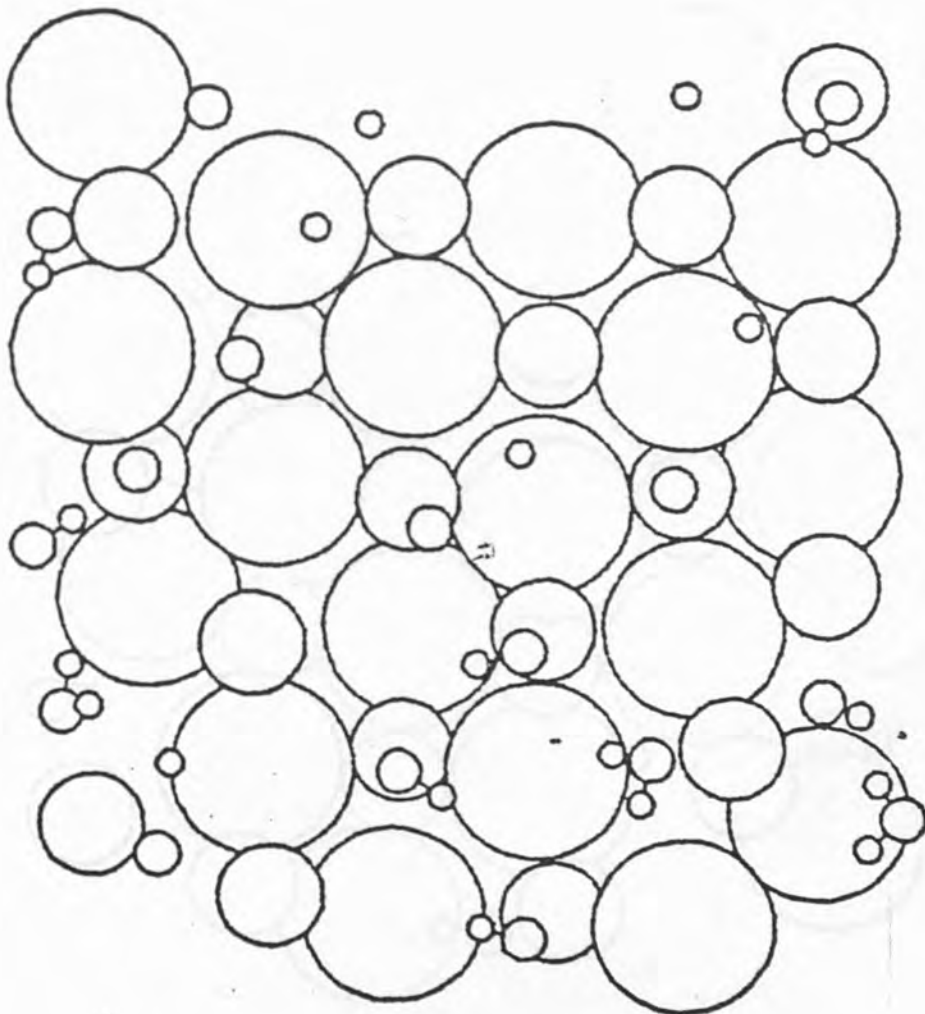


FIG. 5.7

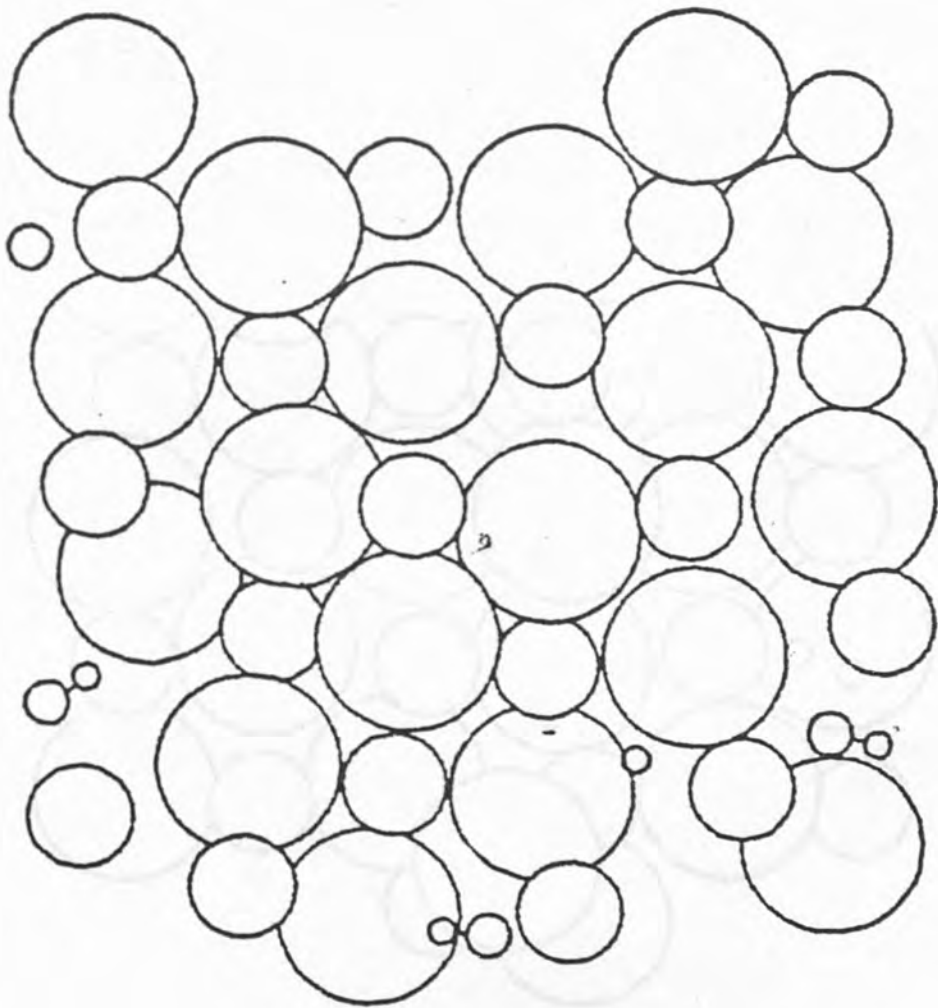
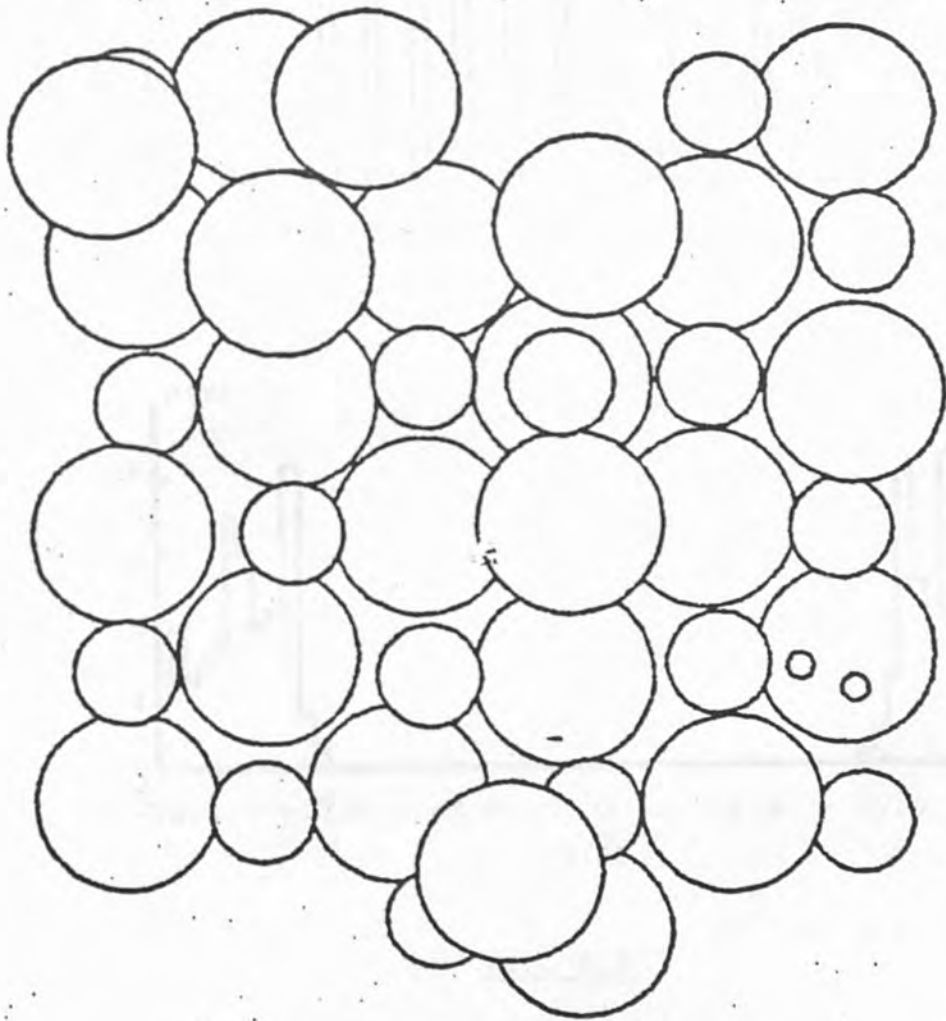


FIG. 5.8



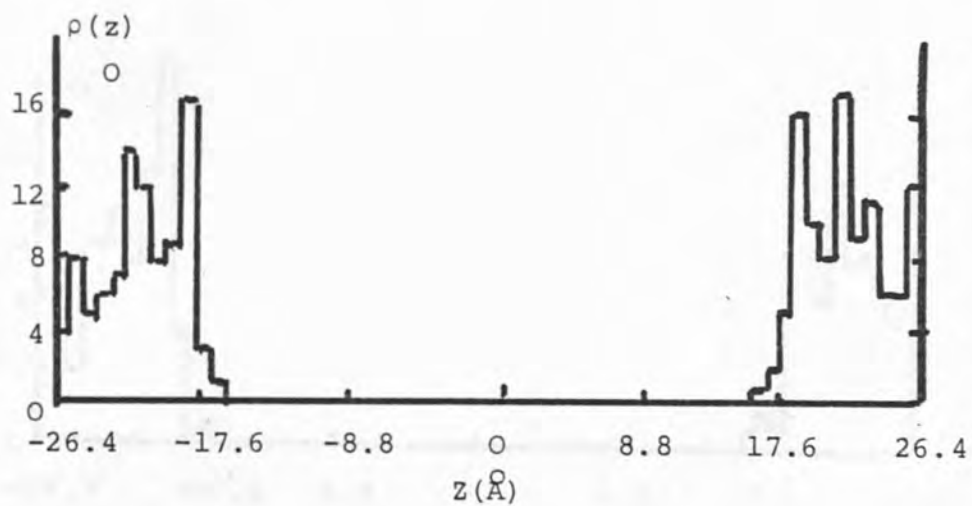
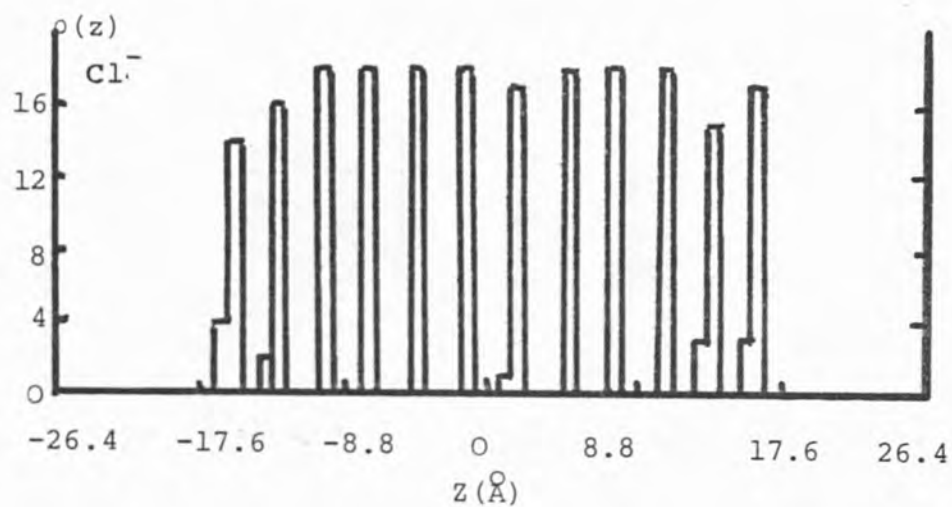
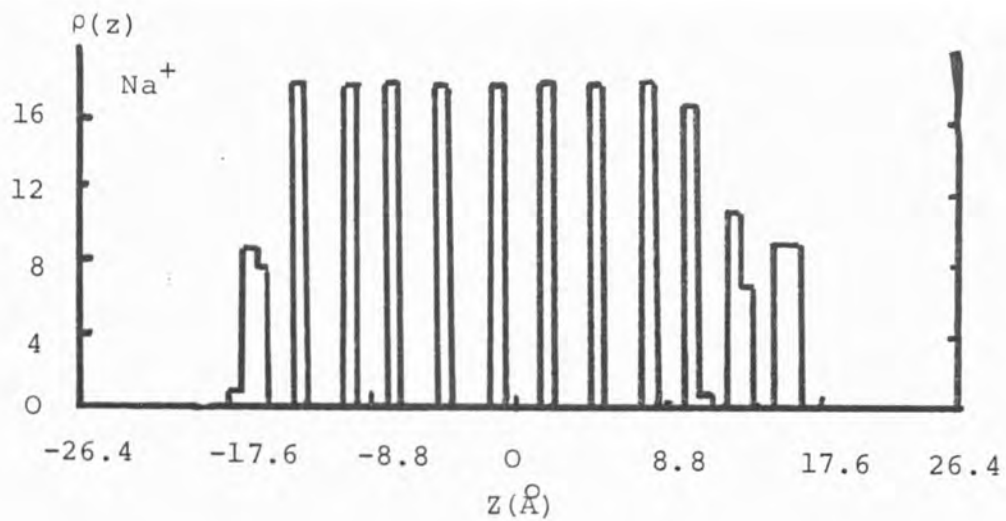


FIG. 5.9

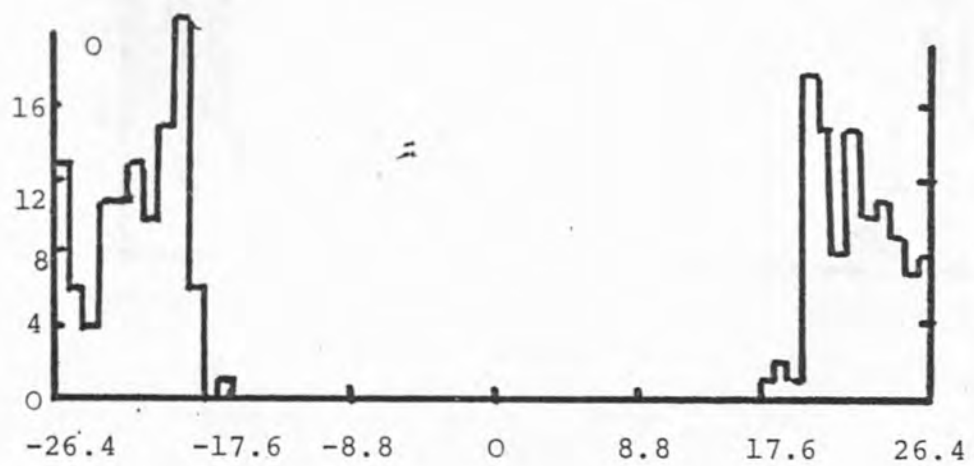
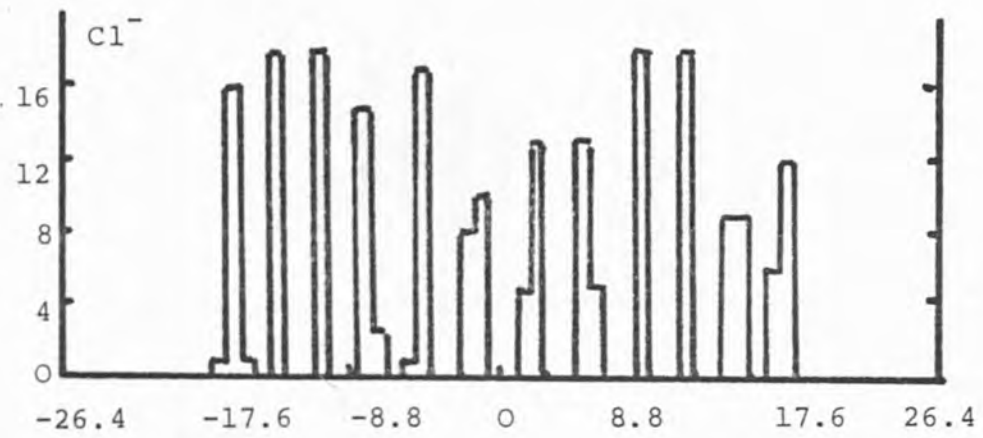
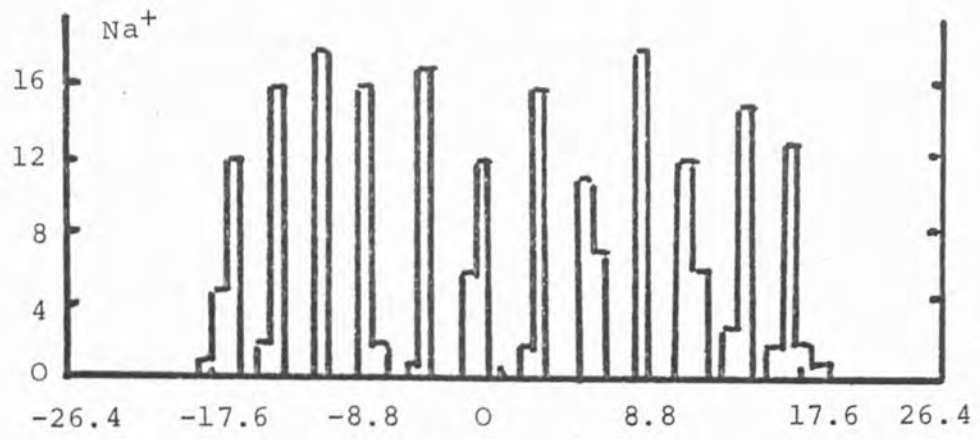


FIG. 5.10

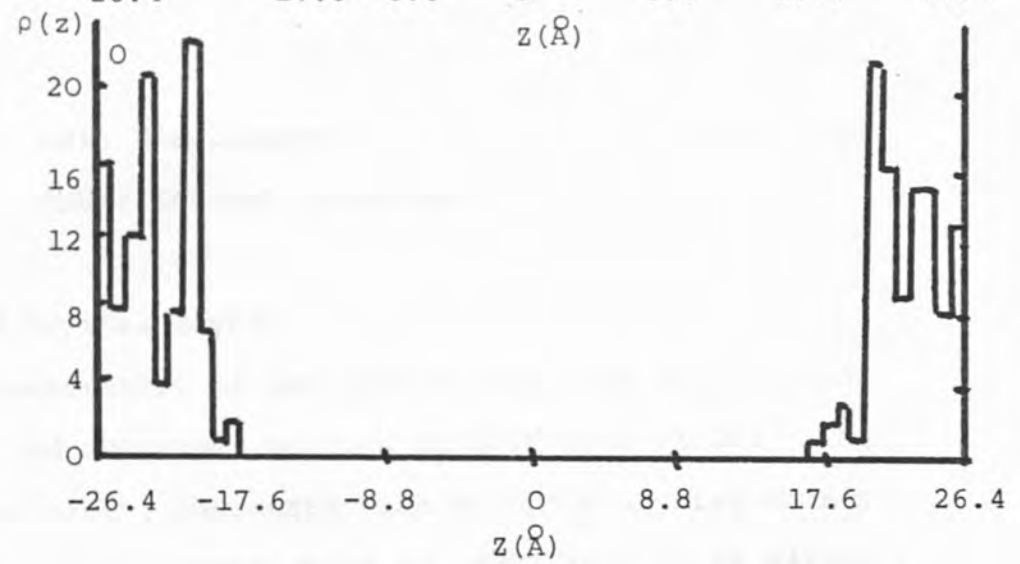
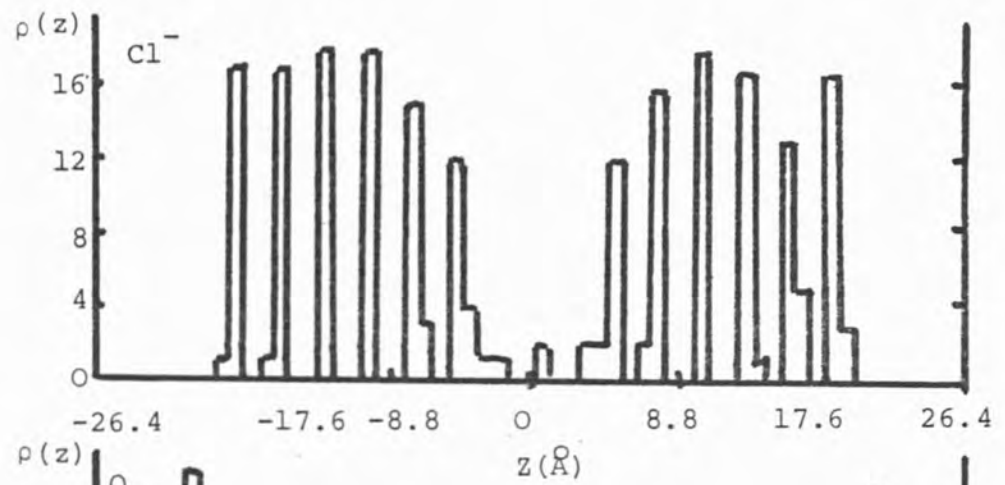
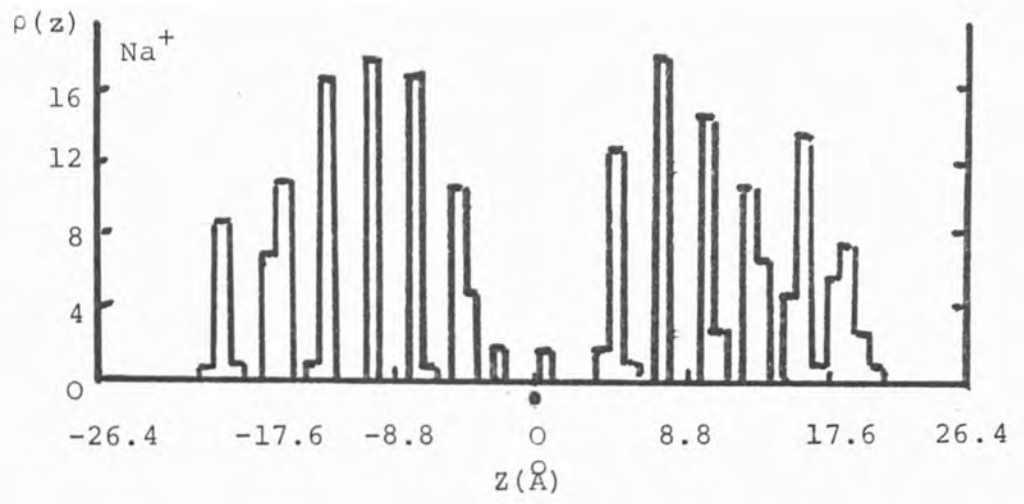


FIG. 5.11

$\Delta z (\text{\AA})$				
$t = 0.05\text{ps}$			$t = 2\text{ps}$	
LAYER	Na^+	Cl^-	Na^+	Cl^-
1.	-0.18	-0.09	-3.26	-2.82
2.	-0.18	0	-3.17	-2.99
3.	-0.18	-0.09	-3.17	-3.07
4.	-0.09	-0.09	-3.17	-3.07
5.	0	0.09	-3.17	-3.07
6.	0.18	-0.18	-2.90	-2.82
7.	0.18	0.09	2.73	2.55
8.	0.36	0.18	3.17	3.17
9.	0.36	0.18	3.34	3.17
10.	0.45	0.18	3.34	3.17
11.	0.36	0.09	3.43	3.17
12.	0.27	0	3.52	3.07

TABLE 5.1 Mean displacements of the crystal layers from their initial positions.

the second crystal layer.

The temperature of the system rose from 300 to 330K in 0.05ps and continued to rise to 365K after 1.3ps. The temperature having increased mainly at the crystal-water interface. As the dissolution of NaCl in H_2O is slightly endothermic rather than exothermic, it was decided to temperature scale for the rest of the simulation, till 2ps, to avoid further temperature rises. The system was scaled to 330K so as not to change it too significantly. The exothermic process observed in this simulation could be

because that the behaviour at short times i.e. till 2ps, is exothermic particularly at the interface. It is also possible that if a lot more water molecules had been used, and hence a greater bulk region that this temperature rise would not have been so significant. This of course would be computationally far too expensive. Another possibility is that the process is exothermic over the first 2ps and that the overall solution process is endothermic. It is also possible that the ion-water potentials are not totally realistic, as not too many ion-water potentials are known as discussed in Ch. 3.

5.4 Simulation at 480K

The simulation at 300K showed that the ion-water potentials were so attractive that the water at either end of the crystal attracted the crystal towards it, leaving very few ions at the centre of the crystal. In the 300K simulation the water was equilibrated in the presence of the fixed crystal before the beginning of the simulation which caused an increase in density of the water at the water at the surface, and also increased the ion-water attraction.

The simulation at 480K may be looked at in a different manner in that increasing the temperature to 480K is equivalent to being at 300K with a well depth $\epsilon' = \frac{\epsilon}{1.6}$ where ϵ is the original well depth and 1.6 the factor by which the temperature has increased, and the charges changed to $\frac{e}{\sqrt{1.6}}$, where e is the charge on the ions, thus giving a charge on the ions of ~ 0.8 i.e. reducing the ion-water interactions. Also the ion-water interactions

at the beginning of the simulation were lower by not allowing prior equilibration of the water next to the crystal and hence no increase in density of water at the surface.

Table 5.2 shows the mean z displacement of the Na^+ and Cl^- ions in the twelve (001) planes at 0.06ps. After 0.06ps the Na^+ ions at the surface have moved slightly away from the surface towards the water (layers 1 and 12 are the surface layers) and the Cl^- ions a lesser displacement in the opposite direction. Fig. 5.12 shows $\rho(z)$, of Na^+ , Cl^- and H_2O after 0.21ps, the initial slight displacement is seen by the broadening of the peaks, particularly for Na^+ in the outer two layers. The density of water has also now increased at the interface. As the Na^+ ions have moved slightly away from the surface voids are created on the crystal surface where water enters. Fig. 5.13 shows a snapshot of the surface, the Na^+ and Cl^- ions are now not perfectly ordered as seen in Fig. 5.1 but the crystal surface is now quite distorted with water present (the water molecules in the diagram are again not drawn to scale for clarity). This is also illustrated by the density profile at 0.5ps in Fig. 5.14. The crystal layers at the surface are now seen to be quite spread out, and the water to have penetrated the outer crystal layers. Table 5.3 gives the numbers after different times of the three species (Na^+ , Cl^- , H_2O) within space-fixed layers ($\Delta z \sim 2.8\text{\AA}$) corresponding to the initial positions of crystal layers. After 0.5ps seventeen water molecules have entered the two outermost layers 1 and 12. After 1.02ps one water molecule appears in layer 2 and one in layer 11

		$\Delta z (\text{\AA})$			
				$t = 2.35\text{ps}$	
$t = 0.06\text{ps}$					
LAYER	Na^+	Cl^-		Na^+	Cl^-
1.	-0.26	0.26		-1.06	-0.62
2.	0.09	0.09		-0.53	-0.18
3.	-0.09	0.09		-0.26	0.09
4.	0	0		0	0.18
5.	0	0.09		0.26	0.35
6.	0	0		0.35	0.44
7.	0	0		0.53	0.53
8.	0.09	0		0.70	0.62
9.	0.09	-0.09		0.79	0.70
10.	0.18	0		0.97	0.79
11.	0.18	0		1.14	0.88
12.	0.44	-0.09		1.67	1.50

TABLE 5.2 Mean displacement of peaks in the density profile, $\rho(z)$ of ions.



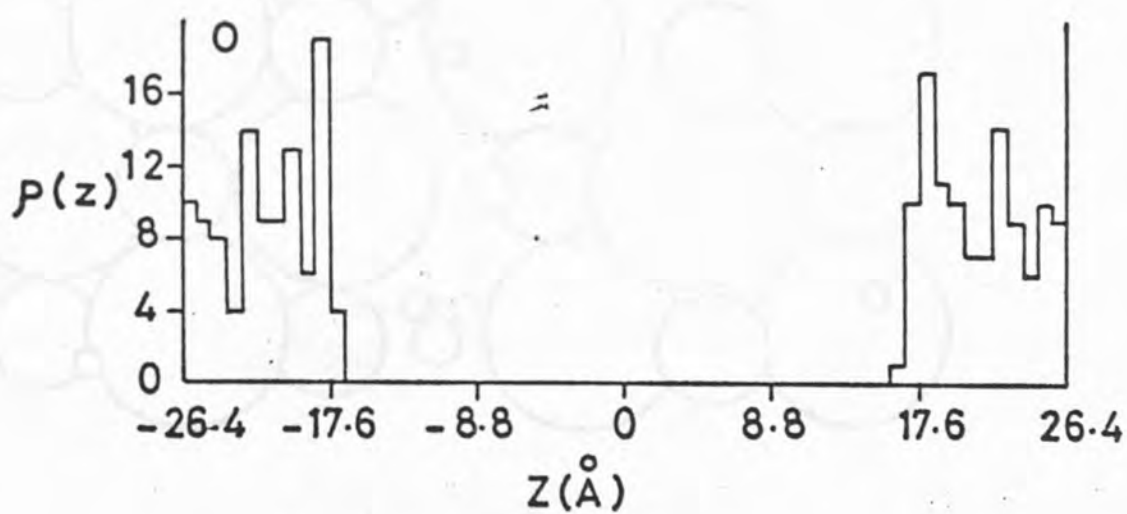
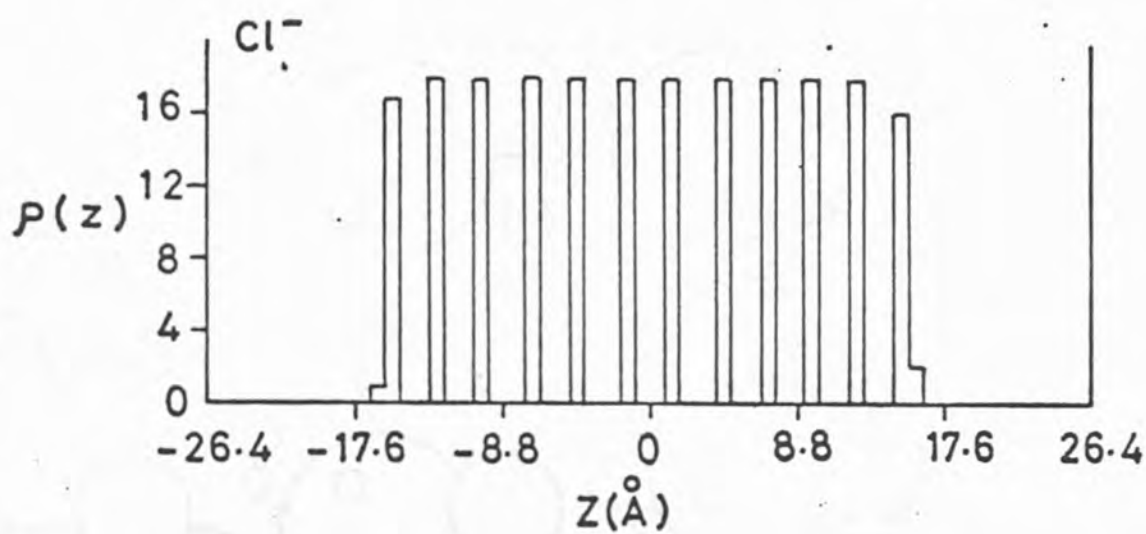
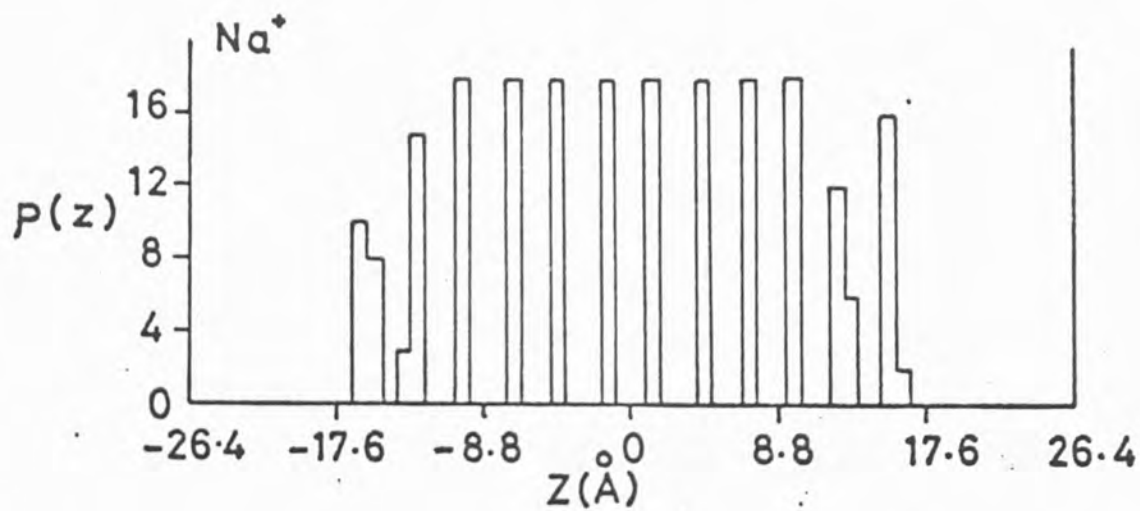


FIG. 5.12

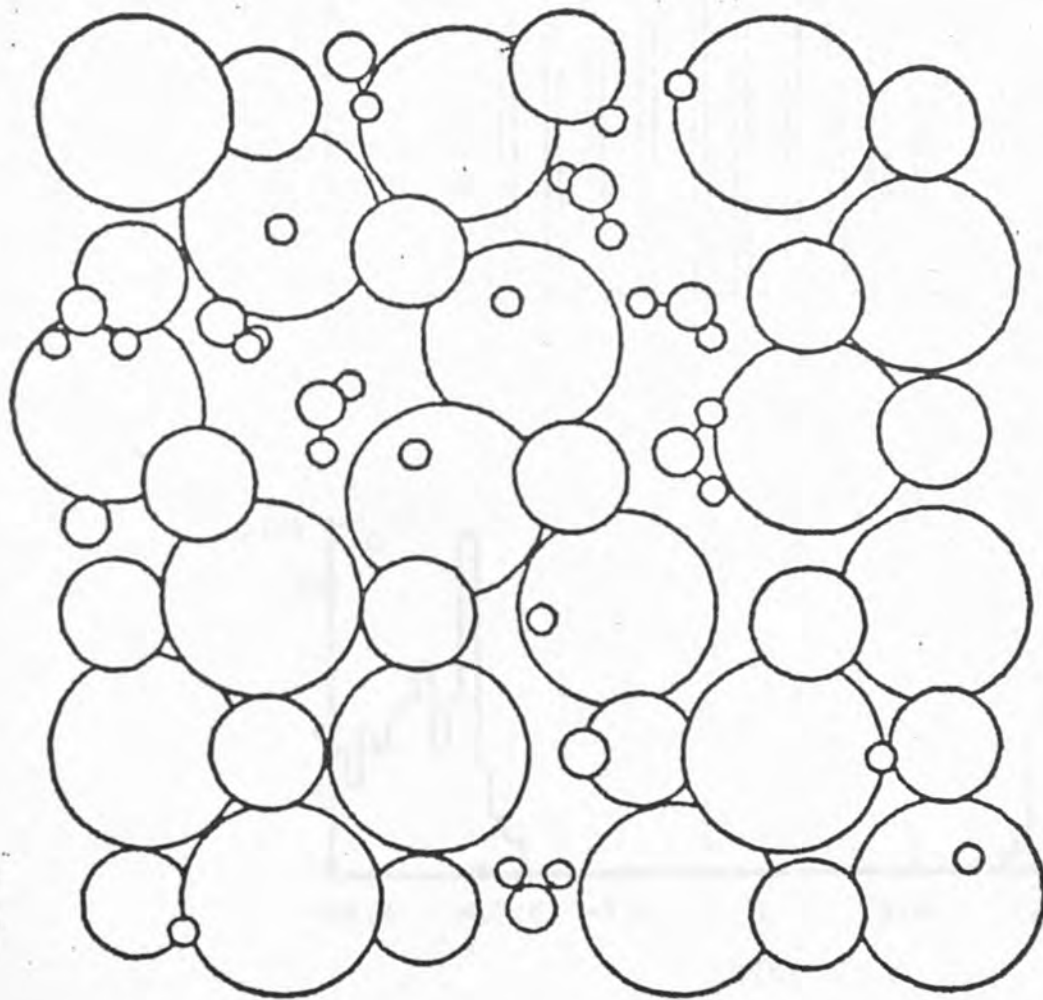


FIG. 5.13

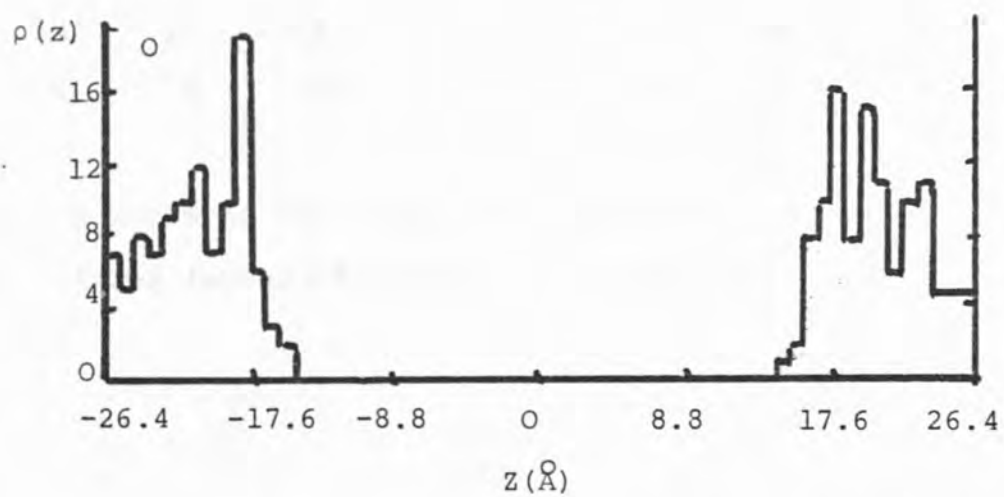
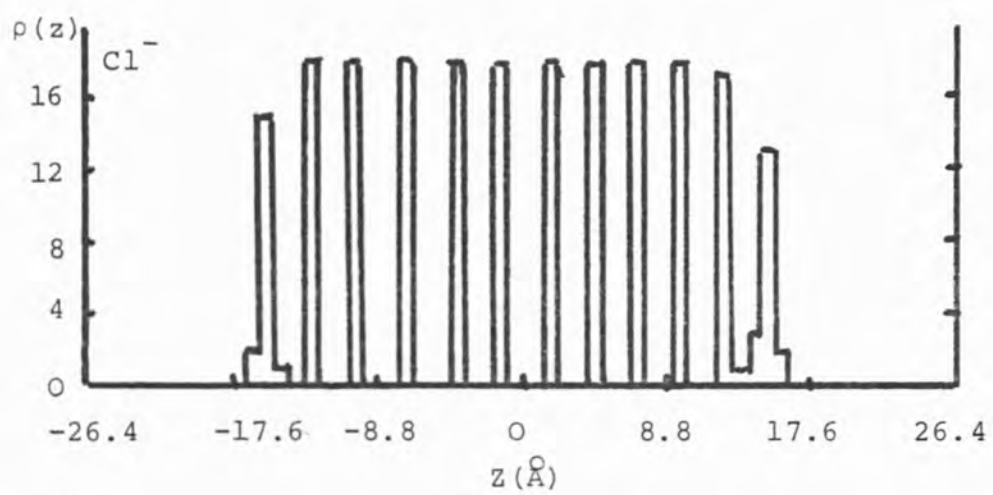
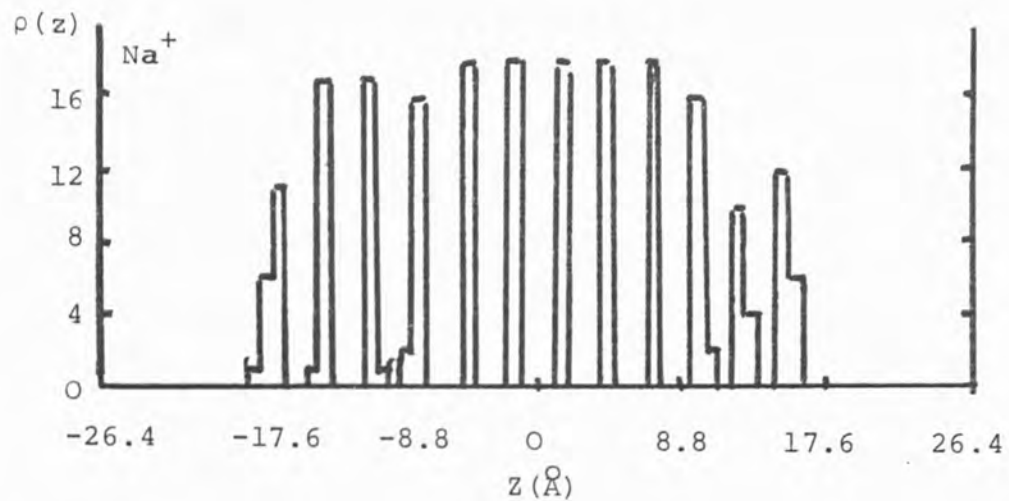


FIG. 5.14

T = 0.5ps

LAYER	1	2	3	10	11	12
Na ⁺	18	18	18	18	18	18
Cl ⁻	18	18	18	18	18	18
H ₂ O	6	0	0	0	0	11

T = 1.02ps

LAYER	1	2	3	10	11	12
Na ⁺	17	18	18	18	18	17
Cl ⁻	18	18	18	18	18	17
H ₂ O	8	1	0	0	1	9

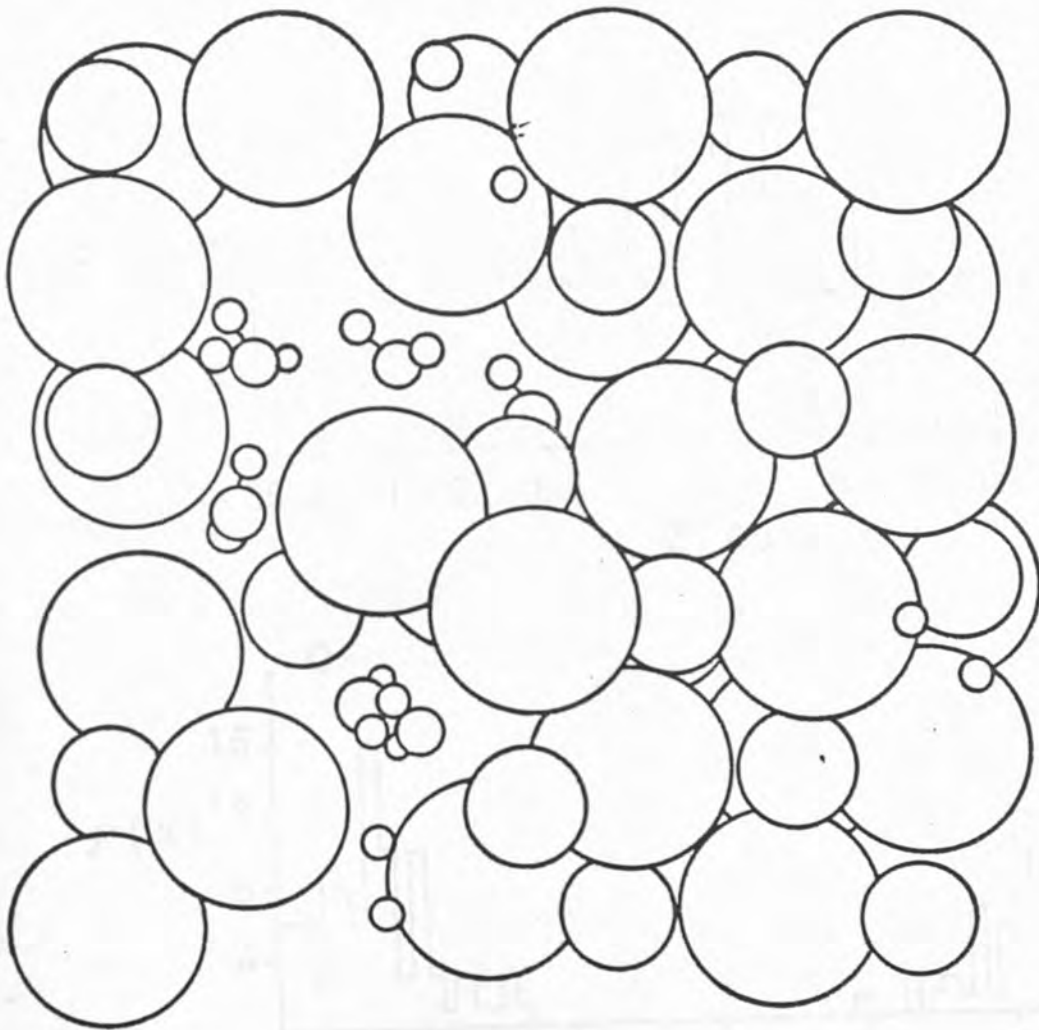
T = 2.35ps

LAYER	1	2	3	10	11	12
Na ⁺	16	15	17	17	13	17
Cl ⁻	14	17	18	17	18	16
H ₂ O	6	5	0	2	3	9

TABLE 5.3 Numbers of Na⁺ ions, Cl⁻ ions and O atoms in fixed layers of width $\Delta z = 2.8\text{\AA}$

while the sum in layers 1 and 12 is still 17. At this stage not more than ion of each species has been lost from layers 1 and 12. After 2.35ps two water molecules have penetrated layer 10; thirteen Na^+ and eight Cl^- ions have disappeared from layers 1-3 and 10-12 while 25 water molecules have appeared in them. All thirteen Na^+ ions are, however, still within $\leq 2.2\text{\AA}$ and seven of the Cl^- ions within $\leq 0.9\text{\AA}$ of the initial phase boundary. This is a reflection of the mean outward displacement of the peaks. This is also shown by Table 5.2 of the mean z displacement of the Na^+ and Cl^- ions from their initial positions. Another indication of the disordered nature of the crystal surface is given by Fig. 5.15 a snapshot of the interface at $t = 1.6\text{ps}$. Fig. 5.16 shows, $\rho(z)$ after 2.35ps the profile is seen to have changed drastically from the beginning of the simulation (see Fig. 5.2). The outer ionic layers have not only moved outwards as shown in Table 5.2 at 2.35ps but also become so diffuse so as to run into one another. The broadening of the peaks now affects all but the 4-5 inner layers. The oxygen profile extends well into the crystalline region. It appears from this simulation that the migration of water into the initially crystalline phase prevails over that of the ions into the aqueous phase. At the end of the simulation only one, a Cl^- ion, has completely broken off the surface by $\Delta z \sim 4.8\text{\AA}$. Despite the dissolution process involved at the interfaces when compared with Fig. 5.2 the overall crystal structure is still quite intact, though it has relaxed outwards slightly. But it has by no means shown the same decrease in density at the centre of the crystal,

FIG. 5.15



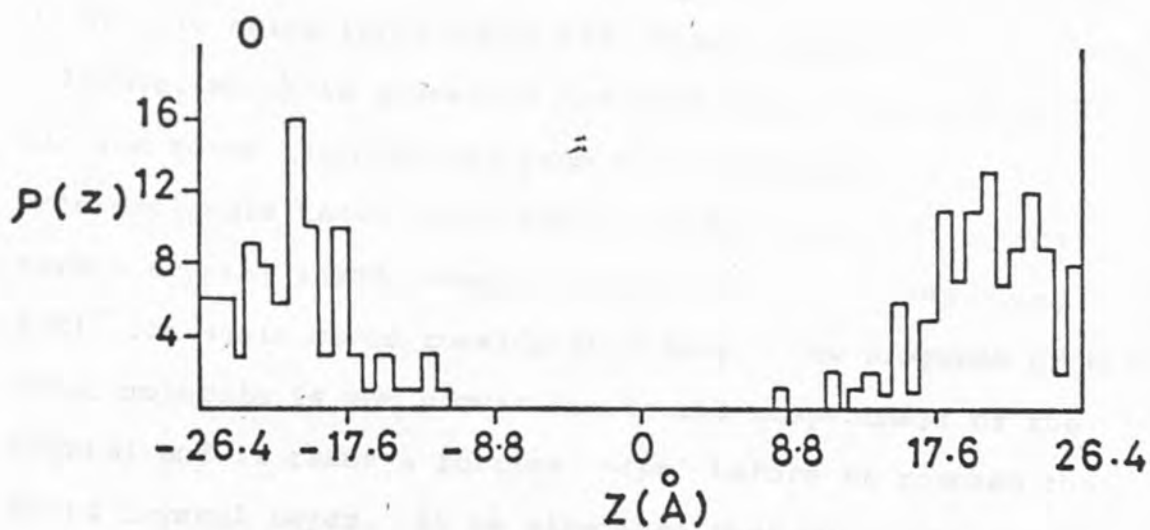
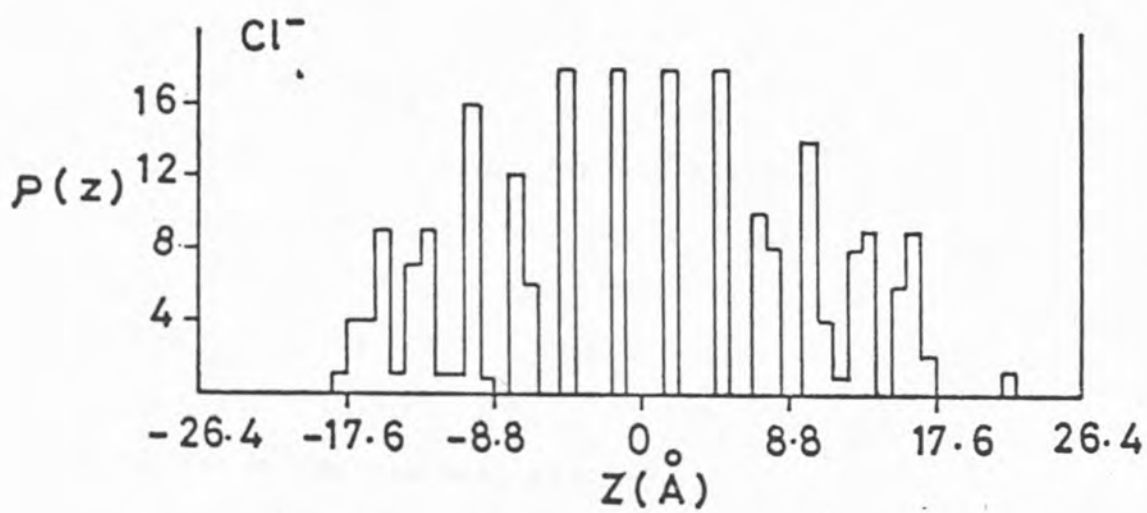
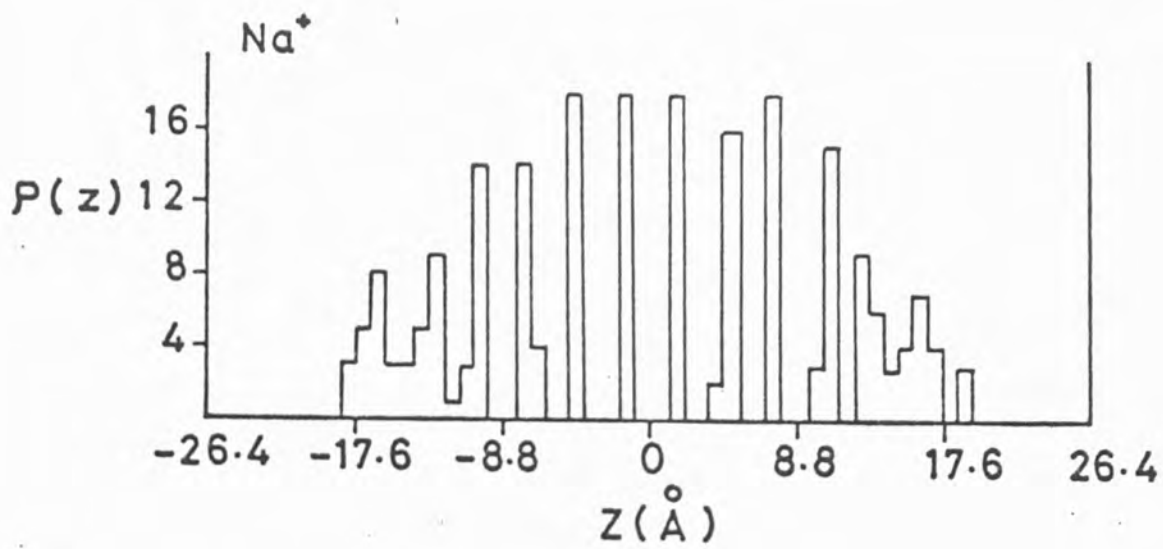


FIG. 5.16

as can be seen by comparing Fig. 5.16 for the 480K simulation with Fig. 5.11 of the 300K simulation. The effective interaction are now not so large and there was now no prior equilibration period for the 480K simulation and thus no increase in density of the water at the surface as in the 300K simulation. This could have allowed Na^+ ions to move outwards slowly but since the water molecules were not necessarily sitting on the Na^+ ions, they soon entered the voids created on the crystal surface caused by the outwards displacement of the Na^+ ions.

The overall temperature change of the 480K simulation, was an increase of about 50-60K though the temperature of this simulation was scaled for the first 0.17ps.

Another study performed was to trace the history of the water molecule that has penetrated the crystal the furthestest from the beginning of this 480K simulation, see Fig. 5.17, this is plotted on the XZ plane. At $t = 0$ the water molecule molecule was near the crystal surface. After a short time the ions moved towards the water, and after 0.5ps a Na^+ is being replaced in its crystal layer by a water molecule, which is almost of the same size. The nearest Cl^- ion moves slightly way from the water molecule. The water molecule takes about another 0.5ps to arrive at the second crystal layer, where it again replaces a Na^+ ion, a Cl^- ion again moves considerably away. The progress of the water molecule is now slower due to the compactness of the crystal and it takes a further 0.5ps before it reaches the third crystal layer. It is also seen that while the water molecules was entering the crystal the inner two layers were not particularly displaced. By the end of the simulation the water molecule has reached the third layer the outer two

$\begin{array}{ccc} + & - & + \\ - & + & - \\ + & - & + \end{array}$	$\begin{array}{ccc} + & - & + \\ & \omega & \\ - & + & - \\ + & - & + \end{array}$
$\begin{array}{ccc} + & - & + \\ - & + & - \\ + & - & + \end{array}$	$\begin{array}{ccc} + & - & + \\ & \omega & + \\ - & & - \\ + & - & + \end{array}$
$\begin{array}{ccc} + & - & + \\ - & + & - \\ + & - & + \end{array}$	$\begin{array}{ccc} + & - & + \\ \omega & & \\ - & + & - \\ + & - & + \end{array}$
$\begin{array}{ccc} + & - & + \\ - & + & - \\ + & - & + \end{array}$	$\begin{array}{ccc} \omega^+ & - & + \\ - & + & - \\ + & - & + \end{array}$

FIG. 5.17

layers are quite distorted are part of the interface.

5.5 Conclusion

The computer simulation studies suggest that at least for some alkali halides the solution process starts by a displacement of the positive ions outwards towards the water. From the simulation at 300K it has been seen that the crystal has been strongly attracted towards the water at either end of it. The simulation at 480K though at a temperature higher than the boiling point of water, may be regarded as a simulation at 300K with charges on the crystal ions of ~ 0.8 , with a change in the depth of the potential well, lessening the ion-water interactions and not causing the crystal as a whole to move towards the water. As the Na^+ move away from the surface since there was no prior equilibration and therefore no water molecules necessarily sitting on the Na^+ ions, the water molecules can enter the interstitial gaps left by the Na^+ ions.

The simulation at 480K has therefore given an interesting indication into the mechanism of the solution process at the interface, this mechanism of water molecules penetrating the crystal as Na^+ ions move out has been observed to a lesser extent at 300K and is therefore likely that at longer time the same kind of process may be involved. The simulations have also shown the solution process at the interface to be exothermic.

CHAPTER 6

FIXED IONIC CRYSTAL-WATER INTERFACE

6.1 Introduction

The molecular dynamics simulation described in Ch.5 was not able to study the nature of the equilibrium ionic crystal-water interface because of the dissolution process involved at short times at the interface. To study properties near a stable interface in which the dissolution process was prevented another simulation was performed with water next to a fixed NaCl crystal. This now enables us to study the water behaviour at the surface averaged over time. The study of water next to a fixed ionic crystal is of relevance in understanding the structural and dynamical properties of water next to an insoluble crystal.

The interaction potentials used are the same as the ones described in Ch.5. Since the ion-ion interactions are not important because the crystal is not allowed to move, for computational economy they were not calculated except in the fourier routine where it would have been more complicated to remove the ion-ion interactions. A timestep of 0.25Fs was used again and the time for each step on the Cray-1 computer was now 2.5s.

The simulations performed were (a) at room temperature, 300K; and (b) at 480K. The simulation at the higher temperature was for the same reason already described in Ch.5. In (b) a simulation with $\text{H}_2\text{O}^{3,18}$ next to a fixed NaCl crystal was also carried out to allow us to use a timestep of 1Fs.

After sufficient equilibration of water next to the fixed sodium chloride the following results were obtained.

6.2 Simulation at 300K

(A) Density profile of water in the z direction.

Fig. 6.1 gives $\rho(z)$ for the oxygens and hydrogens respectively. The hydrogen $\rho(z)$ is divided by a factor of two to make it comparable to the oxygen $\rho(z)$. $\rho(z)$ here compares well with the density profile see Fig. 5.3 observed in Ch.5 before the dissolution process. The density profile in Fig. 6.1 is now an average over 4000 steps \equiv lps, since now dissolution is prevented and the equilibrium properties at the surface are now more clearly observed as an average over time. At both the surfaces it is clearly seen that there is a greater density of water at the surface than in the bulk and that $\rho(z)$ is different to the one of water at $t = 0$ next to the crystal shown in Fig. 5.2, before crystal and water have been allowed to interact. The oxygens are also closer to the crystal surface than the hydrogens, this is more obvious with a smaller Δz in the $\rho(z)$. Further away from the surface the oxygen $\rho(z)$ appears to be oscillatory indicating that the presence of the crystal introduces layering of the water molecules extending at least 2-3 molecular diameters away from the surface. $\rho(z)$ for the hydrogens is slightly less oscillatory because of the greater orientational randomness of the water molecules.

(B) Description of what is happening at the surface.

Fig. 6.2 shows a snapshot which gives a typical picture of the water molecules at either surface. The snapshot is of the xy plane viewed from the z direction. The 6×6 arrangement of Na^+ and Cl^- ions is seen also the first layer of water molecules. The overall picture shows the water

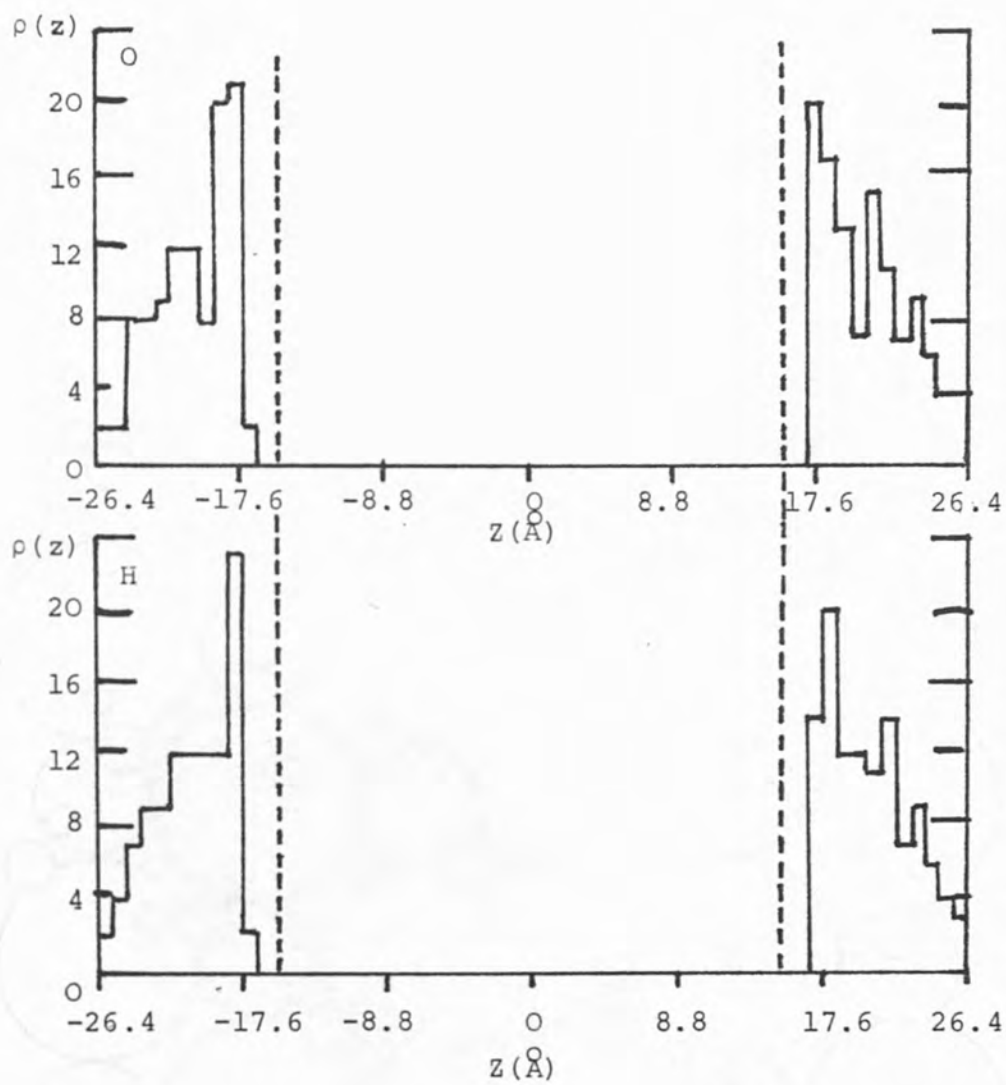
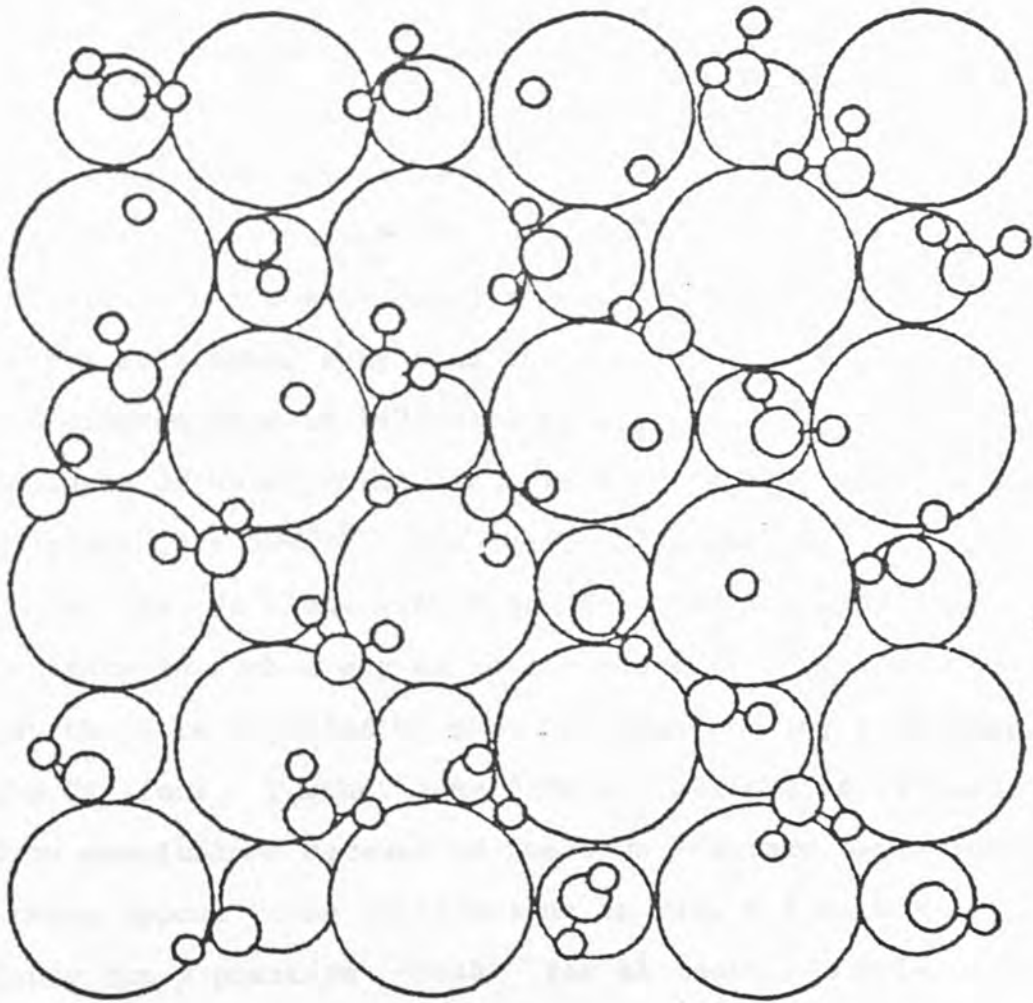


FIG. 6.1

FIG. 6.2



molecules sitting above the Na^+ ions, with a tendency for the hydrogens to point away from chloride ions. The oxygens are also seen to be closer to the surface than the hydrogens as observed in the density profile, see Fig. 6.1.

To confirm the conclusions drawn from the Fig. 6.2 we show a time averaged density profile again over 4000 steps in the x and y directions at both surfaces, see Figs. 6.3 and 6.4. In all instances one clearly sees there are six positions of density maxima corresponding to the water molecules sitting above the Na^+ ions at the surface.

(C) Orientation of the water molecules

The orientation of the water molecules near the crystal surface is shown in Fig. 6.5: by $\langle \cos\theta \rangle$ where θ is the angle between the dipole moment vector of the water molecule and the outward normal to the crystal surface. Near both surfaces the dipole vector points away from the surface i.e. the hydrogens are further away from the surface than the O atom. On the diagram this is indicated by a positive $\langle \cos\theta \rangle$. The first layer of water molecules have a value of $\cos\theta \approx 0.6$ which gives $\theta = 50-60^\circ$. The reasons for this are the oxygens lie above the Na^+ ions with hydrogens pointing away from the surface in such a way as to lie above the chloride ions as (a) they are repelled by the Na^+ ions and (b) attracted by the Cl^- ions. Further away from the surface it is hard to draw conclusions because of the high standard deviations, but there appear to be oscillations in Fig. 6.5 with a tendency for a positive $\langle \cos\theta \rangle$ for at least 2-3 molecular diameters away from the surface. At the edge of the computational box the periodic boundary conditions force $\langle \cos\theta \rangle$ to go to

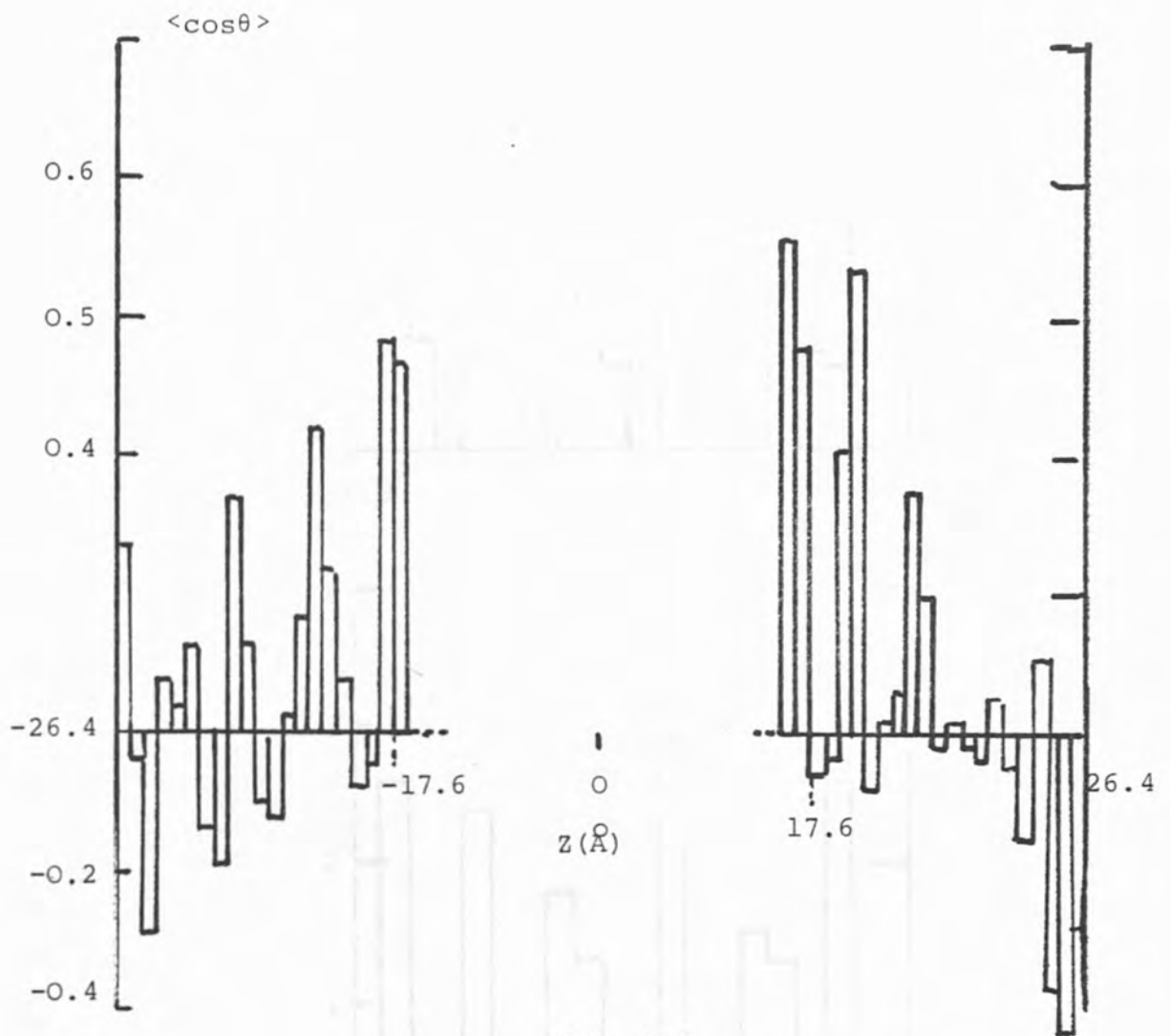


FIG. 6.5

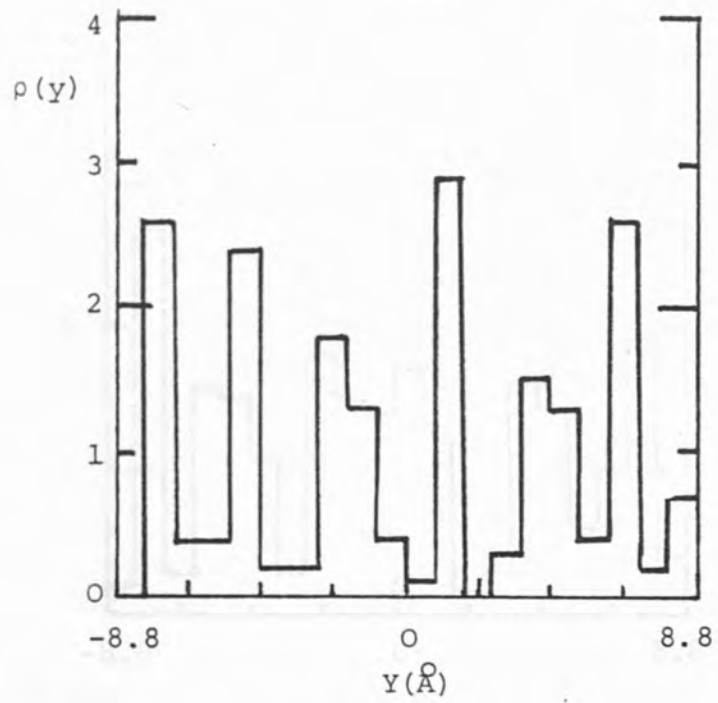
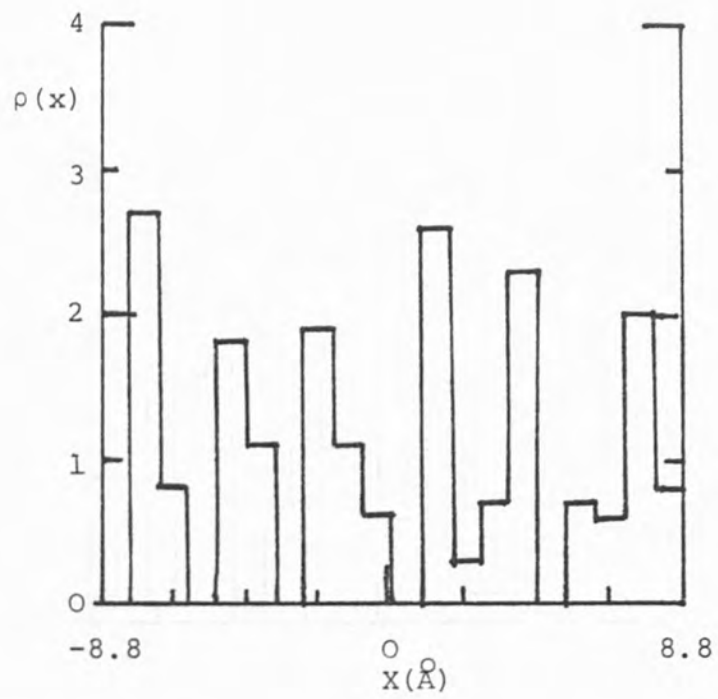


FIG. 6.4

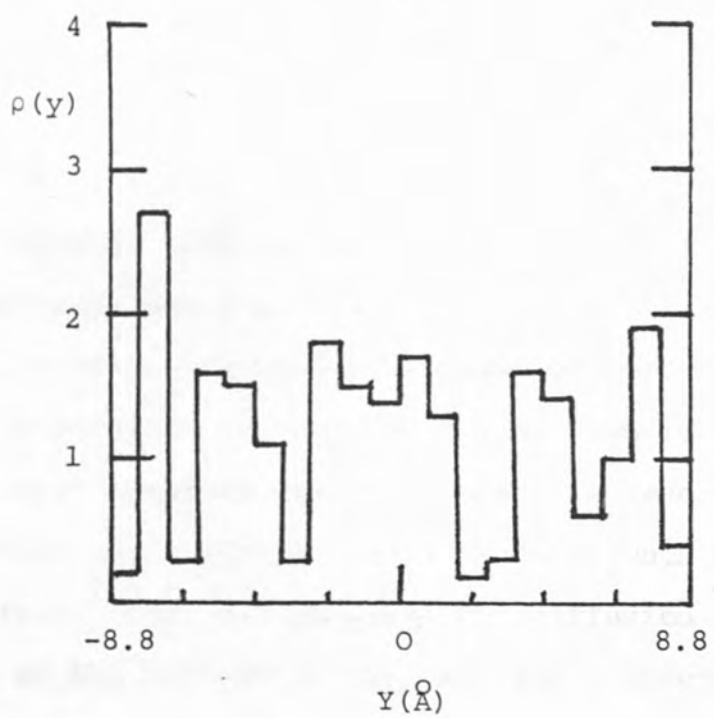
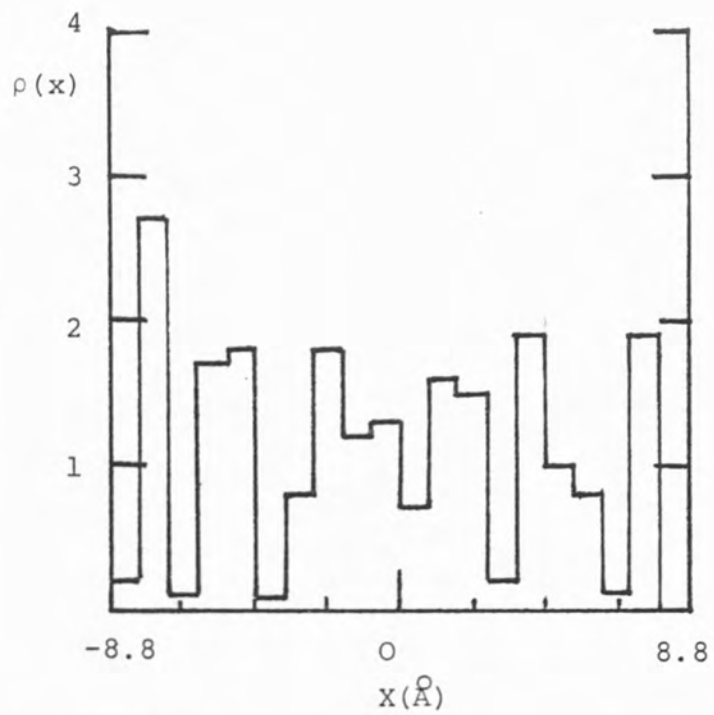


FIG. 6.3

zero. The results are again an average over 4000 steps.

(D) Bond length and angle measurements

In Table 6.1 the mean bond lengths and angle of the water molecules at the surface are compared with the ones in the bulk liquid averaged over 4000 steps.

TABLE 6.1 Bond length and angle measurements.

	$\langle \hat{\text{HOH}} \rangle$	$\langle \text{HH}(\overset{\circ}{\text{O}}) \rangle$	$\langle \text{OH}(\overset{\circ}{\text{O}}) \rangle$
Surface	97.8°	1.476	0.980
Bulk	99.8°	1.491	0.976

The bond angle at the surface is 2° smaller than in the bulk. The molecules at the surface are distorted because of the tendency of the H atoms to point towards the Cl⁻ ions.

(F) Diffusion

The diffusion of the water molecules which have remained in the surface layer is compared with a layer of similar thickness in the bulk, see Fig. 6.6. This is an average over 4000 steps, with a correlation interval of 2000 steps. During this 1ps simulation 37 water molecules have remained in the surface layer compared with 9 in the bulk layer. Fig. 6.6 shows that the diffusion in the bulk is much greater than at the surface. Fig. 6.7 compares the diffusion of the water molecules at the surface in the x, y and z directions. We see that there is greater diffusion in the x and y direction (parallel to the surface) and very little in the z direction (perpendicular to the surface). It appears though that the molecules at the surface are not diffusing away from the Na⁺ ions on the top of which they are sitting.

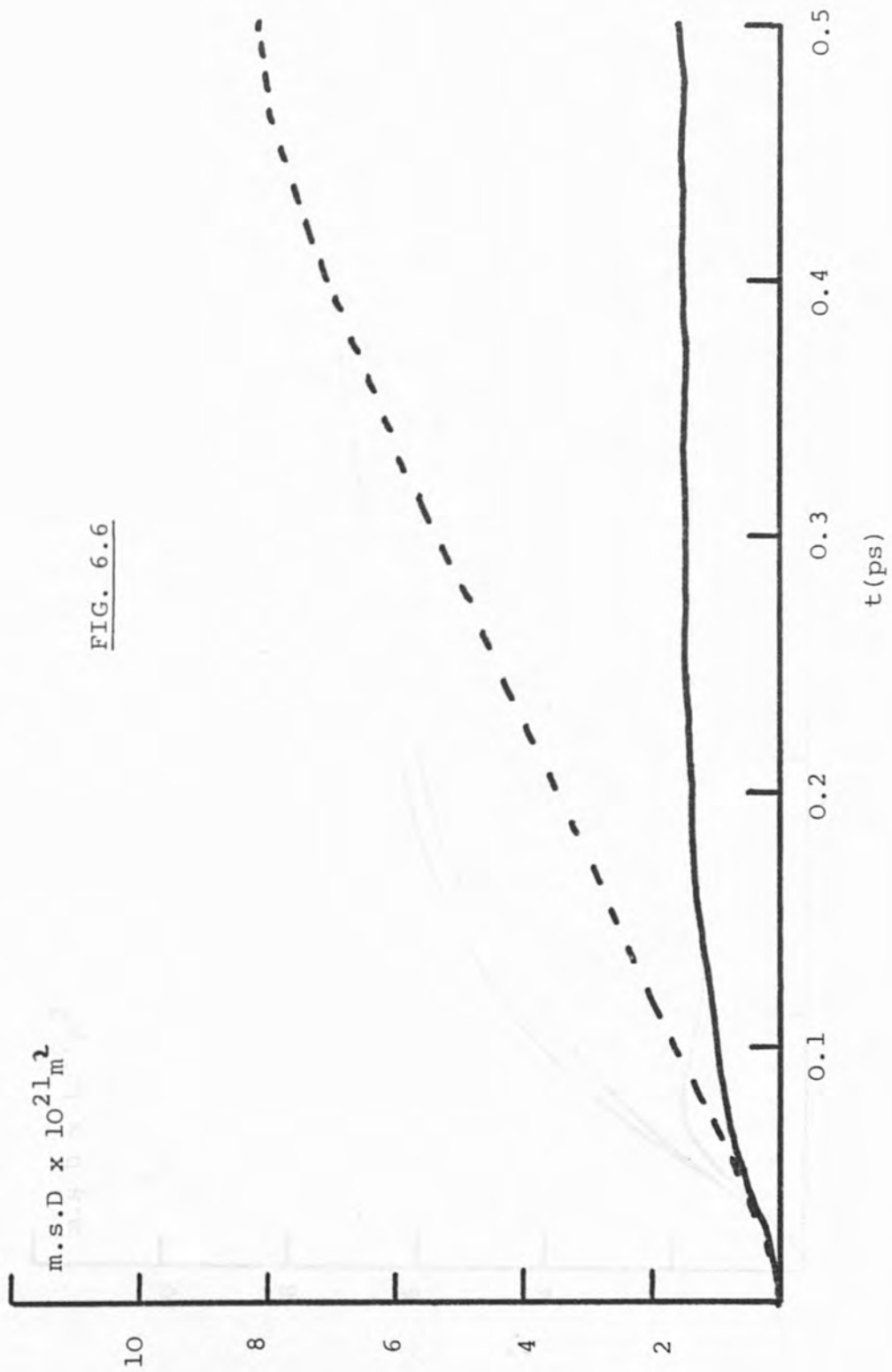
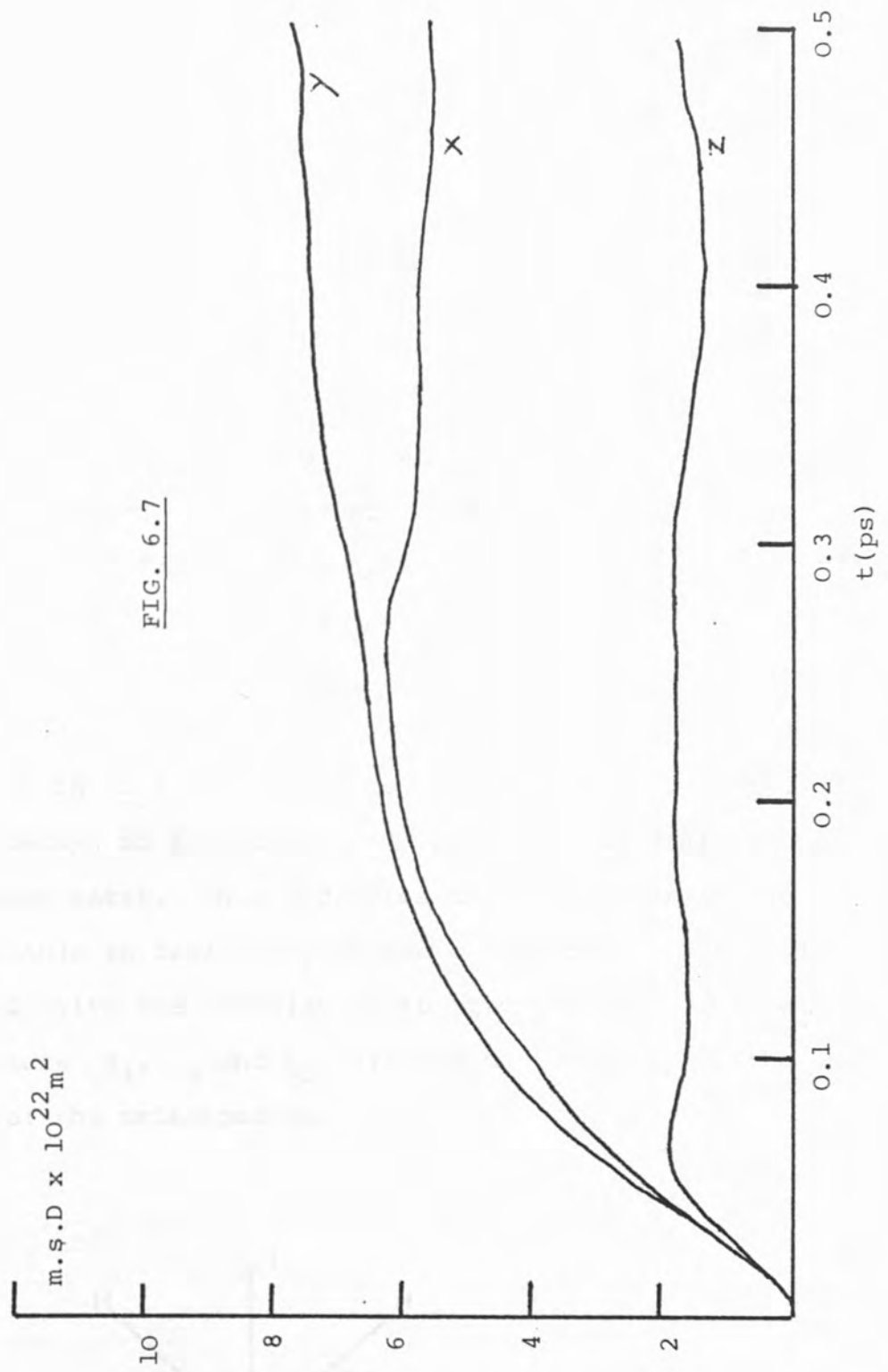


FIG. 6.6



(G) Autocorrelation Functions

Fig. 6.8 gives the angular momentum correlation function, $A_J(t)$ defined by

$$A_J(t) = \frac{\langle \underline{J}(0) \cdot \underline{J}(t) \rangle}{\langle \underline{J}^2 \rangle}$$

where \underline{J} is the angular momentum of the molecule, see Ch.1. All the results described in this section are averaged over 4000 steps with a correlation interval over 2000 steps. We compare the surface (full line) and bulk water molecules (dashed line) that have remained in these layers during the simulation, they are also compared with the angular momentum correlation function of pure water (dotted line). 37 molecules remained in the surface layer, and 9 in the bulk layer $A_J(t)$ decays to zero faster and has a deeper minimum than for the bulk molecules. The surface molecules are in a more dense environment and also next to the crystal surface, causing a faster change in $A_J(t)$. The correlation function for bulk water also decays to zero faster and has a deeper minimum than for pure water. This indicates that the water in the bulk may be able to feel the presence of crystal. Figs. 6.9, 6.10 and 6.11 give the correlation functions for $\langle \underline{J} \cdot \underline{e}_1 \rangle$, $\langle \underline{J} \cdot \underline{e}_2 \rangle$ and $\langle \underline{J} \cdot \underline{e}_3 \rangle$ where \underline{e}_1 , \underline{e}_2 and \underline{e}_3 are the unit vectors in the directions of the principal axis.

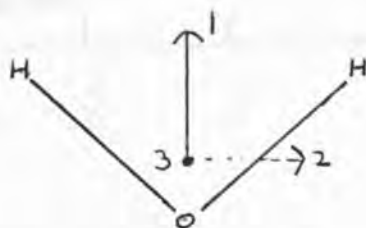


Fig. 6.12

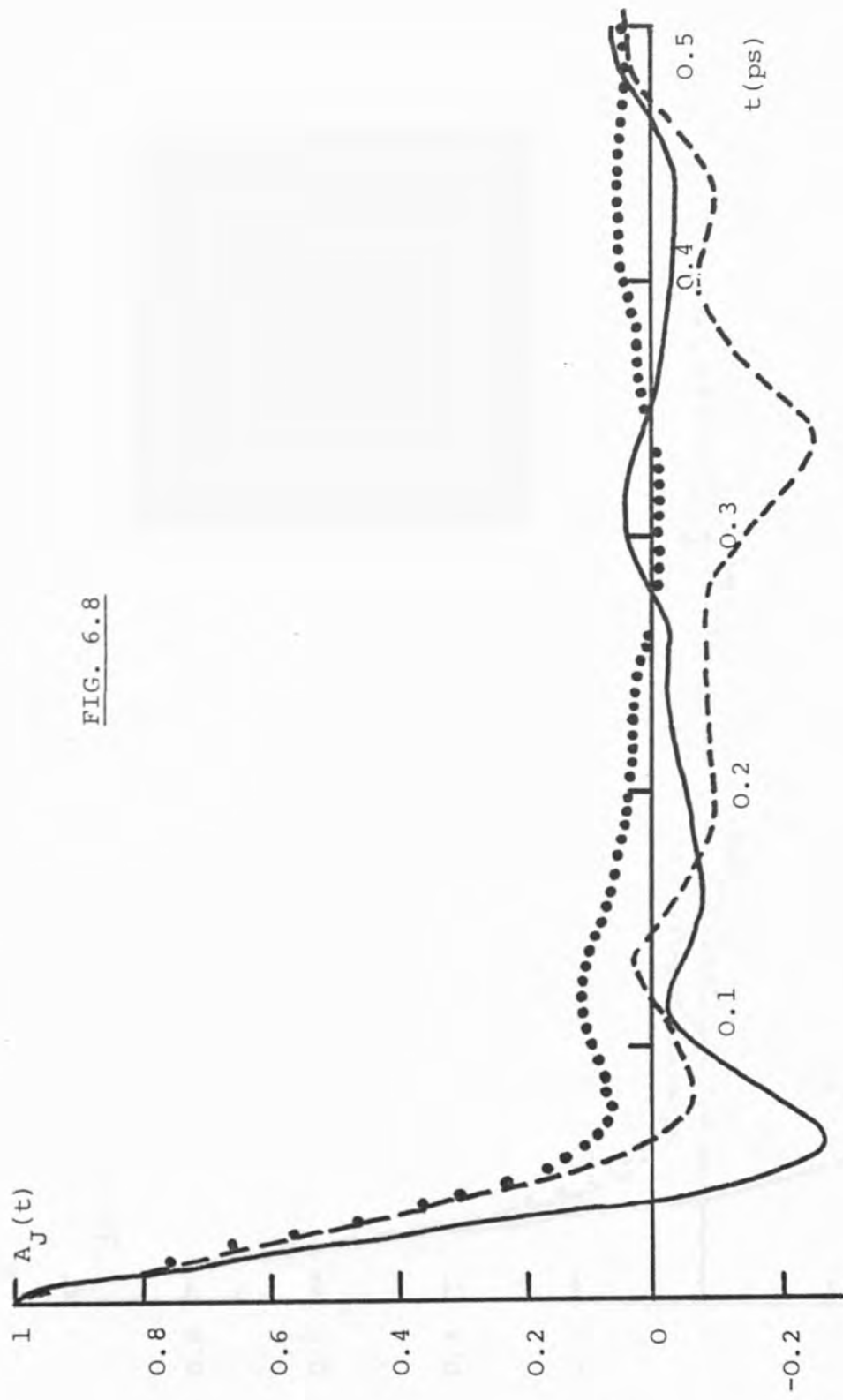


FIG. 6.8

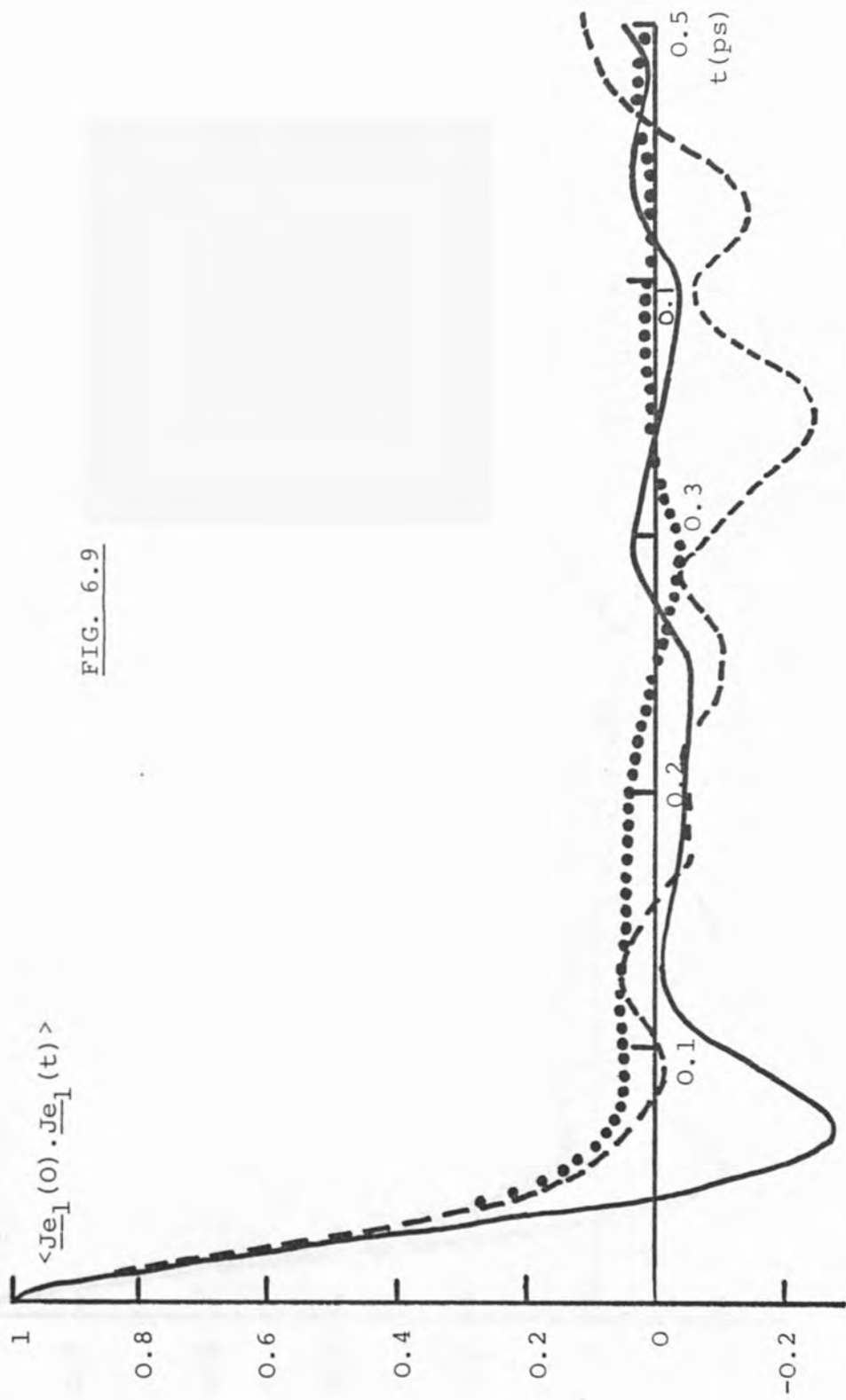


FIG. 6.9

FIG. 6.10

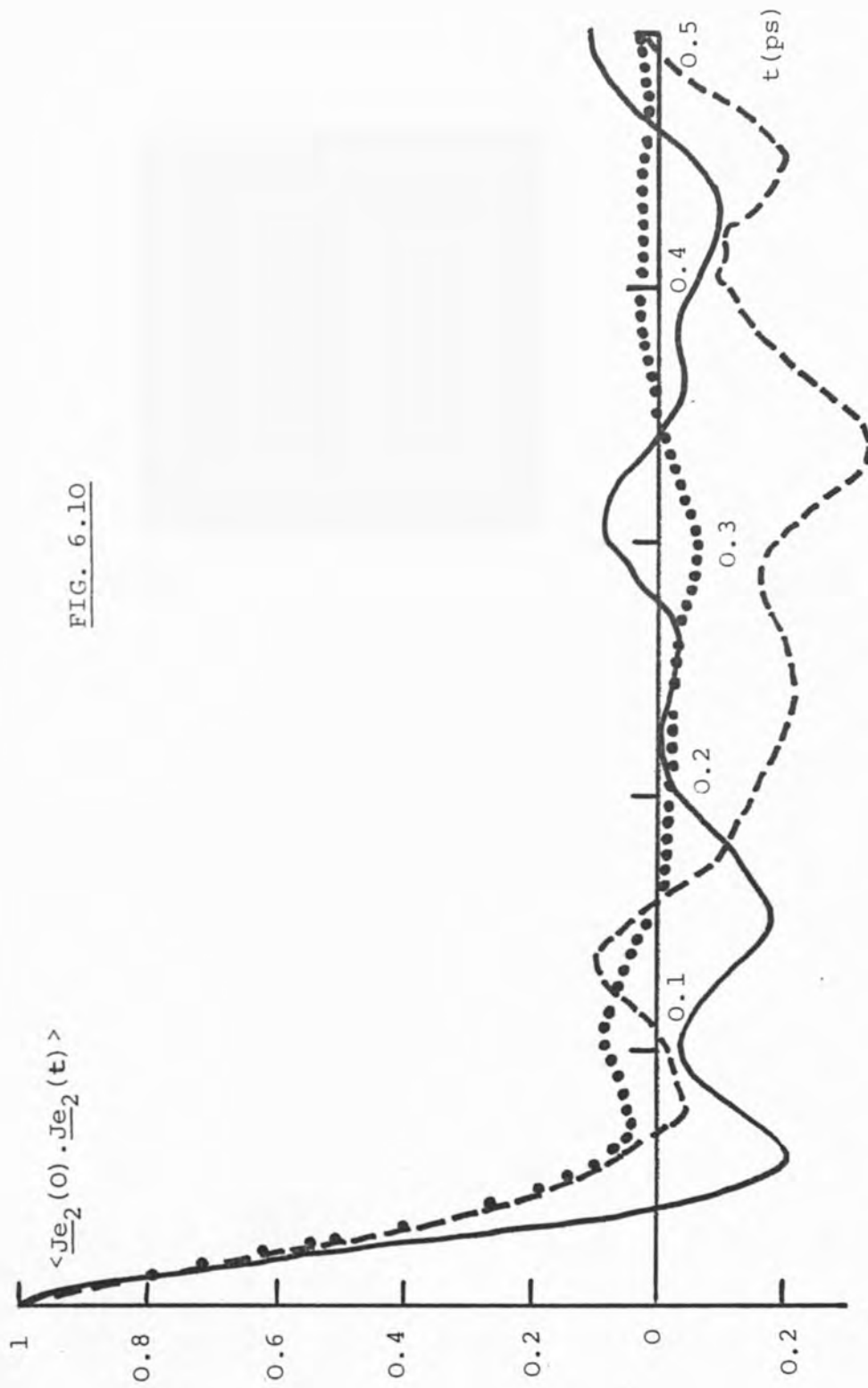
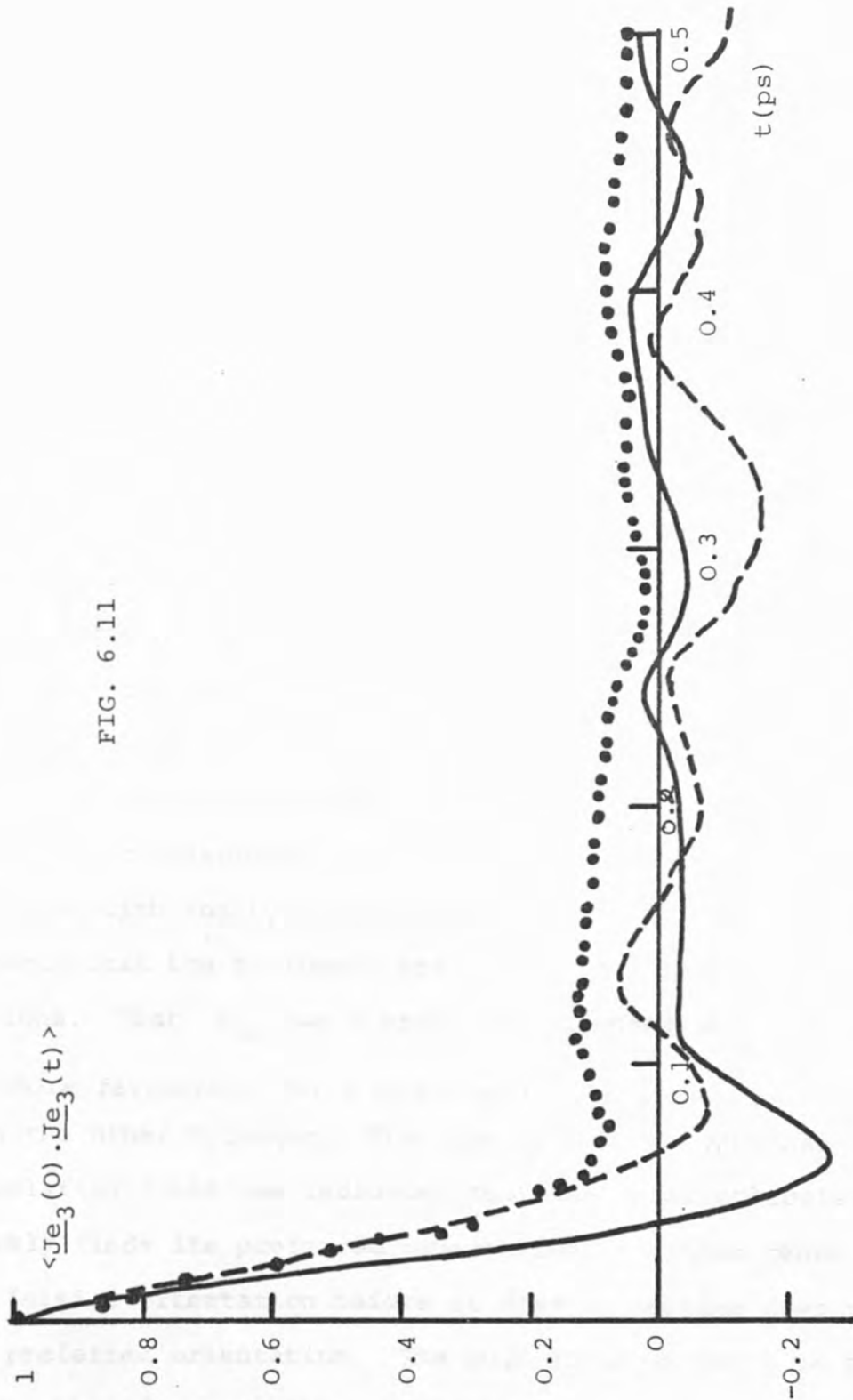
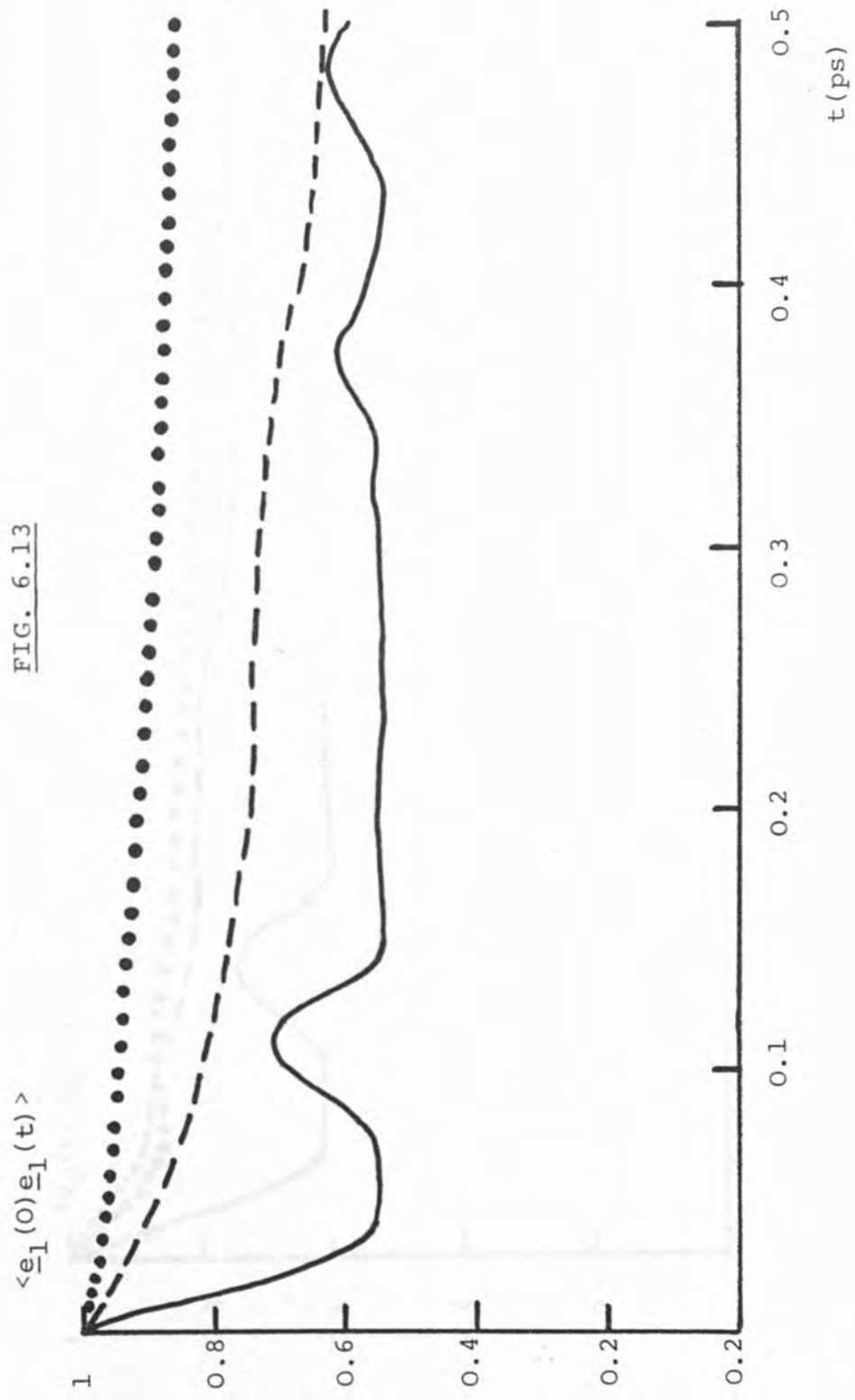


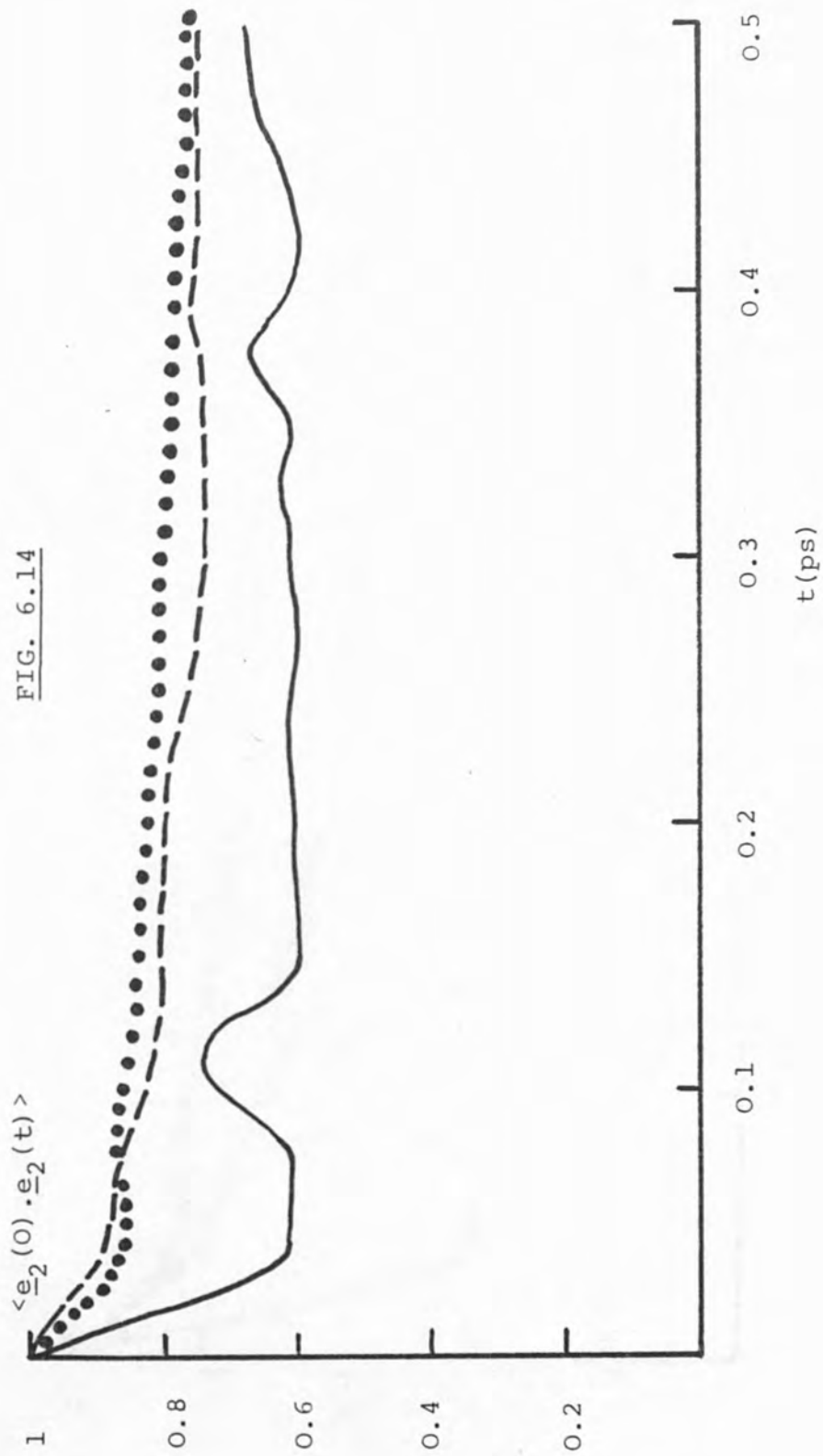
FIG. 6.11



In all cases the correlation function goes to zero and has a deeper minimum for the surface molecules compared to the bulk. The bulk goes to zero faster and has a deeper minimum than for pure water. After 0.2-0.3ps the correlation function for bulk water has a long negative tail, which appears to be too large for noise, this is difficult to interpret though it could be a delayed ordering effect. Figs. 6.13, 6.14 and 6.15 give the act's of \underline{e}_1 , \underline{e}_2 and \underline{e}_3 , the orientational correlation functions about the three axes. These correlation functions all decay to zero much slower than the angular momentum correlation functions. The correlation functions for the surface is faster than for the bulk, but flatten off instead of continuing to zero. This means that there is a preferred orientation, for \underline{e}_1 , it flattens off at about 0.57, $\underline{e}_1(0) \cdot \underline{e}_1(t) = \cos\theta$, this is in agreement with Fig. 6.5 for the orientation of the water molecules at the surface; so the water molecules as previously discussed lie above the Na^+ ions, with the hydrogens closer and the value of $\langle \cos\theta \rangle$ suggests that the hydrogens are trying to align above the Cl^- ions. That \underline{e}_2 has a preferred orientation suggests it is more favourable for 1 hydrogen to lie above one Cl^- more than the other hydrogen. The hump in the orientational correlation functions indicates that the water molecules quickly finds its preferred orientation, but then tends to its initial orientation before it finally settles down to the preferred orientation. The bulk again is going to zero faster than for pure water indicating a long range ordering.

FIG. 6.13





Equilibrium properties of water near the surface of a crystal at 480K. Fig. 6.15 gives the time evolution of the correlation function $\langle \vec{e}_3(0) \cdot \vec{e}_3(t) \rangle$ for water molecules at the surface. The solid line shows the correlation function for water molecules at the surface, and the dashed line shows the correlation function for water molecules in the bulk. The dotted line shows the correlation function for water molecules at the surface, but with the hydrogen atoms removed. The correlation function for water molecules at the surface (solid line) starts at 1.0 at $t=0$ and decays to approximately 0.4 at $t=0.5$ ps. The correlation function for water molecules in the bulk (dashed line) starts at 1.0 at $t=0$ and decays to approximately 0.4 at $t=0.5$ ps. The correlation function for water molecules at the surface with hydrogen atoms removed (dotted line) starts at 1.0 at $t=0$ and decays to approximately 0.4 at $t=0.5$ ps.

FIG. 6.15

$$\langle \vec{e}_3(0) \cdot \vec{e}_3(t) \rangle$$

t (ps)

6.3 Simulation at 480K

(A) Equilibrium properties

Fig. 6.16 gives the density profile of water next to a fixed crystal at 480K. The density of water is greater at the surface than in the bulk and the oxygens slightly closer to the surface than the hydrogen. Comparing with Fig. 6.1 the density is slightly less at the surface at 480K. Again there is evidence of layering away from the surface. Fig. 6.17 shows a snapshot of the water molecules sitting on the Na^+ ions with the hydrogens attempting to align above the Cl^- ions. Figs. 6.18 and 6.19 give the density profile of water in the x and y directions at both the surfaces. Six positions of density maxima are seen corresponding to the water molecules sitting above the Na^+ ions.

The orientation of the water molecules is shown in Fig. 6.20 by $\langle \cos\theta \rangle$, θ being the angle between the dipole moment vector of the water molecule and the outward normal to the crystal surface. Near both interfaces the dipole vector points away from the surface, this is indicated by a positive $\langle \cos\theta \rangle$ again showing that the oxygens are closer to the surface. At the surface $\langle \cos\theta \rangle \approx 0.6$, which gives $\theta = 50-60^\circ$. θ being reduced from 90° as the hydrogens try to align above the Cl^- ions. The tendency for a positive $\langle \cos\theta \rangle$ is maintained further away from the surface, though there are now large standard deviations. The bond angle at the surface is as at 300K 2° smaller, and the OH bond length slightly greater, see Table 6.2.

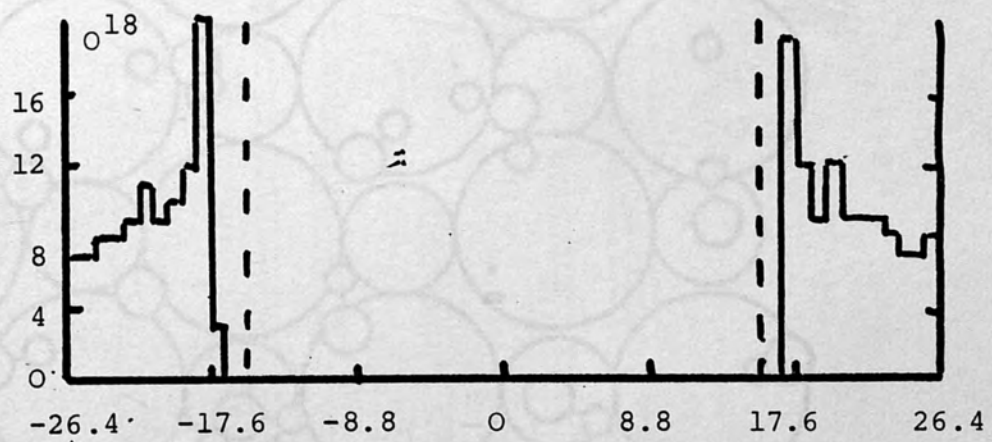
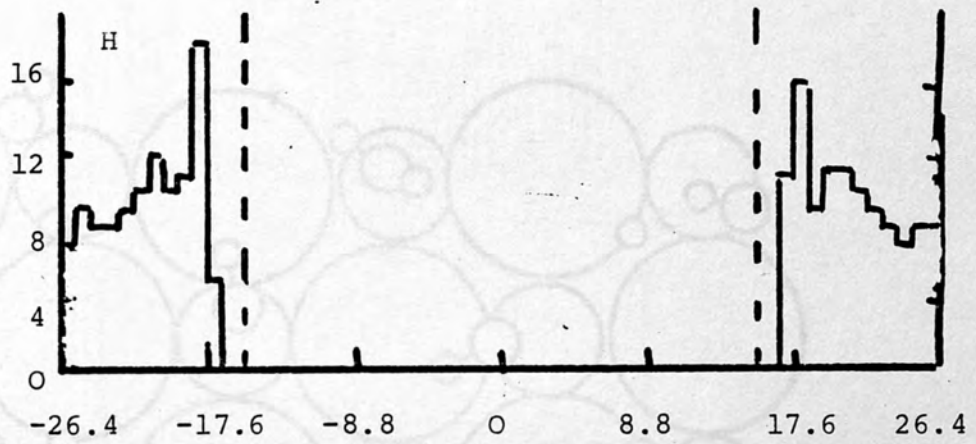
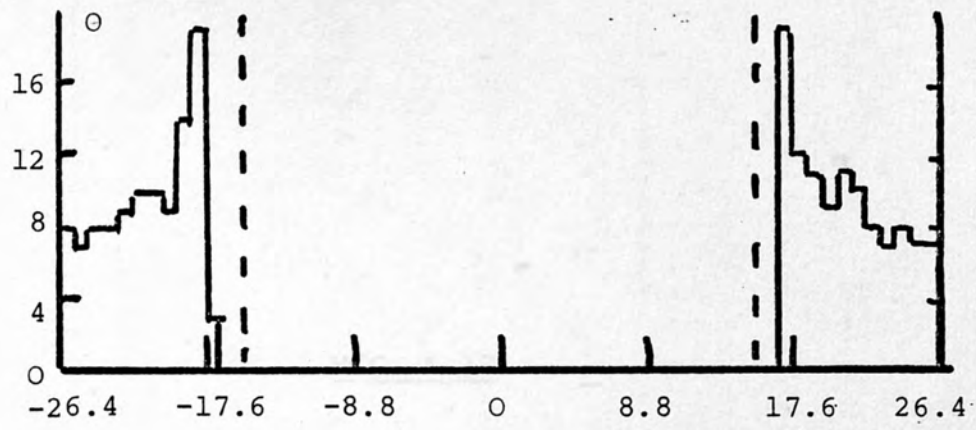


FIG. 6.16

FIG. 6.17

FIG. 6.17

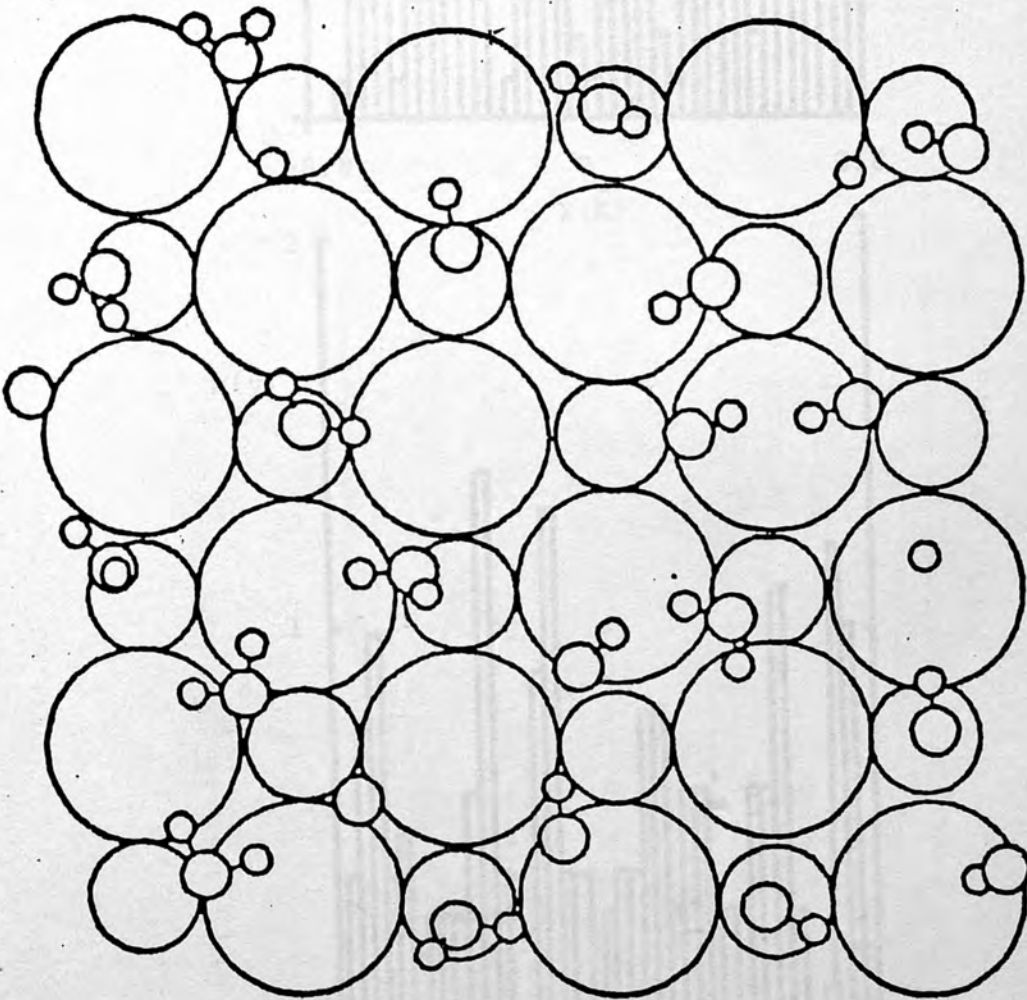


FIG. 6.18

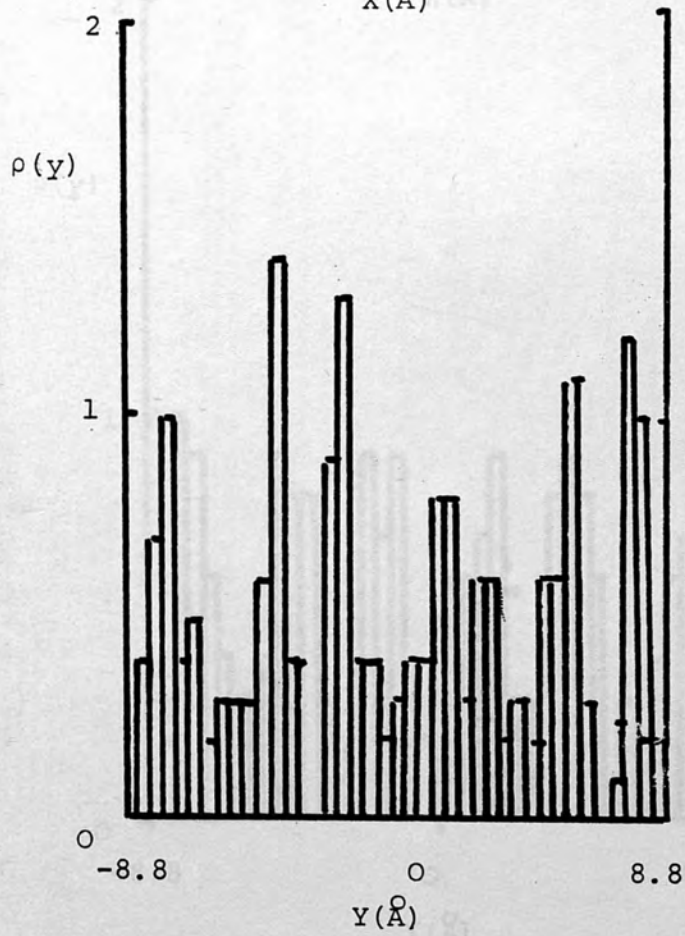
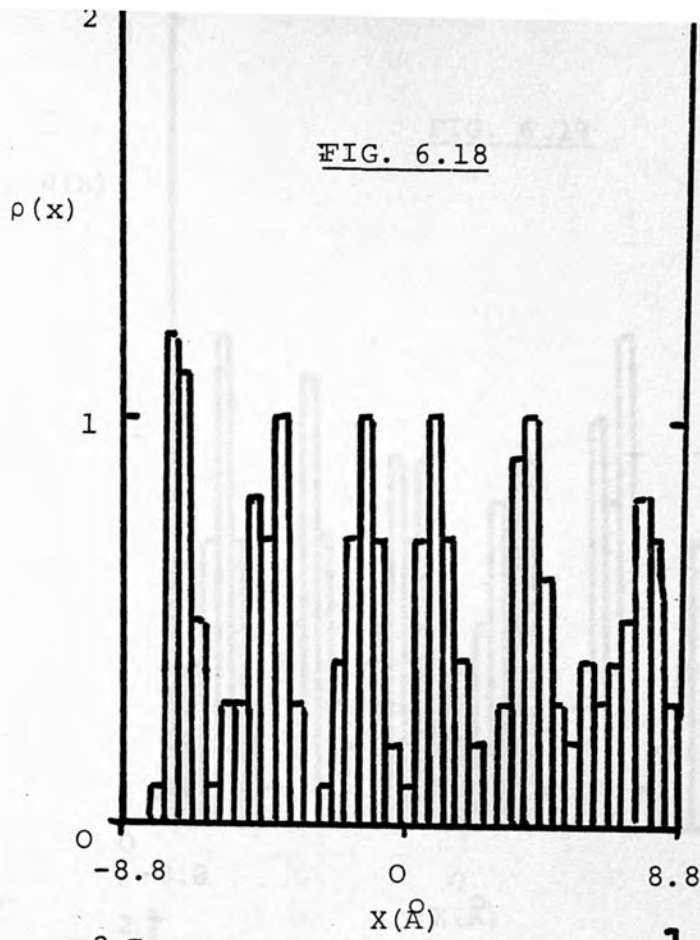


FIG. 6.19

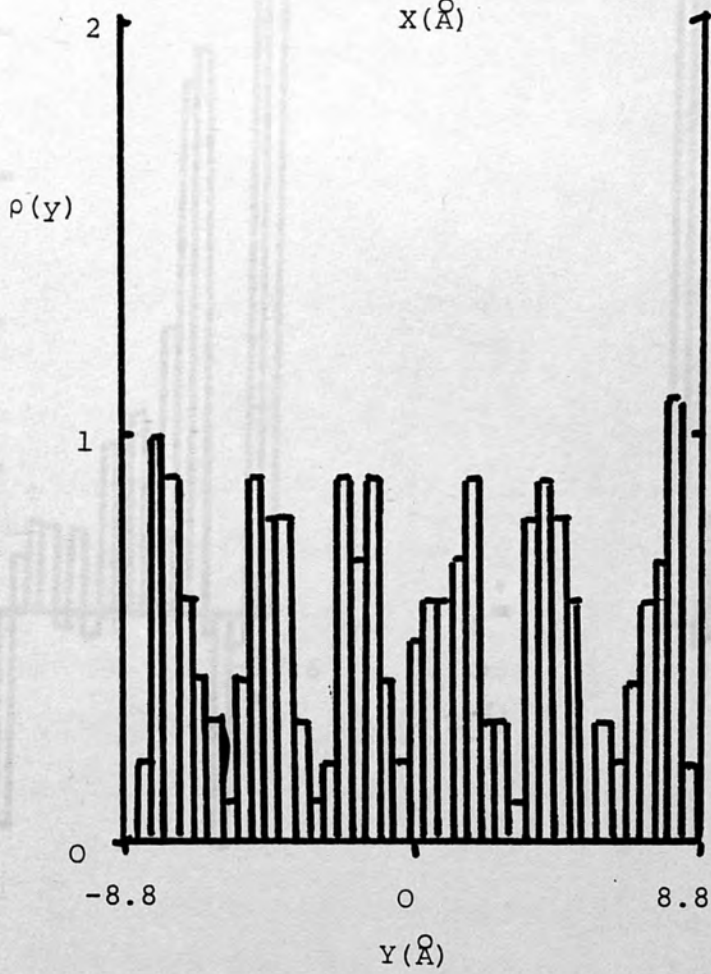
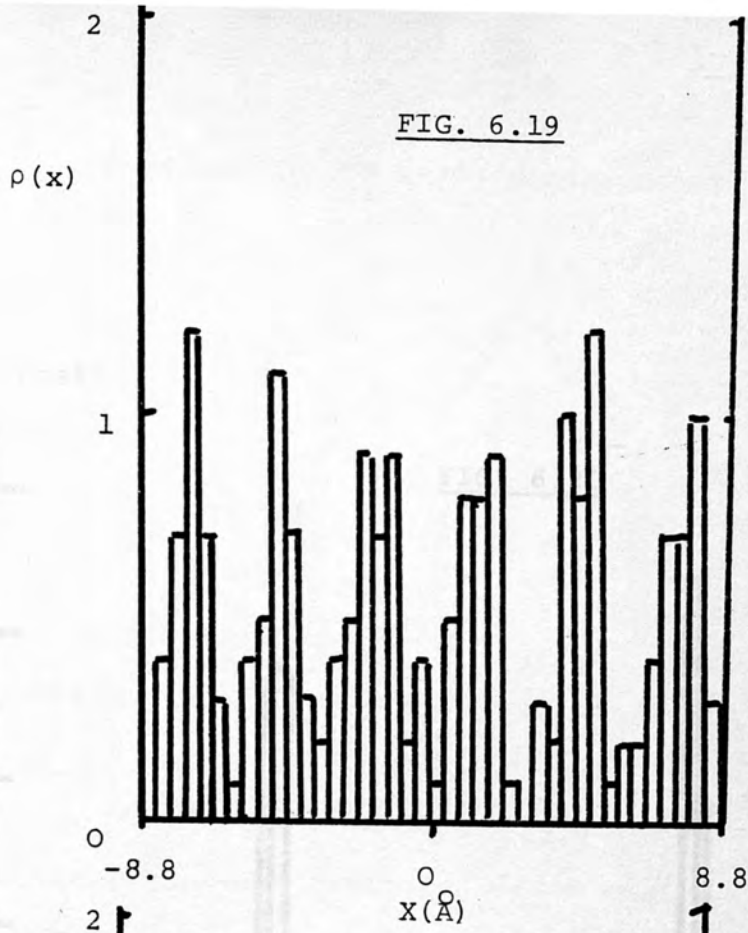


TABLE 6.2 Bond length and angle measurements

	$\langle \text{HOH} \rangle$	$\langle \text{OH}(\text{\AA}) \rangle$	$\langle \text{OH}(\text{\AA}) \rangle$
Water	104.5°	1.498	0.978
Ice	103.8°	1.502	0.973

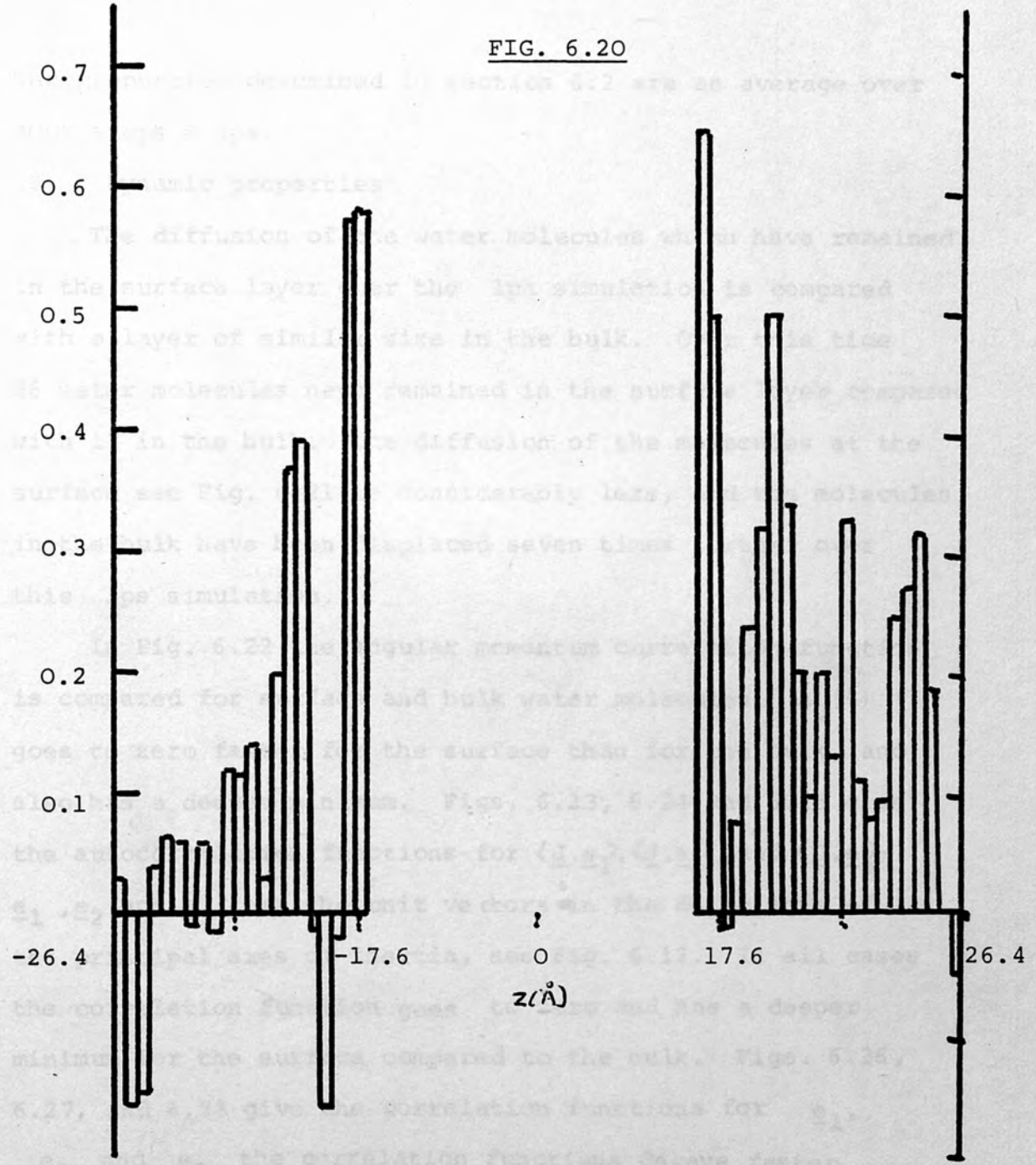


TABLE 6.2 Bond length and angle measurements

	$\hat{\langle \text{HOH} \rangle}$	$\langle \text{HH}(\text{\AA}) \rangle$	$\langle \text{OH}(\text{\AA}) \rangle$
Surface	99.5°	1.498	0.978
Bulk	101.6°	1.502	0.973

The properties described in section 6.2 are an average over 4000 steps = 1ps.

(B) Dynamic properties

The diffusion of the water molecules which have remained in the surface layer over the 1ps simulation is compared with a layer of similar size in the bulk. Over this time 26 water molecules have remained in the surface layer compared with 17 in the bulk. The diffusion of the molecules at the surface see Fig. 6.21 is considerably less, and the molecules in the bulk have been displaced seven times further over this 1ps simulation.

In Fig. 6.22 the angular momentum correlation function is compared for surface and bulk water molecules. $A_J(t)$ goes to zero faster for the surface than for the bulk, and also has a deeper minimum. Figs. 6.23, 6.24 and 6.25 give the autocorrelation functions for $\langle \underline{J} \cdot \underline{e}_1 \rangle$, $\langle \underline{J} \cdot \underline{e}_2 \rangle$ and $\langle \underline{J} \cdot \underline{e}_3 \rangle$; \underline{e}_1 , \underline{e}_2 and \underline{e}_3 are the unit vectors in the directions of the principal axes of inertia, see Fig. 6.12. In all cases the correlation function goes to zero and has a deeper minimum for the surface compared to the bulk. Figs. 6.26, 6.27, and 6.28 give the correlation functions for \underline{e}_1 , \underline{e}_2 and \underline{e}_3 the correlation functions decays faster for the surface than the bulk. After the initial rapid change the correlation functions at the surface do not go to zero but flatten off indicating a preferred orientation

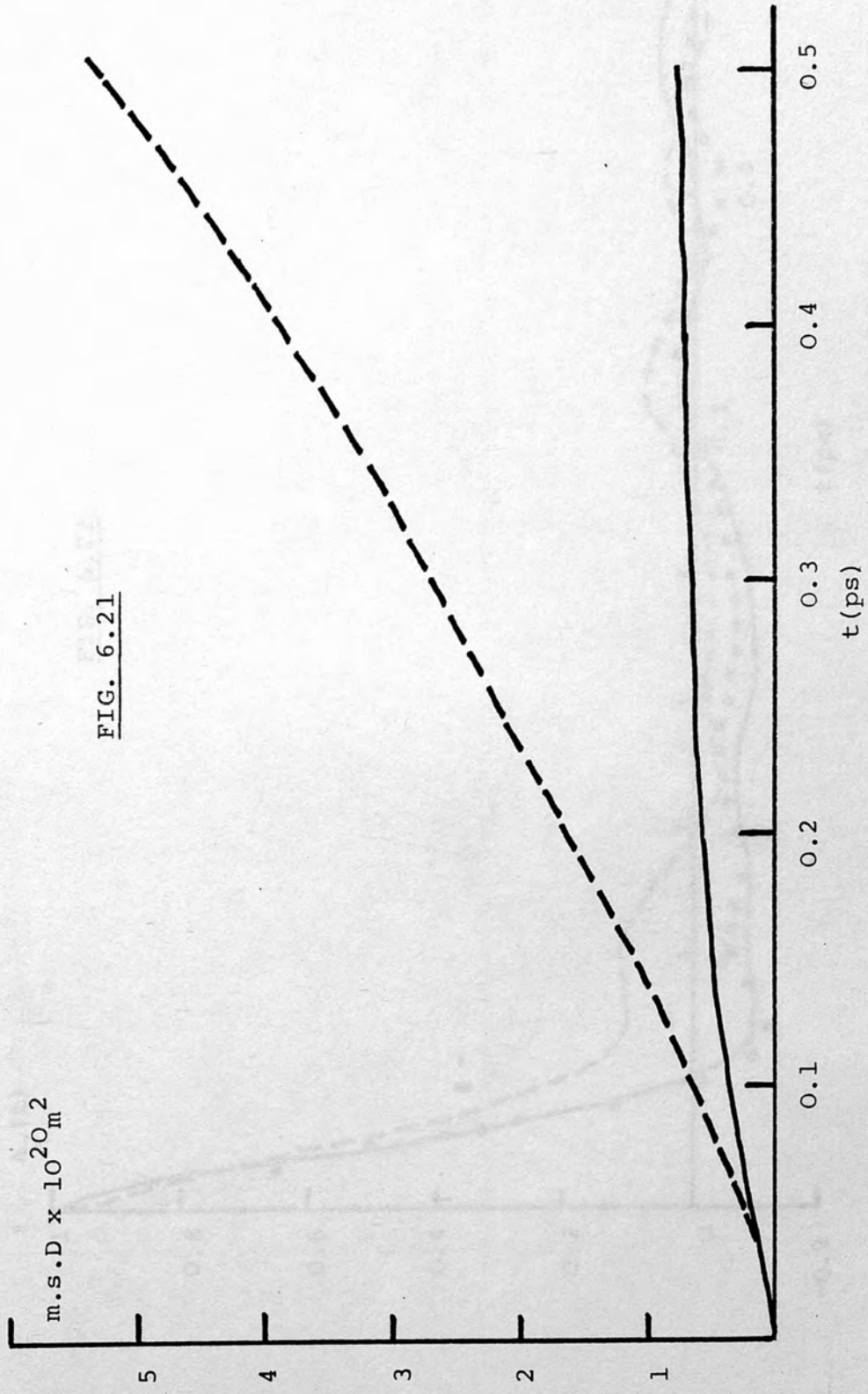


FIG. 6.21

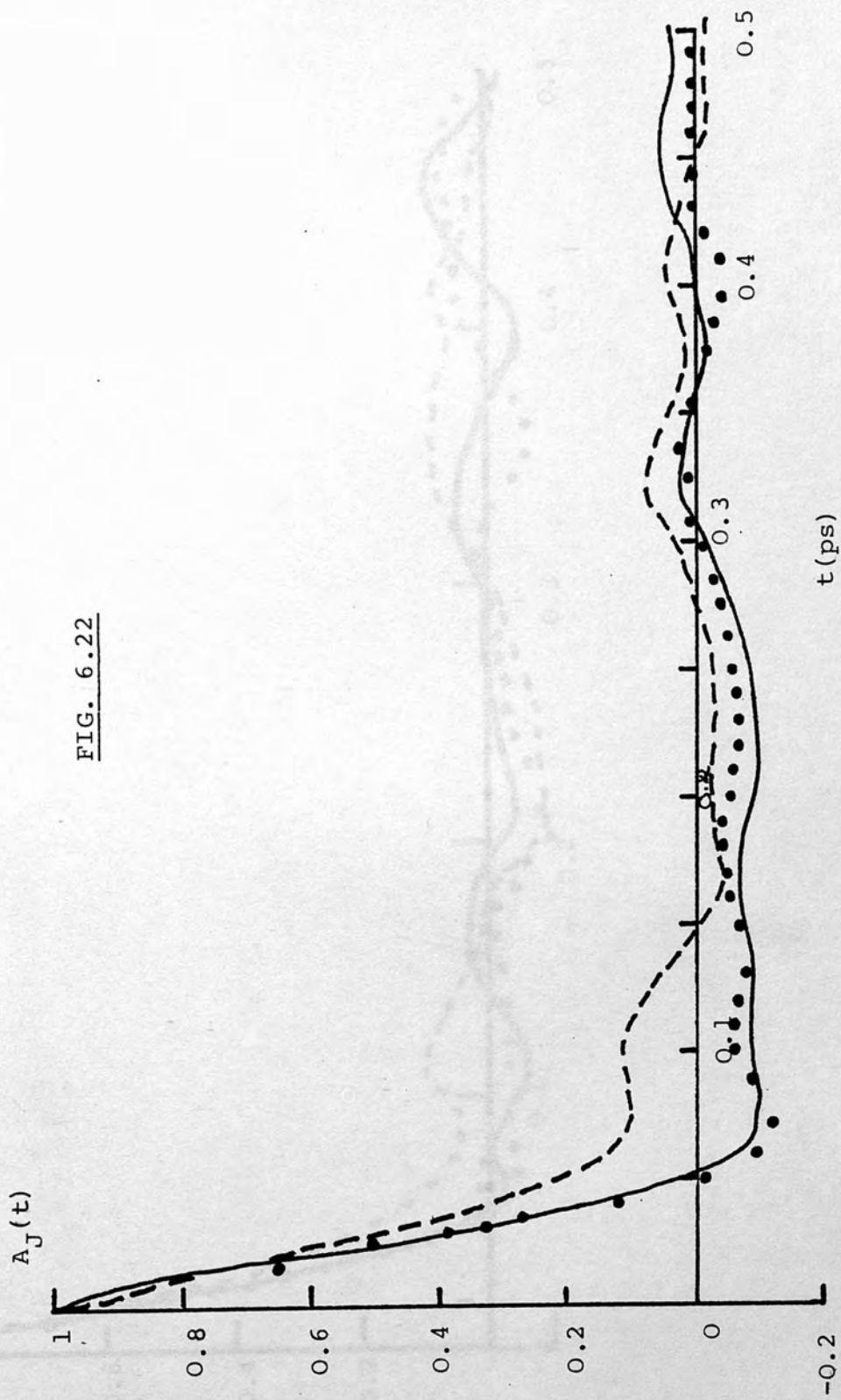


FIG. 6.22

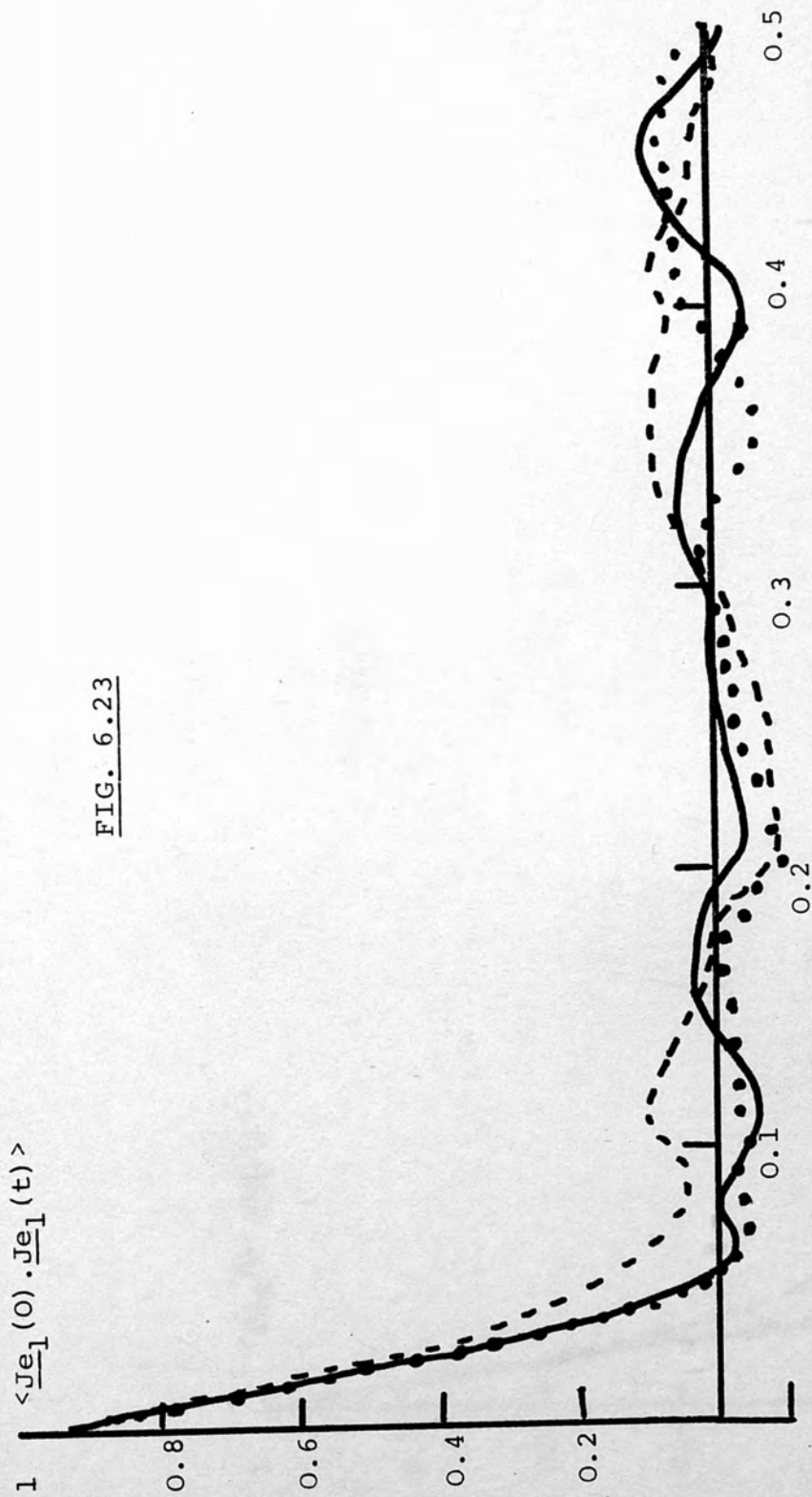


FIG. 6.23

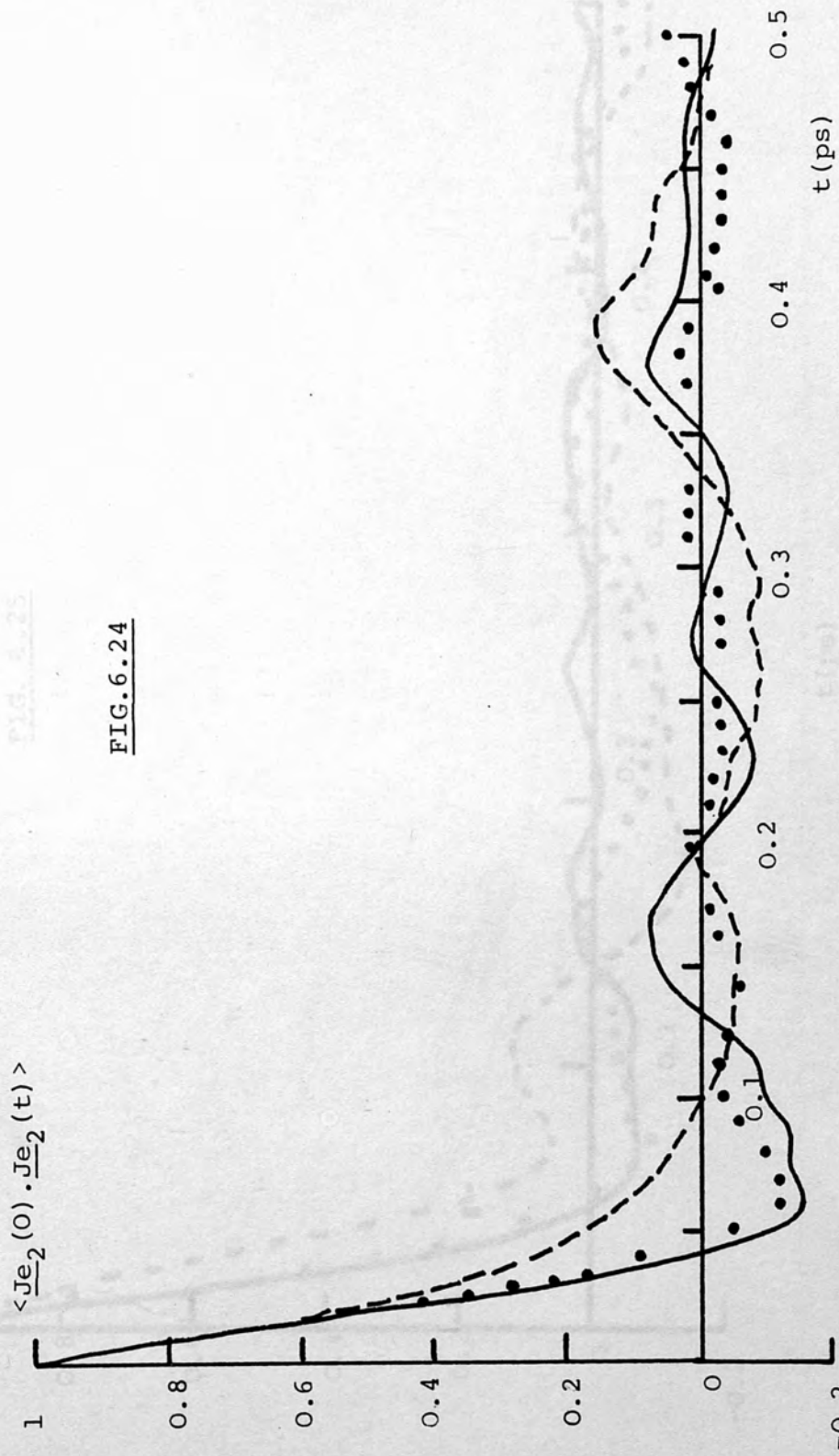


FIG. 6.24

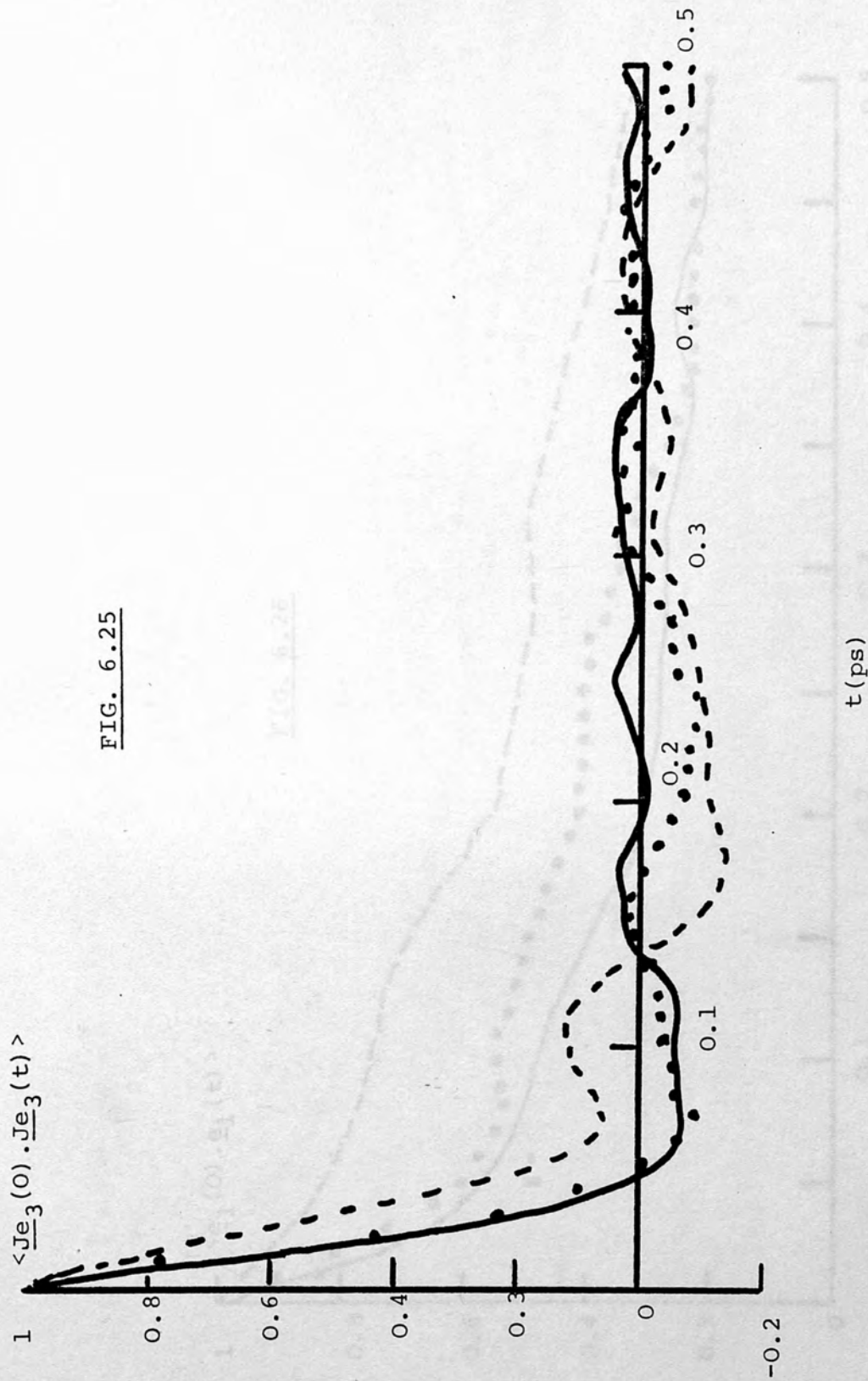
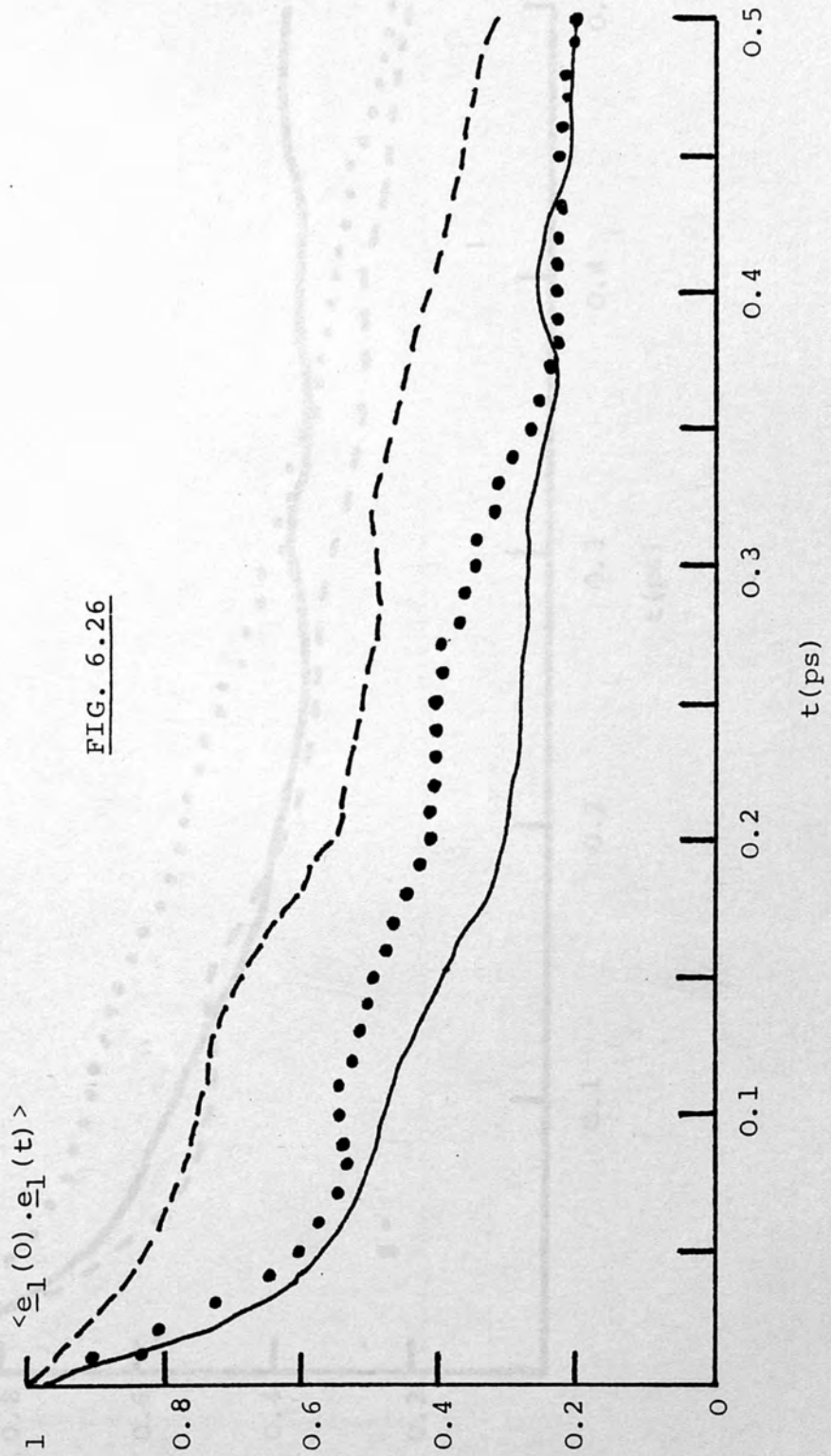
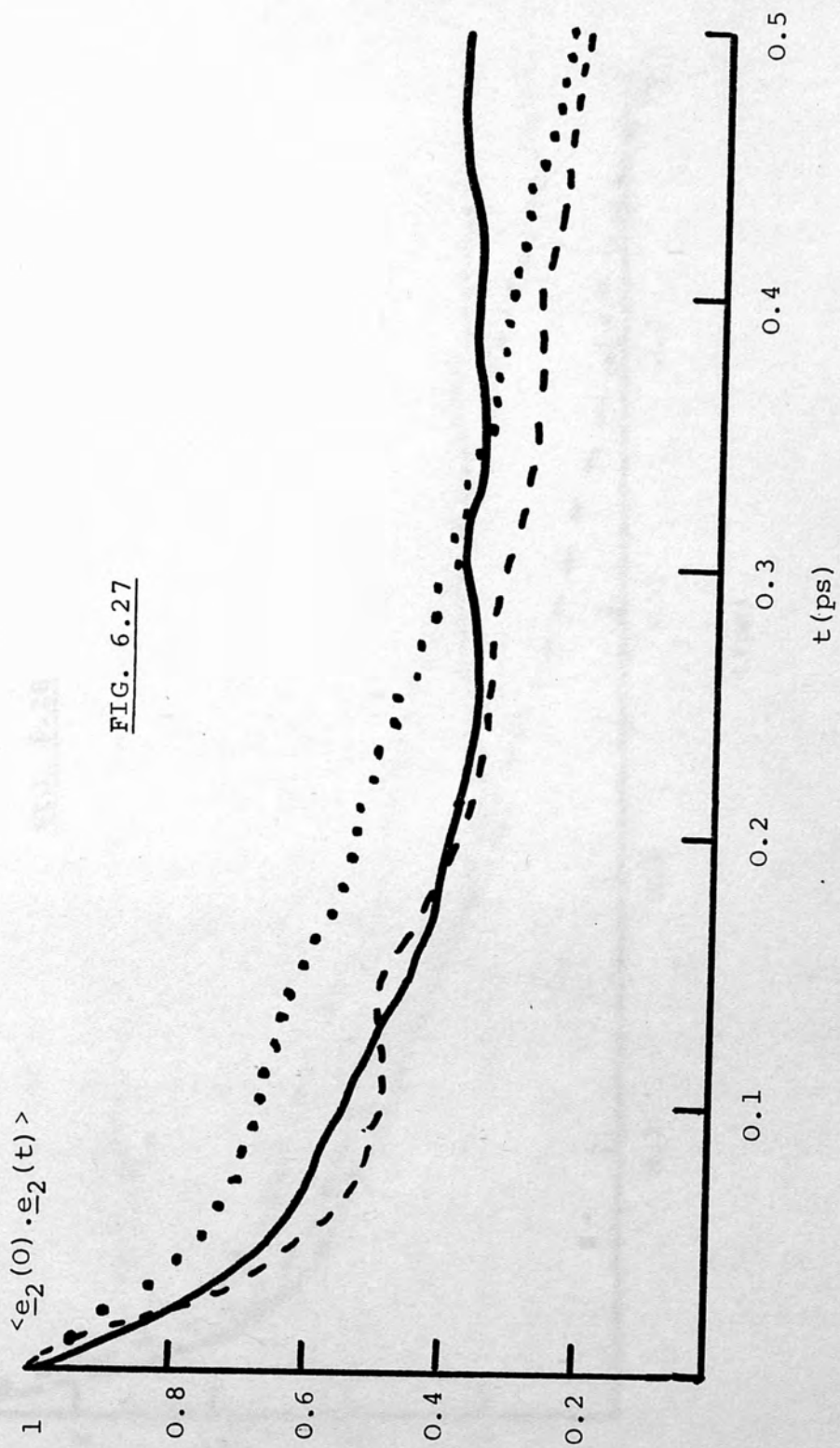


FIG. 6.25

FIG. 6.21

FIG. 6.26





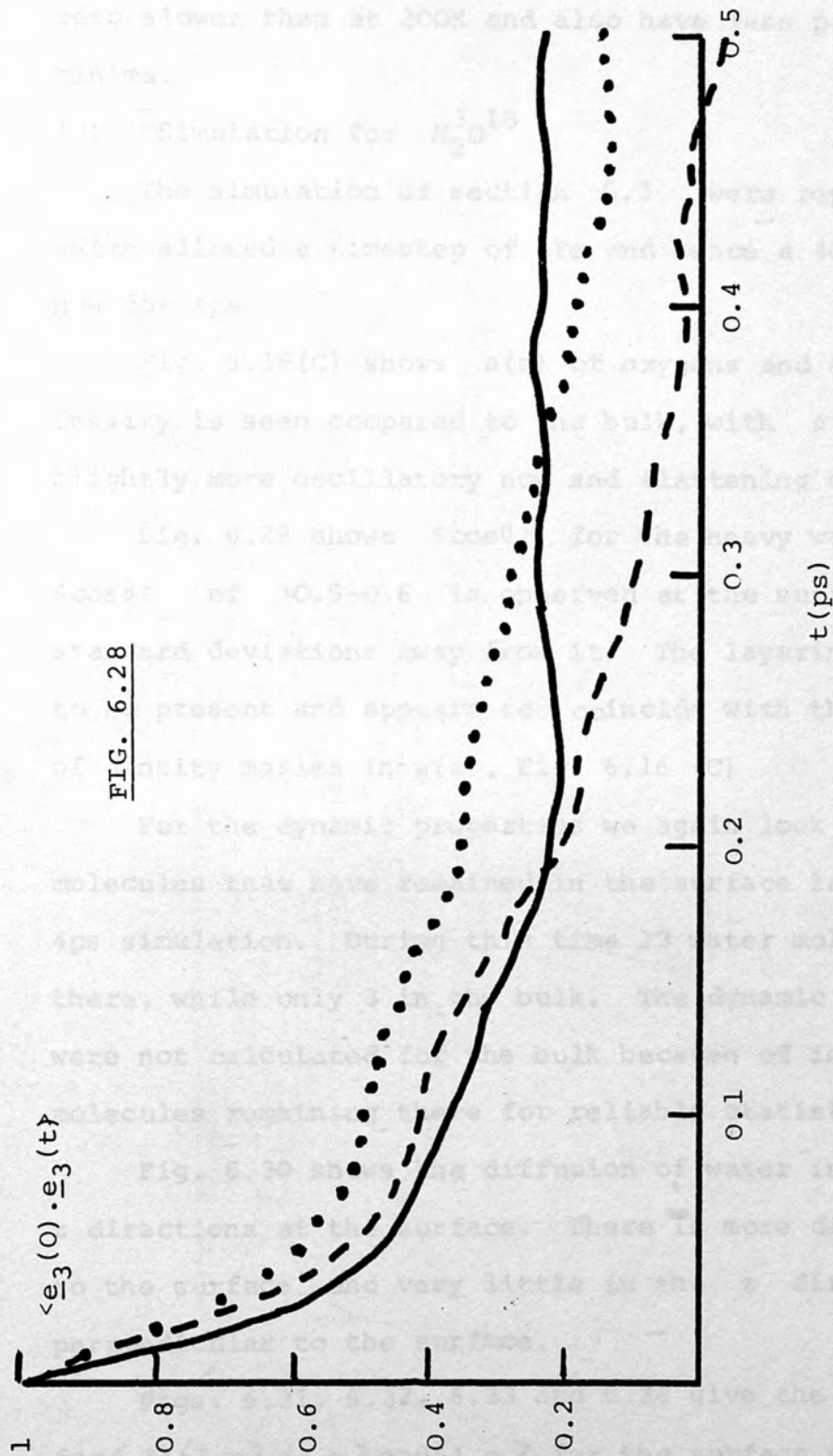


FIG. 6.28

at the surface. The correlation functions at 480K go to zero slower than at 300K and also have less pronounced minima.

(C) Simulation for H_2^{318}O

The simulation of section 6.3 were repeated with H_2^{318}O which allowed a timestep of 1fs and hence a 4000 step run was now for 4ps.

Fig. 6.16(C) shows $\rho(z)$ of oxygens and again the greater density is seen compared to the bulk, with $\rho(z)$ being slightly more oscillatory now and flattening off at the bulk.

Fig. 6.29 shows $\langle \cos\theta \rangle$ for the heavy water, again a $\langle \cos\theta \rangle$ of $\sim 0.5-0.6$ is observed at the surface and large standard deviations away from it. The layering does seem to be present and appears to coincide with the positions of density maxima in $\rho(z)$, Fig. 6.16 (C)

For the dynamic properties we again look at the water molecules that have remained in the surface layer during the 4ps simulation. During this time 13 water molecules had remained there, while only 3 in the bulk. The dynamic properties were not calculated for the bulk because of insufficient molecules remaining there for reliable statistics.

Fig. 6.30 shows the diffusion of water in the x, y and z directions at the surface. There is more diffusion parallel to the surface, and very little in the z direction, perpendicular to the surface.

Figs. 6.31, 6.32, 6.33 and 6.34 give the correlation function for $\langle \underline{J} \rangle$, $\langle \underline{J} \cdot \underline{e}_1 \rangle$, $\langle \underline{J} \cdot \underline{e}_2 \rangle$ and $\langle \underline{J} \cdot \underline{e}_3 \rangle$ for the surface molecules. The pattern is similar to the one observed for normal water as previously described and the correlation functions oscillate

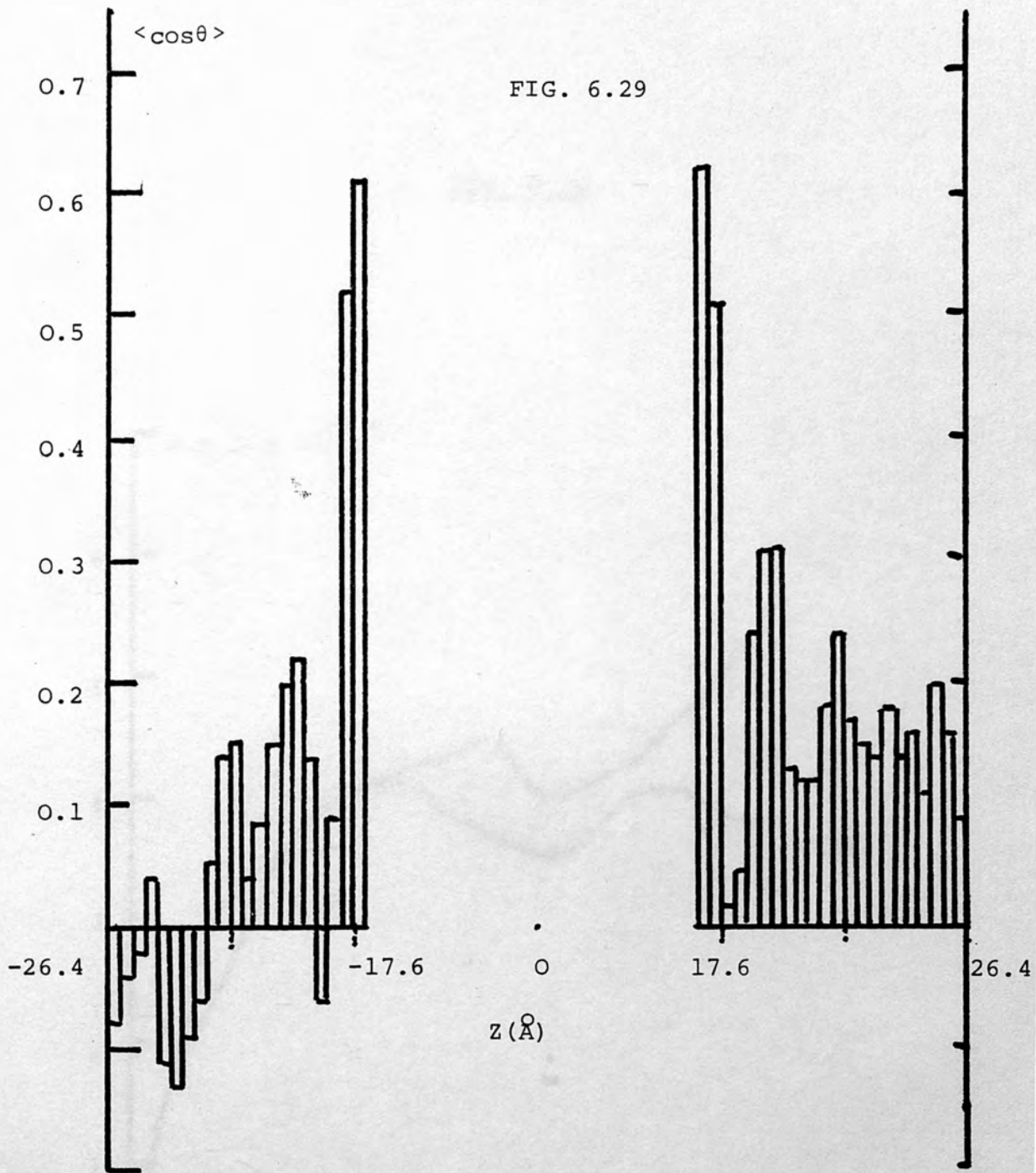
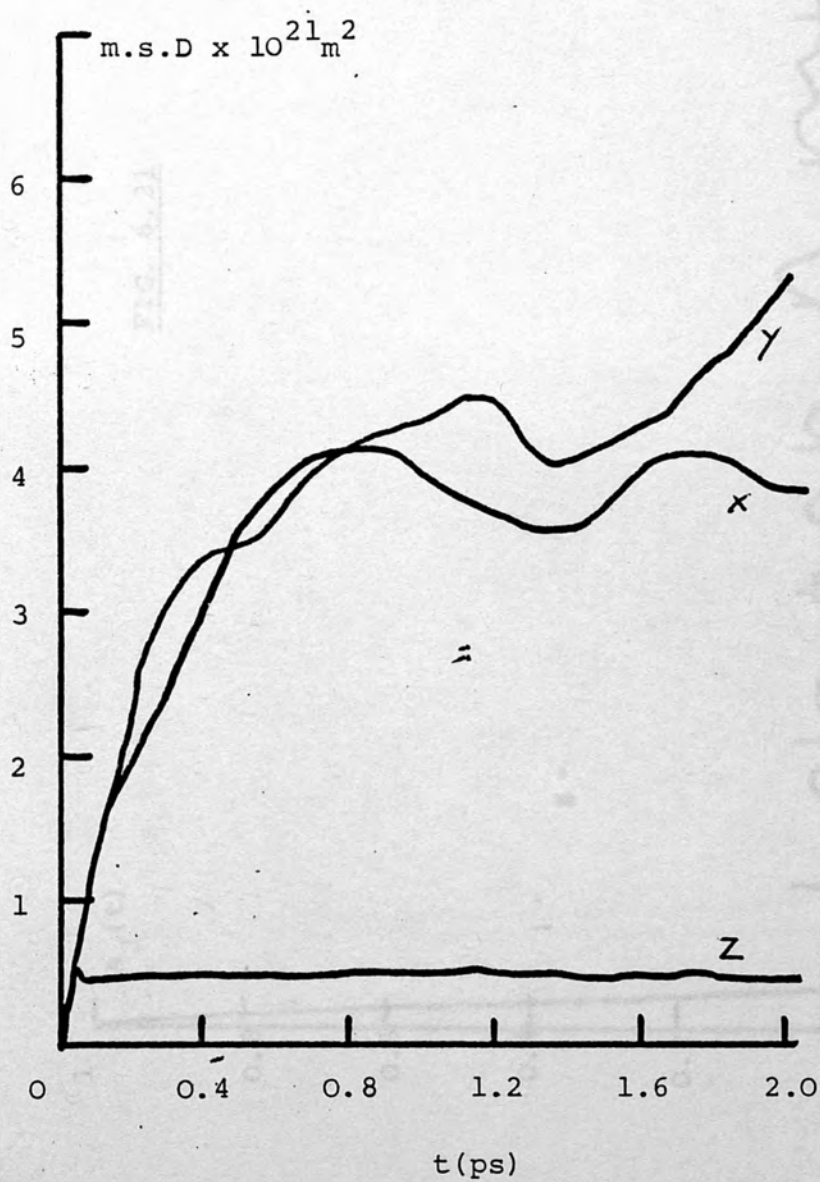
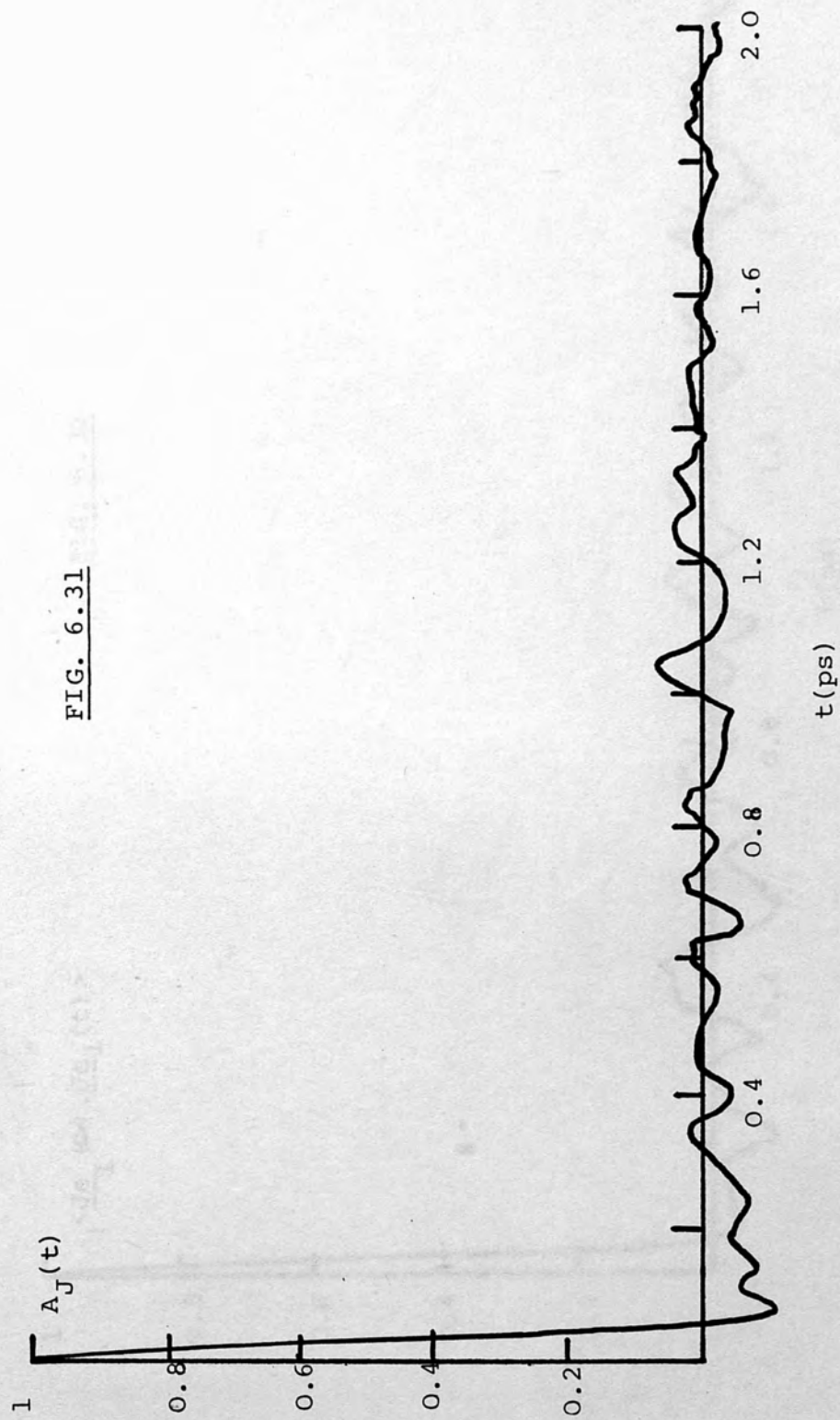


FIG. 6.30





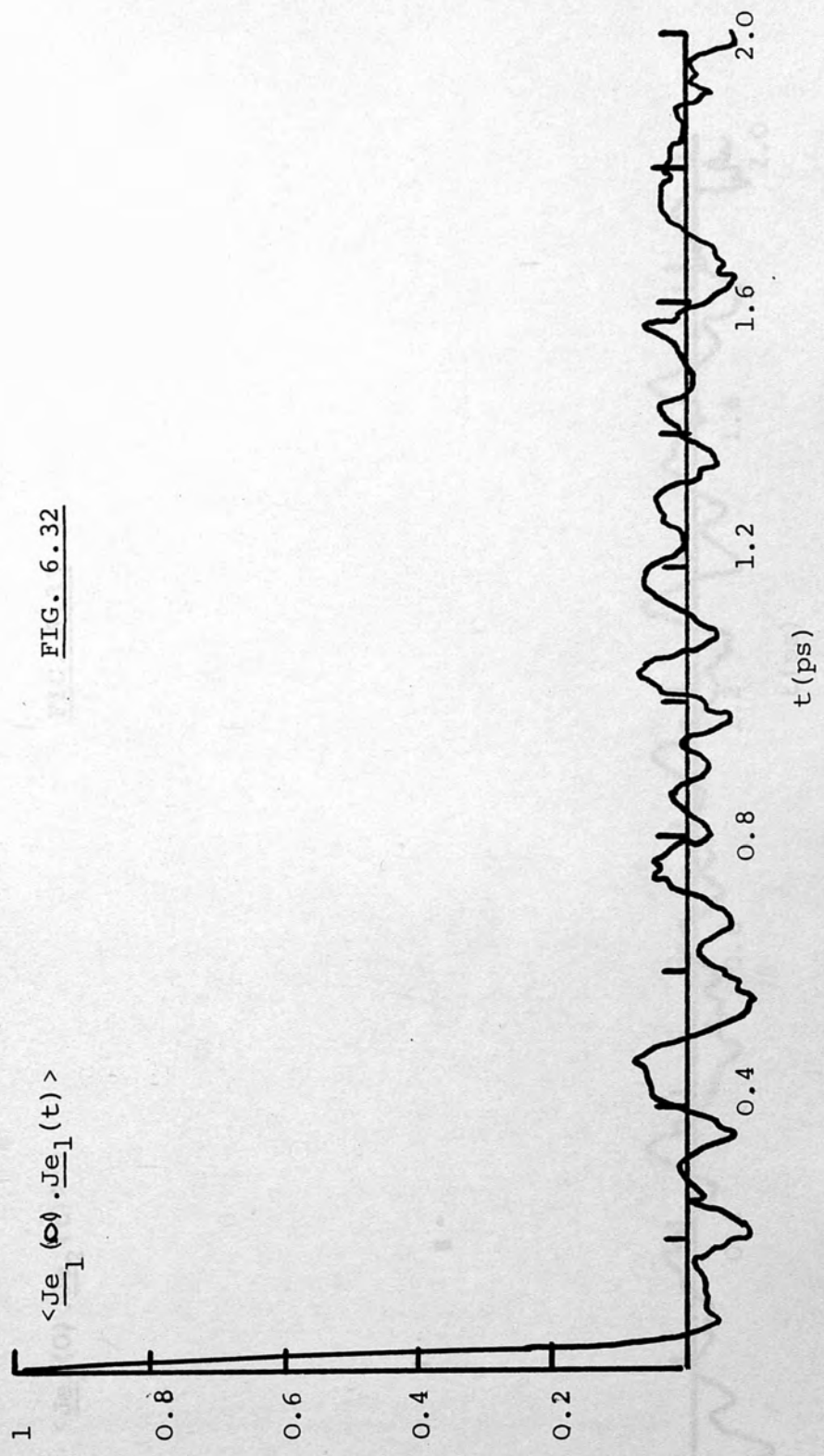


FIG. 6.32

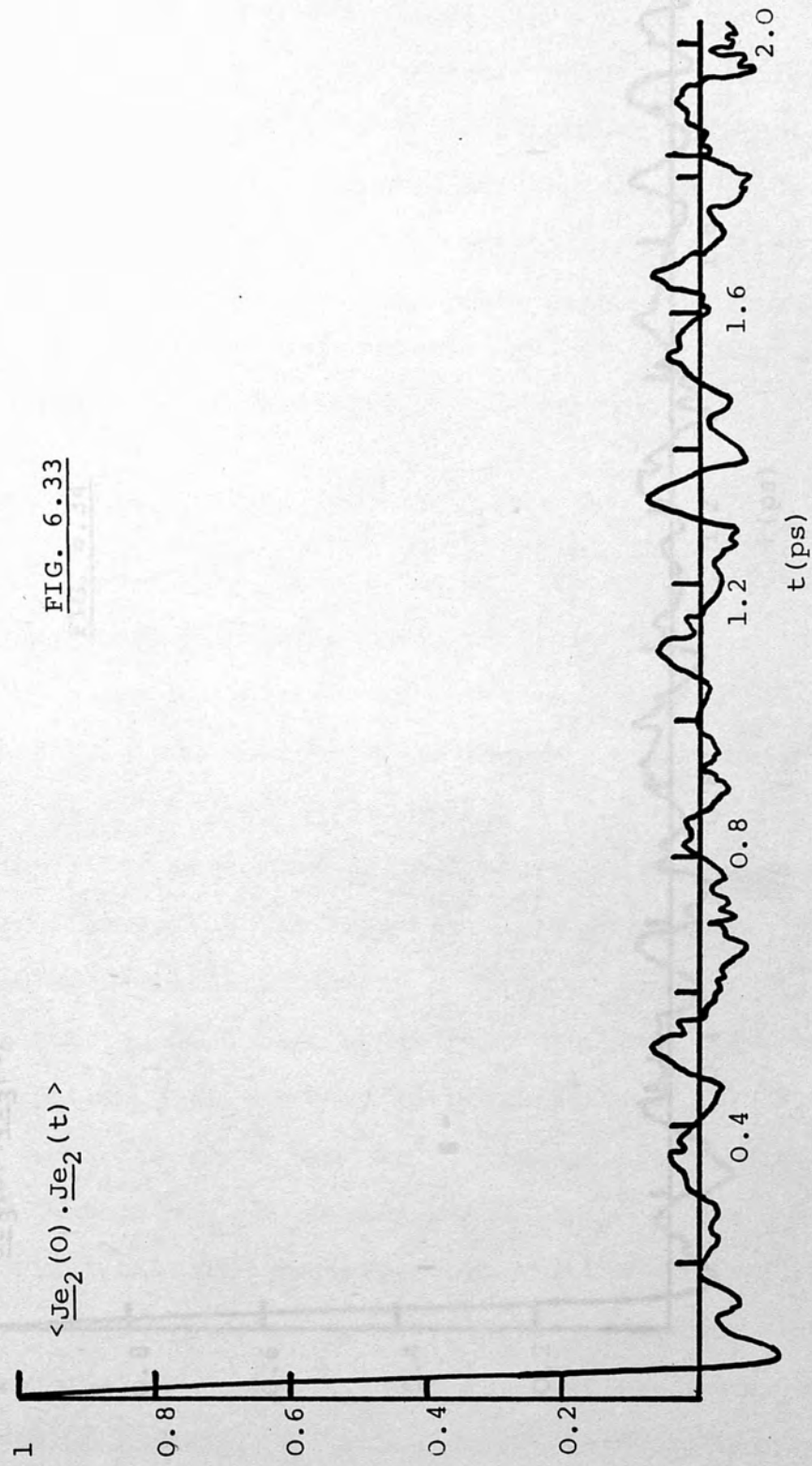


FIG. 6.33

... until the end of the simulation. Figs. 5.22, 5.23, 5.24 and 5.25 also compare the correlation functions for the surface molecules of H_2O and D_2O for the surface molecule, the only difference being that for the heavy water the z component correlates more. Figs. 5.26, 5.27 and 5.28 compare the orientational correlation functions at the surface for normal and heavy water, and in all cases it is slower for heavy water. Figs. 5.29, 5.30 and 5.31 show the z component of the correlation functions for heavy water for the whole simulation, the correlation functions are seen to be flattened off showing the preferred orientation at the surface.

5.4 Conclusions

In Ch. 5 we were not able to study time averaged processes due to the distribution process there at short times. Ch. 5 therefore describes simulations of water next to a fixed crystal, this work may also be of relevance to other crystals.

The simulation performed at 300K and 400K in good agreement substantiating the important results presented in Ch. 5 for the simulations at 400K.

The results in Ch. 6 have shown that a greater density of water is observed at the surface compared to the bulk. The oxygen atoms lie above the Na^+ ions and are closer to the surface than the H atoms, which try to get above the Cl^- ions. The preferred orientation observed at the surface is also seen in the orientational correlation functions at the surface flattening off instead of decaying to zero indicating the preferred orientation. The diffusion of the water at the surface has also been shown to be very

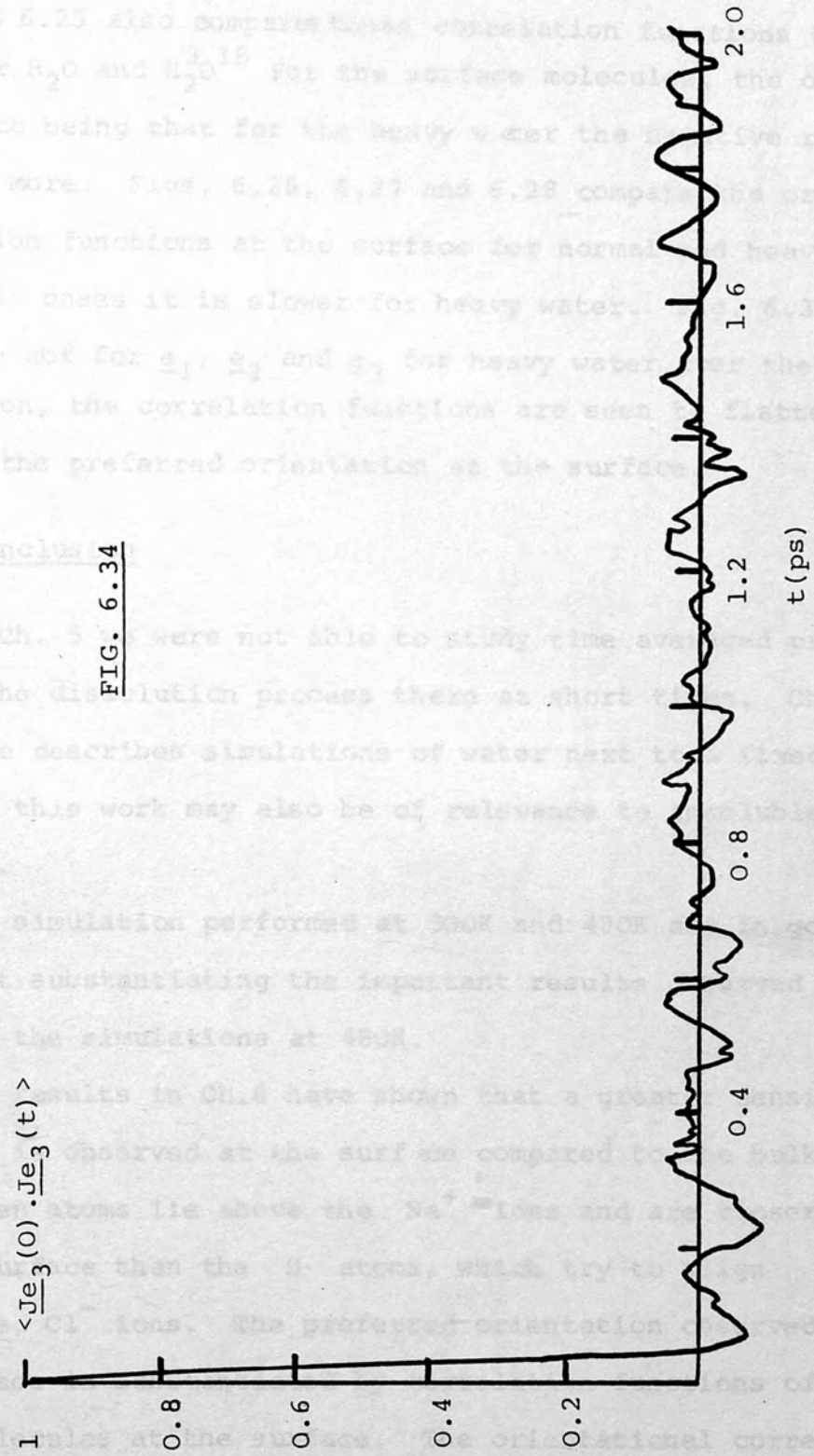


FIG. 6.34

about zero till the end of the simulation. Figs. 6.22, 6.23, 6.24 and 6.25 also compares these correlation functions till 0.5ps for H_2O and H_2O^{318} for the surface molecules, the only difference being that for the heavy water the negative region persists more. Figs. 6.26, 6.27 and 6.28 compare the orientational correlation functions at the surface for normal and heavy water, and in all cases it is slower for heavy water. Fig. 6.35 gives the acf for e_1 , e_2 and e_3 for heavy water over the whole simulation, the correlation functions are seen to flatten off showing the preferred orientation at the surface.

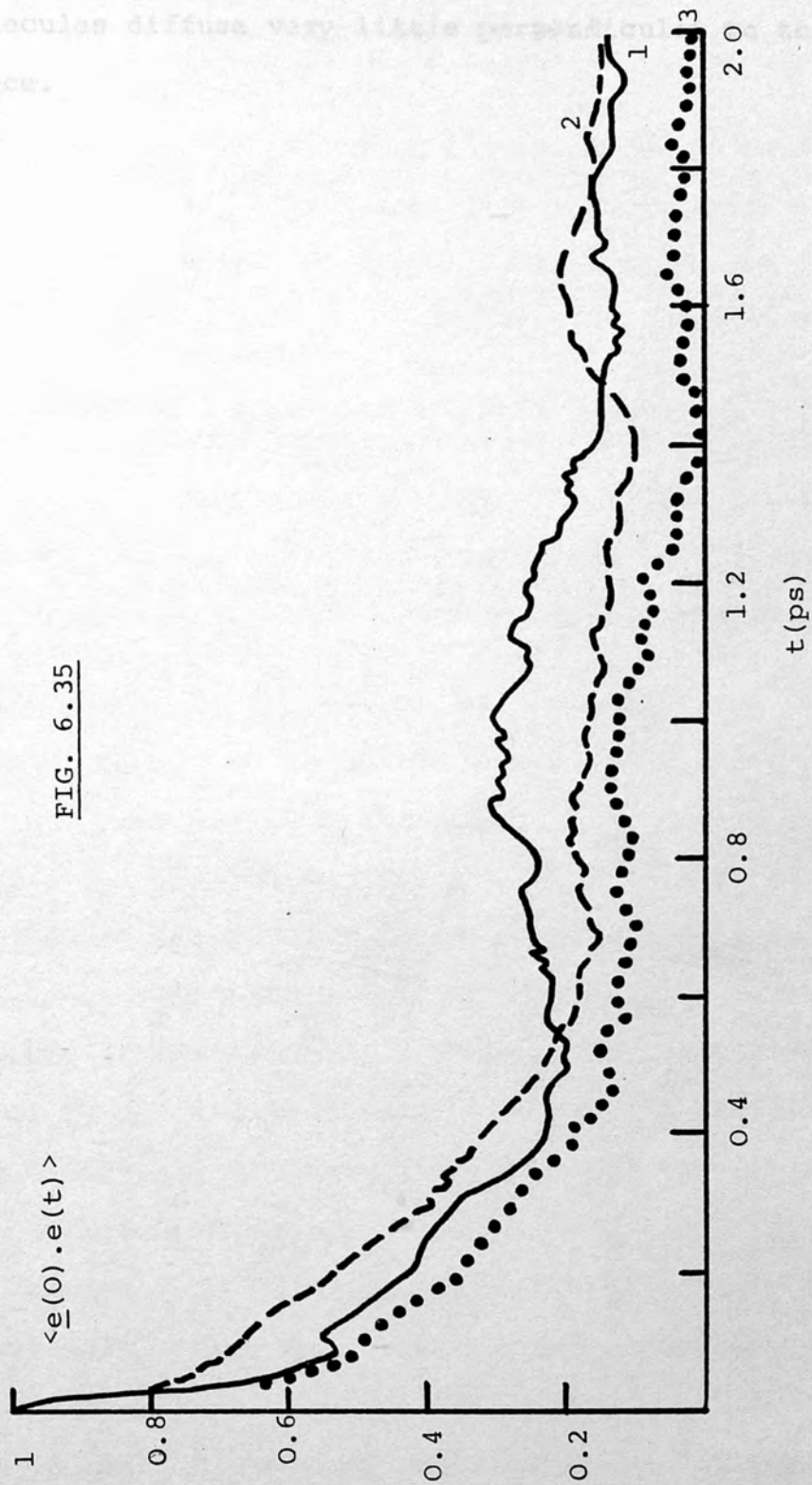
6.4 Conclusion

In Ch. 5 we were not able to study time averaged processes due to the dissolution process there at short times. Ch.6 therefore describes simulations of water next to a fixed crystal, this work may also be of relevance to insoluble crystals.

The simulation performed at 300K and 480K are in good agreement substantiating the important results observed in Ch.5 for the simulations at 480K.

The results in Ch.6 have shown that a greater density of water is observed at the surface compared to the bulk. The oxygen atoms lie above the Na^+ ions and are closer to the surface than the H atoms, which try to align above the Cl^- ions. The preferred orientation observed at the surface is substantiated by correlation functions of the water molecules at the surface. The orientational correlational functions at the surface flattening off instead of decaying to zero indicating the preferred orientation. The diffusion of the water at the surface has also been shown to be very

limited compared to the diffusion in the bulk, in particular
the water molecules diffuse very little parallel to the
crystal surface.



limited compared to the diffusion in the bulk, in particular the water molecules diffuse very little perpendicular to the crystal surface.

- (1) J.P. Valleau and B.E. Whittington, "A guide to Monte Carlo for statistical mechanics" in Statistical Mechanics Part A Ch.4, ed. B.J. Berne, Plenum Press, New York (1977).
- (2) J.P. Valleau and G.M. Torris, "A guide to Monte Carlo for statistical mechanics" in Statistical Mechanics Part A Ch.5, ed. B.J. Berne, Plenum Press, New York (1977).
- (3) I.R. McDonald, "Molecular dynamics: principles and applications" in Microscopic Structure and Dynamics of Liquids, ed. J. Dupuy and A.J. Dianzani, Plenum Press, New York (1978).
- (4) N.A. Metropolis, A.W. Rosenbluth, M.N. Rosenbluth, A.H. Teller and E. Teller, J. Chem. Phys. 21, 1087 (1953).
- (5) W.W. Wood and F.R. Parker, J. Chem. Phys. 27, 120 (1957).
- (6) W.W. Wood, "Monte Carlo studies of simple liquid models" in Physics of Simple Liquids, ed. H.N.V. Temperley, J.S. Rowlinson and G.J. Rushbrooke, North-Holland Publishing Company, Amsterdam (1968).
- (7) B.G. Alder and T.W. Wainwright, J. Chem. Phys. 31, 459 (1959).
- (8) A. Rahman, Phys. Rev. 135, 405 (1964).
- (9) L. Verlet, Phys. Rev. 159, 97 (1967).
- (10) L. Verlet and D. Levesque, Physica 16, 254 (1967).
- (11) I.R. McDonald and K. Singer, Discuss. Far. Soc. 41, 40 (1966).
- (12) I.R. McDonald and K. Singer, J. Chem. Phys. 47, 4705 (1967).
- (13) I.R. McDonald and K. Singer, J. Chem. Phys. 39, 2908 (1963).
- (14) J.A. Barker and A. Espey, Aust. J. Chem. 11, 1583 (1958).
- (15) I.R. McDonald and K. Singer, Mol. Phys. 12, 29 (1968).
- (16) J.V.L. Singer and K. Singer, Mol. Phys. 13, 279 (1968).
- (17) J.V.L. Singer and K. Singer, Mol. Phys. 14, 557 (1968).
- (18) I.R. McDonald, Chem. Phys. Lett. 1, 241 (1963).
- (19) I.R. McDonald, Mol. Phys. 11, 31 (1968).
- (20) G.D. Harp and B.J. Berne, J. Chem. Phys. 42, 1749 (1965).
- (21) B.J. Berne and G.D. Harp, Adv. Chem. Phys. 17, 63 (1970).
- (22) J. Barajas, D. Levesque and B. Quentrecq, Phys. Rev. A7, 1097 (1973).

REFERENCES

- (1) J.P. Valleau and S.E. Whittington, "A guide to Monte Carlo for statistical mechanics" in Statistical Mechanics Part A Ch.4, ed. B.J. Berne, Plenum Press, New York (1977).
- (2) J.P. Valleau and G.M. Torrie, "A guide to Monte Carlo for statistical mechanics" in Statistical Mechanics Part A Ch.5, ed. B.J. Berne, Plenum Press, New York (1977)
- (3) I.R. McDonald, "Molecular dynamics: principles and applications" in Microscopic Structure and Dynamics of Liquids, ed. J. Dupuy and A.J. Dianoux, Plenum Press, New York (1978).
- (4) N.A. Metropolis, A.W. Rosenblut, M.N. Rosenblut, A.H. Teller and E. Teller, J. Chem. Phys. 21, 1087 (1953).
- (5) W.W. Wood and F.R. Parker, J. Chem. Phys. 27, 720 (1957).
- (6) W.W. Wood, "Monte Carlo studies of simple liquid models" in Physics of Simple Liquids, ed. H.N.V. Temperley, J.S. Rowlinson and G.S. Rushbrooke, North-Holland Publishing Company, Amsterdam (1968).
- (7) B.J. Alder and T.W. Wainwright, J. Chem. Phys. 31 459 (1959).
- (8) A. Rahman, Phys. Rev. A136, 405 (1964).
- (9) L. Verlet, Phys. Rev. 159, 98 (1967).
- (10) L. Verlet and D. Levesque, Physica 36, 254 (1967).
- (11) I.R. McDonald and K. Singer, Discuss. Far. Soc. 43, 40 (1967)
- (12) I.R. McDonald and K. Singer, J. Chem. Phys. 47, 4766 (1967).
- (13) I.R. McDonald and K. Singer, J. Chem. Phys. 50, 2308 (1969).
- (14) J.A. Barker and A. Pompe, Aust. J. Chem. 21, 1683 (1968).
- (15) I.R. McDonald and K. Singer, Mol. Phys. 23, 29 (1972).
- (16) J.V.L. Singer and K. Singer, Mol. Phys. 19, 279 (1970).
- (17) J.V.L. Singer and K. Singer, Mol. Phys. 24, 557 (1972).
- (18) I.R. McDonald, Chem. Phys. Lett. 3, 241 (1969).
- (19) I.R. McDonald, Mol. Phys. 23, 41 (1972).
- (20) G.D. Harp and B.J. Berne, J. Chem. Phys. 49, 1249 (1968).
- (21) B.J. Berne and G.D. Harp, Adv. Chem. Phys. 17, 63 (1970).
- (22) J. Barojas, D. Levesque and B. Quentree, Phys. Rev. A7, 1092 (1973).

- (23) P.S.Y. Cheung and J.G. Powles, *Mol. Phys.* 30, 921 (1975).
- (24) K. Singer, A. Taylor and J.V.L. Singer, *Mol. Phys.* 33, 1757 (1977).
- (25) K. Singer, J.V.L. Singer and A. Taylor, *Mol. Phys.* 37, 1239 (1979).
- (26) C.S. Murthy, K. Singer, M.L. Klein and I.R. McDonald, *Mol. Phys.* 41, 1387 (1980).
- (27) C.S. Murthy, K. Singer and I.R. McDonald, *Mol. Phys.* 44, 135 (1981).
- (28) A. Rahman and F.H. Stillinger, *J. Chem. Phys.* 55, 3336 (1971).
- (29) L.V. Woodcock and K. Singer, *Trans. Far. Soc.* 67, 12 (1971).
- (30) K.S. Liu, *J. Chem. Phys.* 60, 4226 (1974).
- (31) F.F. Abraham, D.E. Schreiber and J.A. Barker, *J. Chem. Phys.* 62, 1958 (1975).
- (32) S. Toxvaerd, *J. Chem. Phys.* 62, 1589 (1975).
- (33) M. Rao and D. Levesque, *J. Chem. Phys.* 65, 3233 (1976).
- (34) G.A. Chapela, G. Saville and J.S. Rowlinson, *Far. Disc. Chem. Soc.* 59, 22 (1975).
- (35) S.M. Thompson and K.E. Gubbins, *J. Chem. Phys.* 74, 6467 (1981).
- (36) D.M. Heyes, M. Barber and J.H.R. Clarke, *J.C.S. Far. II* 1485 (1977).
- (37) D.M. Heyes, M. Barber and J.H.R. Clarke, *J.C.S. Far. II* 1469 (1979).
- (38) D.M. Heyes, M. Barber and J.H.R. Clarke, *J.C.S. Far. II*, 1484 (1979).
- (39) S. Toxvaerd, *J. Chem. Phys.* 74, 1998 (1981).
- (40) I. Snook, W. van Megan, *J. Chem. Phys.* 70, 3099 (1979).
- (41) J.N. Cape and L.V. Woodcock, *J. Chem. Phys.* 73, 2420 (1980).
- (42) S. Toxvaerd and E. Praestgaard, *J. Chem. Phys.* 67, 5291 (1977).
- (43) J.Q. Broughton, A. Bonissent and F.F. Abraham, *J. Chem. Phys.* 74, 4029 (1981).
- (44) N.I. Christou, J.S. Whitehouse, D. Nicholson and N.E. Parsonage, *Faraday Symposia of the Chemical Society* 16 (1981).
- (45) D.P. Woodruff, "The Solid-Liquid Interface", Cambridge University, London (1973).

- (46) I.R. McDonald and K. Singer, *J. Chem. Phys.* 50, 2308 (1969).
- (47) R.W. Hockney, *Meth. Comp. Phys.* 9, 136 (1970).
- (48) L. Verlet, *Phys. Rev.* 159, 98 (1967).
- (49) P.S.Y. Cheung, *Mol. Phys.* 33, 519 (1977).
- (50) B.J. Berne in *Adv. Treatise of Phys. Chem.* vol. 8B, ed. H. Eyring, D. Henderson, and W. Joost, Academic Press, London: New York (1970).
- (51) J.W.E. Lewis, K. Singer and L.V. Woodcock, *J.C.S. Far. II*, 301 (1975).
- (52) J. Copley and A. Rahman, *Phys. Rev.* A13, 2276 (1976).
- (53) B. Larsen, T. Fjørland and K. Singer, *Mol. Phys.* 26, 1521 (1973).
- (54) A. Rahman, R.N. Fowler and A.H. Narten, *J. Chem. Phys.* 57, 3010 (1972).
- (55) J.P. Hansen and I.R. McDonald, *Phys. Rev.* A11 2111 (1976).
- (56) F. Lantelme, P. Turc, B. Quentrec and J.W.E. Lewis, *Mol. Phys.* 28, 1537 (1974).
- (57) D.J. Adams and I.R. McDonald, *Physica* 79B, 159 (1975).
- (58) M. Dixon and M.J.L. Sangster, *J. Phys. C* 9, 3381 (1976).
- (59) M.J.L. Sangster and M. Dixon, *Advan. Phys.* 25, 247 (1976).
- (60) J.W.E. Lewis and K. Singer, *J.C.S. Far. II*, 41 (1975).
- (61) F.H. Stillinger, J.G. Kirkwood and P.J. Wojtowicz, *J. Chem. Phys.* 32, 1837 (1976).
- (62) G. Jacucci, I.R. McDonald and K. Singer, *Phys. Lett.* A50, 141 (1974).
- (63) M. Dixon and M.J.L. Sangster, *J. Phys.* C8, L8 (1975).
- (64) M.P. Tosi and F.G. Fumi, *J. Phys. Chem. Solids*, 25, 45 (1964)
- (65) J.E. Meyer, *J. Chem. Phys.* 1, 270 (1933).
- (66) L. Pauling, *Z. Kristallogr*, 67, 377 (1928).
- (67) L. Pauling, *J. Amer. Chem. Soc.* 50, 1036 (1928).
- (68) P.P. Ewald, *Ann. Physik*, 21, 1087 (1921).
- (69) J.W. Eastwood, *J. Comp. Phys.* 18, 1 (1975).
- (70) N. Anastasiou and D. Fincham, *Comp. Phys. Comm.* 25, 159 (1982)
- (71) J.W. Eastwood, R. W. Hockney and D.N. Lawrence, *Comp. Phys. Comm.* 19, 215 (1980).

- (72) S. W. de Leeuw, J.W. Perram and E.R. Smith, Proc. R. Soc. Lond. A373, 27 (1980).
- (73) S. W. de Leeuw and J.W. Perram, Physica 107A, 179 (1981).
- (74) M. Abramowitz and I.A. Stegun (eds) in "Handbook of Mathematical Functions", National Bureau of Standards, equation 7.1.26, Washington (1965).
- (75) F.H. Stillinger and A. Rahman, J. Chem. Phys. 68, 666 (1978)
- (76) J.W. Eastwood, R.W. Hockney and D.N. Lawrence "P³M 3DP - The Three Dimensional Periodic Particle - Particle/Particle-Mesh Program", Reading University Computer Science Report, RCS 113 (1978).
- (77) J.W. Eastwood and R.W. Hockney, J. Comp. Phys. 16, 342 (1974).
- (78) R.W. Hockney, Meth. Comp. Phys. 9, 176 (1970).
- (79) J.W. Cooley and J.W. Tukey, Meth. Comp. Phys. 19, 297 (1965)
- (80) R.M. Russell, Comm. ACM 21, 63 (1978).
- (81) D. Fincham and B.J. Ralston, Comp. Phys. Comm. 23, 127 (1981)
- (82) J.D. Bernal and R.H. Fowler, J. Chem. Phys. 1, 515 (1933).
- (83) S.W. Peterson and H.A. Levey, Acta. Cryst. 10, 70 (1957).
- (84) I. Pauling, J. Amer. Chem. Soc. 57, 2680 (1935).
- (85) E.J.W. Verwey, Recl. Trav. Chim. Pays. Bes. 60, 881 (1941).
- (86) J.S. Rowlinson, Trans. Far. Soc. 47, 120 (1951).
- (87) N. Bjerrum, Science 115, 385 (1952).
- (88) J.A. Barker and R.O. Watts, Chem. Phys. Lett. 3, 144 (1969).
- (89) A. Ben-Naim and F.H. Stillinger, "Aspects of the Statistical Mechanical Theory of Water", in Structure and Transport Processes in Water and Aqueous Solutions, ed. R.H. Horne, Wiley-Interscience, New York (1972).
- (90) F.H. Stillinger and A. Rahman, J. Chem. Phys. 60, 1545 (1974)
- (91) A.H. Narten and H.A. Levy, J. Chem. Phys. 55, 2268 (1971).
- (92) P. Barnes, J.L. Finney, J.D. Nicholas and J.E. Quinn, Nature 282, 459 (1979).
- (93) A. Rahman and F.H. Stillinger, J. Amer. Chem. Soc. 95, 7943 (1973)
- (94) H. Popkie, H. Kistenmacher and E. Clementi, J. Chem. Phys. 59, 1325 (1973).
- (95) O. Matsuoka, E. Clementi and M. Yoshime, J. Chem. Phys. 64, 1351 (1976).

- (96) F.H. Stillinger, *Adv. Chem. Phys.* 31, 1 (1975).
- (97) G.C. Lie and E. Clementi, *J. Chem. Phys.* 64, 5308 (1976).
- (98) R.O. Watts, *Chem. Phys.* 26, 367 (1977).
- (99) I.R. McDonald and M.L. Klein, *J. Chem. Phys.* 68, 4875 (1978).
- (100) A.D. Buckingham, *Quart. Rev. Chem. Soc.* 13, 183 (1959).
- (101) C.A. Coulson and D. Eisenberg, *Proc. Roy. Soc.* A291, 445 (1966).
- (102) W.E. Sharp, "The Structure and Properties of Water", eds. D. Eisenberg and W. Kauzmann, Clarendon Press, Oxford (1969).
- (103) M.D. Morse and S.A. Rice, *J. Chem. Phys.* 76, 650 (1982).
- (104) J-P Rychaert, G. Ciccotti and H.J.C. Berensden, *J. Comp. Phys.* 23, 327 (1977).
- (105) J. Barojas, D. Levesque and B. Quentrec, *Phys. Rev.* A7, 1092 (1973).
- (106) A.J.C. Ladd, *Mol. Phys.* 28, 1069 (1977).
- (107) P. Bopp, W. Dietz and K. Heinzinger, *Z. Naturforsch* 34a, 1424 (1979).
- (108) A. Rahman, F.H. Stillinger and H.L. Lemberg, *J. Chem. Phys.* 63, 5223 (1975).
- (109) K. Heinzinger and P.C. Vogel, *Z. Naturforsch* 29a, 1164 (1974).
- (110) P.C. Vogel and K. Heinzinger, *Z. Naturforsch* 30a, 789 (1975).
- (111) K. Heinzinger and P.C. Vogel, *Z. Naturforsch* 31a, 463 (1976).
- (112) P.C. Vogel and K. Heinzinger, *Z. Naturforsch* 31a, 476 (1976).
- (113) G. Polinkas, W.O. Riede and K. Heinzinger, *Z. Naturforsch*, 32a, 1137 (1977).
- (114) G.I. Szász and K. Heinzinger, *Z. Naturforsch* 34a, 840 (1979).
- (115) G.I. Szász, W.O. Riede and K. Heinzinger, *Z. Naturforsch* 34a, 1083 (1979).
- (116) G. Palinkás, T. Radnai, G. Szász and K. Heinzinger, *J. Chem. Phys.* 74, 3522 (1981).
- (117) H. Kistenmacher, P. Popkie and E. Clementi, *J. Chem. Phys.* 58, 1689 (1973).
- (118) H. Kistenmacher, H. Popkie and E. Clementi, *J. Chem. Phys.* 59, 5842 (1973).

- (119) H. Kistenmacher, H. Popkie and E. Clementi, J. Chem. Phys. 61, 799 (1974).
- (120) E. Clementi and H. Popkie, J. Chem. Phys. 57, 1077 (1971).
- (121) H. Kistenmacher, H. Popkie, and E. Clementi, J. Chem. Phys. 61, 799 (1974).
- (122) M. Mezei and D.L. Beveridge, J. Chem. Phys. 74, 622 (1981).
- (123) M. Mezei and D.L. Beveridge, J. Chem. Phys. 74, 6902 (1981).
- (124) G. Bolis and E. Clementi, J. Amer. Chem. Soc. 99, 5550 (1977).
- (125) E. Clementi, F. Cavallone and R. Scordamaglia, J. Amer. Chem. Soc. 99, 5531 (1977).
- (126) E. Clementi, G. Ranghino and R. Scordamaglia, Chem. Phys. Lett. 49, 218 (1977).
- (127) R. Scordamaglia, F. Cavallone and E. Clementi, J. Amer. Chem. Soc. 99, 5545 (1977).
- (128) P. Schuster, W. Jakubetz and W. Marius, Top. Curr. Chem. 60, 1 (1975).
- (129) A. Geiger, A. Rahman and F.H. Stillinger, J. Chem. Phys. 70, 263 (1979).
- (130) C. Pangali, M. Rao and B.J. Berne, J. Chem. Phys. 71, 2975 (1979).
- (131) S. Swaminathan and D.L. Beveridge, J. Amer. Chem. Soc. 101, 5832 (1980).
- (132) G.N. Patey and J.P. Valleau, J. Chem. Phys. 63, 2334 (1975).
- (133) I.R. McDonald and J.C. Rasaiah, Chem. Phys. Lett. 34, 382 (1975).
- (134) D.J. Adams and J.C. Rasaiah, Far. Disc. Chem. Soc. 64, 22 (1977).
- (135) E.M. Gosling and K. Singer, Chem. Phys. Lett. 39, 361 (1976).
- (136) J.Q. Broughton and L.V. Woodcock, J. Phys. C. 11, 2743 (1978).
- (137) A.J.C. Ladd and L.V. Woodcock, J. Phys. C. 11, 3565 (1978).
- (138) C.S. Hsu and A. Rahman, J. Chem. Phys. 71, 4974 (1979).
- (139) J.L. Tallon, W.H. Robinson and S.I. Smedley, J. Phys. Chem. 82, 1277 (1978).
- (140) F.W. de Wette and G.P. Alldredge, Meth. Comp. Phys. 15, 163 (1976).
- (141) S. Srinivason and G. Lakshmi, Surf. Sci. 43, 617 (1974).
- (142) D.M. Heyes and J.H.R. Clarke, J.C.S. Far. Trans. II, 1240 (1979).

- (143) C.A. Croxton, "Atomic Processes at the Liquid Surface" in Progress in Liquid Physics, ed. C.A. Croxton, Wiley-Interscience (1978).
- (144) D.M. Heyes, Ph.D. Thesis, U.M.I.S.T. (1977).
- (145) F.F. Abraham, in CRC Critical Reviews in Solid State and Materials Science 10, 169 (1981).
- (146) R.O. Watts, Mol. Phys. 28, 1069 (1974).
- (147) B. Jönsson, Chem. Phys. Lett. 82, 520 (1981).